A Computational Fluid Dynamics Study of Fluid Flow and Heat Transfer in a Micro channel

Submitted in partial fulfillment
of the requirements for the degree of

MASTER OF TECHNOLOGY

IN

CHEMICAL ENGINEERING

By

ASHISH KUMAR PANDEY
Roll No: 209CH1059
Session: 2010-2011

Under the Supervision of

Dr. BASUDEB MUNSHI

NATIONAL INSTITUTE OF TECHNOLOGY, ROURKELA
ROURKELA (ORISSA) – 769 008, INDIA

NATIONAL INSTITUTE OF TECHNOLOGY, ROURKELA
(ORISSA), INDIA

CERTIFICATE

This is to certify that the dissertation report entitled**, "A Computational Fluid Dynamics Study of Fluid Flow and Heat Transfer in a Micro channel"** is submitted by **Ashish Kumar Pandey**, Roll. No. 209CH1059 for Dissertation (CH 692) course. It is required in partial fulfillment for the award of M. Tech. Degree in Chemical Engineering. The matter embodies original work done by him under my supervision.

Signature in full of the Supervisor	_____
Name in capital block letters	**Prof. BASUDEB MUNSHI**
Designation	Associate Professor Department of Chemical Engineering National Institute of Technology, Rourkela

Date:

Acknowledgments

I would like to express my sincere gratitude to Prof. Basudeb Munshi for his guidance and assistance in this thesis. The technical discussions with Prof. Munshi were always been very insightful, and I will always be indebted to his for all the knowledge he shared with me. His prompt responses and availability despite his constantly busy schedule were truly appreciated. The reality is that Prof. Munshi was much more than an advisor for me. He always helped me in all the technical and non-technical issues during the production of this work. His encouragement and efforts led this report to successful completion in a timely fashion.

I would also like to thank Prof. M. Kundu for being a uniformly excellent advisor. She was always open minded, helpful and provided us with a strong broad idea.

I am also thankful to all the staff and faculty members of Chemical Engineering Department, National Institute of Technology, Rourkela for their consistent encouragement.

I would like to extend my sincere thanks to my friends and colleagues. Last but not least I am also thankful to Mr. Akhilesh khapre for his unconditional assistance and support.

Ashish Kumar Pandey

Roll No. 209CH1059

Contents

Abstract i

List of Figures ii

List of Tables v

Chapters

1. INTRODUCTION

1.1 MICROCHANNEL AND ITS USE 1

1.2 USE OF NANO PARTICLES 3

1.3 APPLICATION OF COMPUTATIONAL FLUID DYNAMICS (CFD) 3

1.4 OBJECTIVES OF THE PRESENT WORK 4

1.5 OUTLINE OF THE REPORT 5

2. LITERATURE REVIEW

2.1 EXPERIMENTAL STUDY OF FLUID FLOW AND HEAT TRANSFER IN MICRO CHANNELS 7

2.2 NUMERICAL STUDY OF FLUID FLOW AND HEAT TRANSFER IN MICRO CHANNELS 9

2.3 NANOFLUIDS AS HEAT ENHANCER 15

3. COMPUTATIONAL FLUID DYNAMICS MODEL EQUATIONS

3.1 SINGLE PHASE MODELING EQUATIONS 20

3.1.1 Mass Conservation Equation 20

3.1.2 Momentum Conservation Equation 20

3.1.3 Energy equation 21

3.2 TWO PHASE MODELING EQUATIONS 22

3.2.1 Volume of Fluid (VOF) Model 23

3.2.1.1 Volume Fraction Equation 23

3.2.1.2 Material Properties 23

3.2.1.3 Momentum Equation 24

3.2.1.4 Energy Equation 24

3.2.2 Mixture Model 25

3.2.2.1 Continuity Equation 25

3.2.2.2 Momentum Equation 25
3.2.2.3 Energy Equation 26
3.2.2.4 Volume Fraction Equation for the Secondary Phases 27
4. SIMULATION OF SINGLE PHASE FLUID FLOW IN A CIRCULAR MICRO CHANNEL
4.1 SPECIFICATION OF PROBLEM 27
4.2 GEOMETRY IN ANSYS WORKBENCH 28
4.3 MESHING OF GEOMETRY 29
4.4 PHYSICAL MODELS 29
4.5 MATERIAL PROPERTIES 29
4.6 GOVERNING EQUATIONS 30
4.7 BOUNDARY CONDITIONS 33
4.8 METHOD OF SOLUTIONS 33
4.9 RESULTS AND DISCUSSIONS 34
4.10 CONCLUSIONS 49
5. MODELING OF SINGLE PHASE FLUID FLOW IN RECTANGULAR MICRO CHANNEL
5.1 PROBLEM SPECIFICATION 51
5.2 GEOMETRY OF THE COMPUTATIONAL DOMAIN 52
5.3 MESHING OF THE COMPUTATIONAL DOMAIN 53
5.4 PHYSICAL MODEL 53
5.5 FLUID PROPERTIES 53
5.6 ASSOCIATED EQUATIONS 54
5.7 BOUNDARY CONDITIONS 55
5.8 SOLUTION METHODS 56
5.9 RESULTS AND DISCUSSIONS 56
5.10 CONCLUSIONS 74
6. CONCLUSIONS AND FUTURE SCOPE OF WORK
6.1 CONCLUSIONS 75
6.2 FUTURE SCOPE OF WORK 76
7. REFERENCES 77

Abstract

A theoretical study of single phase microchannel heat exchanger has been carried out. The computational fluid dynamics (CFD) model equations are solved to predict the hydrodynamic and thermal behaviour of the exchanger. The geometry of the problem and meshing of it have been made in ANSYS Workbench. The models have been solved by ANSYS Fluent 12.0 solver.

The utility of nonmaterial as a heat enhancer has been justified by studying a circular microchannel thermal behaviour. Water and its nanofluids with alumina (Al_2O_3) are used as the coolant fluid in the microchannel heat sink. The present CFD calculated heat transfer coefficient values have compared with the analytical values and very close agreement is observed. The result shows that nanofluids help to increase the heat transfer coefficient by 15% and 12% respectively in laminar and turbulent zone. Thus use of nanofluids has been found beneficial both in laminar and turbulent zone. The relation between heat transfer coefficient and thermal conductivity of the fluid i.e. $h \propto k$ is proved in the present study. The entrance length for the fully developed velocities depends on Reynolds number. The temperature rise between outlet and inlet depends on the Reynolds number, Re and Peclet number, Pe. Temperature distribution is found to be independent of radial position even for $Pe << 1.0$. The hydrodynamic and thermal behaviour of the system have been studied in terms of velocity, pressure and temperature contours. The velocity contours at the exit show that wall effect penetrates more towards the center and the thicknes of the zone with maximum velocity shrinks with increase in Re. The pressure drop across the channel increases with increase in Re.

The experimental work done by Lee and Mudawar (2007) has been predicted by the present CFD results. The hydrodynamics and thermal behaviour of a rectangular microchannel are studied here. The variation wall temperature, pressure drop in the channel and the friction factors calculated using ANSYS Fluent can well predict the experimental data. The effect of Re on the behaviour the channel are also studied. Its behaviour also have been analysed with the help of temperature, pressure and velocity contours.

Key Words: microchannels, heat exchangers, nanoparticles, nanofluids, Fluent, CFD, heat transfer coefficient, pressure drop, friction factor

List of Figures

		Page Number
Figure 4.1	Fluid flow through a circular micro channel of constant cross-section	27
Figure 4.2	Computational Domain of Circular Micro channel	28
Figure 4.3	Two dimensional geometry of circular micro channel with structured mesh	29
Figure 4.4	Velocity profile at centerline in the circular micro channel at Re =1278. Pr_{Water} =5.53 , $Pr_{2\%}$ = 5.40, $Pr_{5\%}$ = 5.20.	34
Figure 4.5	Velocity profile at centerline in the circular micro channel at Re =12780. Pr_{Water} =5.53 , $Pr_{2\%}$ =5.40 , $Pr_{5\%}$ =5.20.	35
Figure 4.6	Variation heat transfer coefficient for laminar flow (Re =1278.0) in circular micro channel for water and its nanofluid	37
Figure 4.7	Variation heat transfer coefficient for turbulent flow (Re=12780.0) in circular micro channel for water and its nanofluid	37
Figure 4.8	Variation wall temperature for laminar flow (Re =1278.0) in circular micro channel for water and its nanofluid	39
Figure 4.9	Variation wall temperature for turbulent flow (Re =12780.0) in circular micro channel for water and its nanofluid	39
Figure 4.10	Variation wall temperature for Re = 0.1 in circular micro channel for water and its nanofluid	40
Figure 4.11	Variation of wall temperature with axial distant for different value of Reynolds number and Peclet number. Water is used as the fluid in the heat exchanger.	41
Figure 4.12	Variation of velocity of water in radial direction at different values of X for (a) Re = 0.1 (b) Re = 25 (c) Re = 50. Water is used as the fluid in the heat exchanger.	43
Figure 4.13	Temperature of pure water at different position in X direction for diffrent values of Re (a) Re = 0.1 (b) Re = 25 (c) Re = 50. Water is used as the fluid in the heat exchanger.	44
Figure 4.14	Water velocity contour plot at Re = 0.1 for water (a) Nearer to the entrance (b) Nearer to the exit	45
Figure 4.15	Water velocity contour plot at Re = 25 for water (a) Nearer to the entrance (b)Nearer to the exit. Water is used as the fluid in the heat exchanger.	46
Figure 4.16	Velocity contour plot at Re = 50 for water (a) Nearer to the entrance (b)Nearer to the exit. Water is used as the fluid in the heat exchanger.	46
Figure 4.17	Temperature contour plot at Re = 0.1 (a) Nearer to the entrance (b) Nearer to the exit. Water is used as the fluid in the heat exchanger.	47
Figure 4.18	Temperature contour plot at Re = 50. (a) Nearer to the	47

	entrance (b)Nearer to the exit. Water is used as the fluid in the heat exchanger.	
Figure 4.19	Pressure contour plots Re = 0.1 for water (a) Nearer to the entrace (b)Nearer to the exit. Water is used as the fluid in the heat exchanger.	48
Figure 4.20	Pressure contour plots Re = 25 for water (a) Nearer to the entrace (b)Nearer to the exit. Water is used as the fluid in the heat exchanger.	48
Figure 4.21	Pressure contour plots Re = 50 for water (a) Nearer to the entrace (b)Nearer to the exit. Water is used as the fluid in the heat exchanger.	49
Figure 5.1	Experimental setup with micro channel test module	51
Figure 5.2	Construction of micro channel test module with thermocouple locations	52
Figure 5.3	Computational domain of rectangular micro channel	53
Figure 5.4	Three dimensional geometry of rectangular micro channel with structured mesh	54
Figure 5.5	Velocity profile for water and its nanofluid at Re=140	56
Figure 5.6	Variation of computational and experimental pressure drop and friction factor of water with Re. (a) Pressure drop (b) Friction factor	59
Figure 5.7	Variation of computational and experimental pressure drop and friction factor of 1% Alumina with Re. (a) Pressure drop (b) Friction factor	60
Figure 5.8	Variation of computational and experimental pressure drop and friction factor of 2% Alumina with Re. (a) Pressure drop (b) Friction factor	61
Figure 5.9	Figure 5.9: Variation of Heat Transfer Coefficient for water along micro channel at different Power inputs (a) 100 W (b) 200 W (c) 300 W	62
Figure 5.10	Variation of Heat Transfer Coefficient for Nanofluid with 1% Alumina along micro channel at different Power inputs (a) 100 W (b) 200 W (c) 300 W.	63
Figure 5.11	Variation of Heat Transfer Coefficient for Nanofluid with 2 % Alumina along micro channel at different Power inputs (a) 100 W (b) 200 W (c) 300 W	64
Figure 5.12	Variation of wall temperature at different power inputs along micro channel for Water	65
Figure 5.13	Variation of wall temperature at different power inputs along micro channel for Nanofluid with 1 % Alumina	65
Figure 5.14	Variation of wall temperature at different power inputs along micro channel for Nanofluid with 2 % Alumina	66
Figure 5.15	Varition of wall temperature for pure water at mass flow rate of (a) 2.15 g/s (b)5.55 g/s	67
Figure 5.16	Varition of wall temperature for Nanofluid with 1 % Alumina at mass flow rate of (a) 2.16 g/s (b)5.57g/s	68

Figure 5.16a	Varition of wall temperature for Nanofluid with 2 % Alumina at mass flow rate of (a) 2.09 g/s (b)5.49g/s	69
Figure 5.17	Velocity contour Plot of water At Re = 140 (a) Nearer to inlet (b) Nearer to outlet	70
Figure 5.18	Velocity contour Plot of water At Re = 500 (a) Nearer to inlet (b) Nearer to outlet	70
Figure 5.19	Velocity contour Plot of water At Re = 940 (a) Nearer to inlet (b) Nearer to outlet	71
Figure 5.20	Pressure contour Plot of water At Re = 140 (a) Nearer to inlet (b) Nearer to outlet	71
Figure 5.21	Pressure contour Plot of water At Re = 500 (a) Nearer to inlet (b) Nearer to outlet	72
Figure 5.22	Pressure contour Plot of water At Re = 40 (a) Nearer to inlet (b) Nearer to outlet	72
Figure 5.23	Temperature contour plot for water at Re = 140 (a) Nearer to inlet (b) Nearer to outlet	73
Figure 5.24	Temperature contour plot for water at Re = 500 (a) Nearer to inlet (b) Nearer to outlet	73
Figure 5.25	Temperature contour plot for water at Re=940(a) Nearer to inlet (b) Nearer to outlet	74

List of Tables

		Page Number
Table 4.1	Choice of model based on Reynolds number	29
Table 4.2	Water base fluid properties with different concentration of alumina nanoparticles (Lee and Mudawar, 2007)	29
Table 4.3	Relaxation factor	33
Table 4.4	Comparison of analytical heat transfer coefficient with the present CFD results at laminar (Re == 1278.0) flow for water and nanofluid	36
Table 4.5	Comparison of analytical heat transfer coefficient with the present CFD results at turbulent (Re =12780.0) flow for water and nanofluid.	36
Table 4.6	Validation of laminar flow model based on the relation between heat transfer coefficient and thermal conductivity of the fluid.	38
Table 4.7	Variation of wall temperature with axial distance at different values of Re	41
Table 5.1	Dimension of unit cell micro channel	52
Table 5.1a	Specification of zone type in ANSYS Workbench	55
Table 5.2	Comparison of computation pressure drop and friction factor of water with experimental values (Lee and Qudawar, 2007)	57
Table 5.4	Comparison of computation pressure drop and friction factor of 1% Alumina with experimental values (Lee and Qudawar, 2007)	57
Table 5.5	Comparison of computation pressure drop and friction factor of 2% Alumina with experimental values (Lee and Qudawar, 2007)	58

Chapter 1

INTRODUCTION

Over the last decade, micromachining technology has been increasingly used for the development of highly efficient cooling devices called heat sink because of its undeniable advantages such as less coolant demands and small dimensions. One of the most important micromachining technologies is micro channels. Hence, the study of fluid flow and heat transfer in micro channels which are two essential parts of such devices, have attracted more attentions with broad applications in both engineering and medical problems. Heat sinks are classified into single-phase or two-phase according to whether boiling of liquid occurs inside the micro channels. Primary parameters that determine the single phase and two-phase operating regimes are heat flux through the channel wall and coolant flow rate. For a fixed amount of heat flux (heat load), the coolant may maintain its liquid state throughout micro-channels. With a lower flow rate, the flowing liquid coolant inside the channel may reach its boiling point and thus flow boiling occurs, which results in a two-phase heat sink.

1.1 MICROCHANNEL AND ITS USE

Tuckerman and Pease (1981) first made use of miniaturization for the purposes of heat removal, within the scope of a Ph.D. study in 1981. Their publication titled "High Performance Heat Sinking for VLSI" is credited as the first study on microchannel heat transfer. Their pioneering work has motivated many researchers to focus on the topic and microchannel flow has been recognized as a high performance heat removal tool ever since.

Before proceeding with microchannel flow and heat transfer, it is appropriate to introduce a definition for the term "microchannel". The scope of the term is among the topics of debate between researchers in the field. Mehendale et al. (2000) used the following classification based on manufacturing techniques required to obtain various ranges of channel dimensions, "D", being the smallest channel dimension:

$1\mu m < D < 100\mu m$: Microchannels

$100\mu m < D < 1\ mm$: Minichannels

$1\ mm < D < 6\ mm$: Compact Passages

$6\ mm < D$: Conventional Passages

Kandlikar and Grande (2003) adopted a different classification based on the rarefaction effect of gases in various ranges of channel dimensions, "*D*" being the smallest channel dimension:

$1\mu m < D < 10\mu m$: Transitional Microchannels

$10\mu m < D < 200\ \mu m$: Microchannels

$200\ \mu m < D < 3\ mm$: Minichannels

$3\ mm < D$: Conventional Passages

A simpler classification was proposed by Obot (2003) based on the hydraulic diameter rather than the smallest channel dimension. Obot classified channels of hydraulic diameter under 1 mm ($D_h < 1\ mm$) as microchannels, which was also adopted by many other researchers such as Bahrami and Jovanovich (2006), Bahrami et al. (2006) and Bayraktar and Pidugu (2006). This definition is considered to be more appropriate for the purposes of this thesis.

The higher volumetric heat transfer densities require advanced manufacturing techniques and lead to more complex manifold designs (Kandlikar et al. 2006). Many of the same manufacturing techniques developed for the fabrication of electronic circuits are being used for the fabrication of compact heat exchangers.

Microchannel heat sinks constitute an innovative cooling technology for the removal of a large amount of heat through a small area. It is one of the potential alternatives for replacing conventional finned tube heat exchangers, mainly used in industries such as automobiles, air conditioning and refrigeration at present. The heat sink is usually made from a high thermal conductivity solid such as silicon or copper with the micro-channels fabricated into its surface by either precision machining or micro-fabrication technology. A Micro-channel heat sinks typically contains a large number of parallel micro channels. Coolant is forced to pass through these channels to carry away heat from a hot surface. In Micro channel heat exchangers flow is typically laminar and heat transfer coefficients are proportional to velocity. Micro-channel heat sinks provide very high surface area to volume ratio, large convective heat transfer coefficient, small mass and volume, and small coolant inventory. These attributes render these heat sinks very suitable for cooling devices such as high-performance microprocessors, laser diode arrays, radars, and high-energy-laser mirrors. Micro channel heat exchangers could be easier to repair than their conventional counterparts. It offers other benefits, including increased latent capacity for micro channel evaporators. Micro channel heat exchangers improve heat transfer in two ways. First, the smaller

dimensions of the refrigerant flow passages increase refrigerant-side heat transfer. Second, the flat tube orientation reduces airside flow resistance, leading to either increased airflow or reduced fan power.

A micro reactor is a device in which chemical reactions take place in a confinement with typical lateral dimensions below 1.0 mm. When the temperature of the reactor is required to maintain, micro reactor also act as a micro channel heat exchanger. Micro reactors used in these applications are typically continuous flow reactors rather than batch reactors, with the continuous flow model providing better performance in material synthesis than is possible with batch reactors. The reactors offer many advantages over conventional scale reactors, including vast improvements in energy efficiency, reaction speed and yield, safety, reliability, scalability, on-site/on-demand production, and a much finer degree of process control. It enables miniaturization of the fuel processor because they minimize heat and mass transfer resistance. A micro reactor may also be used to perform reactions on a very small scale to determine the potential for dangerous situations such as runaway reactions or the generation of excessive levels of heat.

1.2 USE OF NANO PARTICLES

In spite of its own advantages micro channel heat exchanger uses nano particles as heat enhancing materials. Fluids with nanoparticles suspended in them are called nanofluids. This term was coined by Choi et al. in 1995 at Argonne National Laboratory of USA. Nanofluids as a new, innovative class of heat transfer fluids represent a rapidly emerging field where nanoscale science and thermal engineering meet. Nanofluids, engineered by dispersing nanometer-sized solid particles in conventional heat transfer fluids have been found to possess superior thermal performance compared to their base fluids. Since a solid metal has a larger thermal conductivity than a base fluid, suspending metallic solid fine particles into the base fluid is expected to improve the thermal conductivity of that fluid. Hence, there is a need for fundamental understanding of the heat transfer behavior of nanofluids in order to exploit their potential benefits and applications. Various potential benefits of the application of nanofluids include: improved heat transfer, heat transfer system size reduction, minimal clogging and micro channel cooling. Nanoparticles are also suitable for use in Microsystems because of their size smaller than the Microsystems.

1.3 APPLICATION OF COMPUTATIONAL FLUID DYNAMICS (CFD)

Numerical methods are extensively used to analyze the performance of the behaviour and also to design the micro channels heat exchanger. Computational Fluid Dynamics (CFD) is a computer-based numerical tool used to study the fluid flow, heat transfer behaviour and also its associated phenomena such as chemical reaction. A set of mathematical model equations are first developed following conservation laws. These equations are then solved using a computer programme in order to obtain the flow variables throughout the computational domain. Examples of CFD applications in the chemical process industry include drying, combustion, separation, heat exchange, mass transfer, pipeline flow, reaction, mixing, multiphase systems and material processing. Validation of CFD models is often required to assess the accuracy of the computational model. This assessment can assist in the development of reliable CFD models. Validation is achieved by comparing CFD results with available experimental, theoretical, or analytical data. Validated models become established as reliable, while those which fail the validation test need to be modified and revalidated. Further model equations can be simulated by CFD method for designing the micro channels and also to do parameter sensitivity analysis.

1.4 OBJECTIVES OF THE PRESENT WORK

As is evident from the diversity of application areas, the study of flow and heat transfer in microchannels is very important for the technology of today and the near future, as developments are following the trend of miniaturization in all fields. Literature shows that the microchannels and microchannels heat sinks were studied extensively, but there is limited research related to the performance study of microchannel heat exchangers using CFD models. Following from the experimental investigation of Lee and Mudawar (2007), this work studies the CFD simulation of micro channel flow and conjugates heat transfer, which couples fluid convection in a rectangular micro channel and heat conduction in the solids.

The present work is undertaken to study the following aspects of

- Computational Fluid Dynamics modeling and simulation of single phase micro channel heat exchanger to understand its hydrodynamic and thermal behaviour.
- Validation of the CFD models by comparing the present simulated results with the data available in the open literature.
- Parameter sensitivity study of micro channel

1.5 OUTLINE OF THE REPORT

Chapter 1 represents complete introduction of project work including definition of micro channel, application of it as heat exchanger, micro reactor etc., definition of nanofluid and its use as heat enhancer, role of CFD and its application.

Chapter 2 is devoted on the extensive literature survey on topic namely experimental and theoretical development of the micro channel, and nanofluid as heat enhancer. In the theoretical survey, more emphasis is given on computational fluid dynamics (CFD) analyses of it.

Chapter 3 represents modeling equation of single phase and two phase flow micro channel. The model equation includes the equation of continuity, momentum equation and energy equation.

Chapter 4 deals with simulation of single phase fluid flow in a circular micro channel. The thermal conductivity and other fluid properties are changed by the nanoparticle inclusion in fluid, and it is the combined effect of these property variations that dictates the overall of heat transfer enhancement in presence of nanofluid. This point is illustrated in this chapter by studying the thermal behaviour of the circular micro channel.

Chapter 5 represents simulation of single phase fluid flow in a rectangular micro channel embedded in a test module. Variations of pressure drop across micro channel with different Reynolds number are found here. The single phase wall heat transfer coefficient is also determined for different heat flux across the wall. The variation of wall temperature along micro channel for different flow rates of water and its nanofluids at different power input is also discussed in this chapter.

Chapter 6 deals with overall conclusion and future recommendations.

Chapter 2

LITERATURE REVIEW

Some experimental and theoretical work on micro channel heat exchanger has been done in the last decades. Both the industrial and academic people have taken interest in this area. The following is a review of the research that has been completed especially on microchannel heat exchangers. The literature survey is arranged according to similarity to the work done in this thesis. In this literature review emphasis is directed on:

- Experimental study of fluid flow and heat transfer in micro channels
- Numerical study of fluid flow and heat transfer in micro channels
- Nano fluid as heat enhancer

2.1 EXPERIMENTAL STUDY OF FLUID FLOW AND HEAT TRANSFER IN MICRO CHANNELS

With the development of micro fabrication technology, microfluidic systems have been increasingly used in different scientific disciplines such as biotechnology, physical and chemical sciences, electronic technologies, sensing technologies etc. Microchannels are one of the essential geometry for microfluidic systems; therefore, the importance of convective transport phenomena in microchannels and microchannel structures has increased dramatically. In recent years, a number of researchers have reported the heat transfer and pressure drop data for laminar and turbulent liquid or gas flow in microchannels. The concept of micro channel heat sink at first proposed by **Tuckermann and Pease (1981)**, they demonstrated that the micro channel heat sinks, consisting of micro rectangular flow passages, have a higher heat transfer coefficient in laminar flow regime than that in turbulent flow through conventionally-sized devices. They said that the heat transfer can be enhanced by reducing the channel height down to micro scale. This pioneering work initiated other studies, some confirmed findings reported by others. Many researchers compared their numerical or analytical studies with Tuckerman and Pease .

Wang and Peng (1995) had investigated experimentally the single-phase forced convective heat transfer characteristics of water/methanol flowing through micro-channels with rectangular cross section of five different combinations, maximum and minimum channel

size varying from (0.6 × 0.7 mm^2) to (0.2 × 0.7 mm^2). The results provide significant data and considerable insight into the behavior of the forced-flow convection in micro-channels

Peng and Peterson (1996) had also investigated experimentally the single-phase forced convective heat transfer micro channel structures with small rectangular channels having hydraulic diameters of 0.133–0.367 mm and distinct geometric configurations. The results indicate that geometric configuration had a significant effect on single-phase convective heat transfer and flow characteristics. The laminar heat transfer found to be dependent upon the aspect ratio i.e. the ratio of hydraulic diameter to the centre to centre distance of micro channels. The turbulent flow resistance was usually smaller than predicted by classical relationships [3].

Fedorov and Viskanta (2000) developed a three dimensional model to investigate the conjugate heat transfer in a micro channel heat sink with the same channel geometry used in the experimental work done by Kawano et al (1998). This investigation indicated that the average channel wall temperature along the flow direction was nearly uniform except in the region close to the channel inlet, where very large temperature gradients were observed. This allowed them to conclude that the thermo–properties are temperature dependent. The modifications of thermo-physical properties in the numerical process are very difficult as temperature and velocity are highly coupled.

Jiang et al. (2001) performed an experimental comparison of microchannel heat exchanger with microchannel and porous media. The effect of the dimensions on heat transfer was analyzed numerically. It was emphasized that the heat transfer performance of the microchannel heat exchanger using porous media is better than using of microchannels, but the pressure drop of the former is much larger.

Qu and Mudawar (2002) have performed experimental and numerical investigations of pressure drop and heat transfer characteristics of single-phase laminar flow in 231 μm by 713 μm channels. Deionized water was employed as the cooling liquid and two heat flux levels, 100 W/cm^2 and 200 W/cm^2, defined relative to the planform area of the heat sink, were tested. Good agreement was found between the measurements and numerical predictions, validating the use of conventional Navier–Stokes equations for micro channels. For the channel bottom wall, much higher heat flux and Nusselt number values are encountered near the channel inlet.

Qu and Mudawar (2004) conducted a three-dimensional fluid flow and heat transfer analysis for a rectangular micro channel heat sink using a numerical method similar to that

proposed by both Kawano et al. (1998) , and Fedorov and Viskanta. (2000) This model considered the hydrodynamic and thermal developing flow along the channel and found that the Reynolds number would influence the length of the developing flow region. It was also found that the highest temperature is typically encountered at the heated base surface of the heat sink immediately adjacent to the channel outlet and that the temperature rise along the flow direction in the solid and fluid regions can both be approximated as linear .

Mishan et al. (2007) has worked on heat transfer and fluid flow characteristic of a rectangular microchannel experimentally, having water as a working fluid. The experimental results of pressure drop and heat transfer confirm that including the entrance effects, the conventional theory is applicable for water flow through microchannels. They have developed new method for measurement of fluid temperature distribution and it gives the fluid temperature distribution inside the channel.

Lee and Mudawar (2007) have done experimental work to explore the micro-channel cooling benefits of water-based nanofluids containing small concentrations of Al2O3. It was observed that the presence of nanoparticles enhances the single-phase heat transfer coefficient, especially for laminar flow. Higher heat transfer coefficients were achieved mostly in the entrance region of micro-channels. However, the enhancement was weaker in the fully developed region. Higher concentrations also produced greater sensitivity to heat flux. A large axial temperature rise was associated with the decreased specific heat for the nanofluid compared to the base fluid. For two-phase cooling, nanoparticles caused catastrophic failure by depositing into large clusters near the channel exit due to localized evaporation once boiling commenced.

Chein and Chuang (2007) have addressed microchannel heat sink (MCHS) performance using nanofluids as coolants. They have carried out a simple theoretical analysis that indicated more energy and lower microchannel wall temperature could be obtained under the assumption that heat transfer could be enhanced by the presence of nanoparticles. The theoretical results were verified by their own experimental results. It was observed that nanofluid-cooled MCHS could absorb more energy than water-cooled MCHS when the flow rate was low. For high flow rates, the heat transfer was dominated by the volume flow rate and nanoparticles did not contribute to the extra heat absorption.

Jung et al (2009) have studied experimentally the heat transfer coefficients and friction factor of Al2O3 with diameter of 170 nm in a rectangular micro channel. Appreciable enhancement of the convective heat transfer coefficient of the nanofluids with the base fluid

of water and a mixture of water and ethylene glycol at the volume fraction of 1.8 volume percent was obtained without major friction loss. It has been found that the Nusselt number increases with increasing the Reynolds number in laminar flow regime, which is contradictory to the result from the conventional analysis.

Ergu et al. (2009) had described the pressure drop and local mass transfer in a rectangular microchannel having a width of 3.70 mm, height of 0.107 mm and length of 35 mm. The pressure drop measurements were carried out with distilled water as working fluid at Reynolds numbers in the range of 100–845, while mass transfer measurements with a chemical solution at Reynolds numbers in the range of 18–552 by using the electrochemical limiting diffusion current technique (ELDCT). Experimental friction factors were found slightly higher than those calculated by theoretical correlation. The Sherwood number correlation was also obtained.

2.2 NUMERICAL STUDY OF FLUID FLOW AND HEAT TRANSFER IN MICRO CHANNELS

To design an effective microchannel heat sink, fundamental understanding of the characteristics of the heat transfer and fluid flow in microchannel are necessary. At the early stages the designs and relations of macroscale fluid flow and heat transfer were employed. The strength of numerical simulations is the possibility to investigate small details that are impossible to observe in experiments.

Liu and Garimella (2004) have studied numerically on fluid flow and heat transfer in micro channels and confirmed that the behavior of micro channels is quite similar to that of conventional channels. And their analysis showed that conventional correlations offer reliable predictions for the laminar flow characteristics in rectangular micro channels over a hydraulic diameter in the range of 244–974 μm.

A numerical study has been performed by **Li et al. (2004)** on the same micro channel heat sink developed by Qu and Mudawar (2000) in order to explore the impact of geometric and thermo physical parameters of the fluid on its flow behavior and heat transfer characteristics. The authors have acknowledged the scattered results obtained in past micro fluidics studies from various authors, and point out the strong differences of empirical correlations derived therein. These differences are especially true when comparing works that studied single micro channels to those who considered entire micro channel heat sinks. Thus, the authors

noted a need to develop numerical models that provide more insight into the fundamental physics of the transport processes involved.

Roy et al. (2004) has studied a steady, laminar flow and heat transfer of a nanofluid flowing inside a radial channel between two coaxial and parallel discs. The non-dimensional governing equations of mass, momentum and energy were solved by computational fluid dynamics method. Results presented in this paper are for a water/aluminium oxide particle nanofluid (H2O–γ Al2O3). Results have shown that the inclusion of nanoparticles in a traditional coolant can provide considerable improvement in heat transfer rates, even at small particle volume fractions. Increases in the resulting wall shear stresses were also noticed.

Gamrat et al. (2005) analyzed three-dimensional flow and associated heat transfer in a rectangular micro channel heat sink numerically. The numerical simulation considered the coupling between convection in micro channels and conduction in the walls and in the complete solid material. The results of numerical simulations using the continuum model (conventional mass, Navier–Stokes and energy equations) were in good agreement with published data on flow and heat transfer in three dimensional channels.

Hetsroni et al. **(2005)** has verified the capacity of conventional theory to predict the hydrodynamic characteristics of laminar Newtonian incompressible flows in micro channels in the range of hydraulic diameter from $D_h = 15$ to $D_h = 4010\ \mu m$. They have compared their results with the data available in open literature. The theoretical models were subdivided in two groups depending on the degree of correctness of the assumptions. The first group includes the simplest one-dimensional models assuming uniform heat flux, constant heat transfer coefficient, etc. The comparison of these models with experiment shows significant discrepancy between the measurements and the theoretical predictions The second group is based on numerical solution of full Navier–Stokes and energy equations, which account the real geometry of the micro-channel, presence of axial conduction in the fluid and wall, energy dissipation, non adiabatic thermal boundary condition at the inlet and outlet of the heat sink, dependence of physical properties of fluid on temperature, etc. These models demonstrate a fairly well correlation with the available experimental data.

Khanafer et al. (2003) has investigated heat transfer enhancement in a two-dimensional rectangular enclosure utilizing nanofluids. The material used is water/cupper. The developed transport equations were solved numerically using the finite-volume approach along with the alternating direct implicit procedure. The effect of suspended ultrafine metallic nanoparticles on the fluid flow and heat transfer processes within the enclosure was analyzed. The heat

transfer correlation of the average Nusselt number for various Grashof numbers and volume fractions was also presented.

Jou and Tzeng (2006) have used the Khanafer's model to analyze heat transfer performance of nanofluids inside an enclosure taking into account the solid particle dispersion. Transport equations were modeled by a stream function-vorticity formulation and solved numerically by finite difference approach. Based upon the numerical predictions, the effects of Rayleigh number (Ra) and aspect ratio on the flow pattern and energy transport within the thermal boundary layer were presented. It was observed that increasing the buoyancy parameter and volume fraction of nanofluids cause an increase in the average heat transfer coefficient. Finally, the empirical equation was built between average Nusselt number and volume fraction.

Li and Peterson (2007) have worked on identification of the possible mechanisms that contribute to the enhanced effective thermal conductivity of nanoparticle suspensions (nanofluids). The mixing effect of the base fluid in the immediate vicinity of the nanoparticles caused by the Brownian motion was analyzed, modeled and compared with existing experimental data available in the literature. The simulation results using CFX 5.5.1 software indicate that this mixing effect can have a significant influence on the effective thermal conductivity of nanofluids. They have found pressure, velocity and temperature profile around the nanoparticles.

A developing laminar forced convection flow of a water–Al2O3 nanofluid in a circular tube, submitted to a constant and uniform heat flux at the wall, has been numerically investigated by Bianco et al. (2009). CFD method was used to simulate the model equations. A single- and two-phase model (discrete particles model) was employed with either constant or temperature dependent properties. The maximum difference in the average heat transfer coefficient between single- and two-phase models results was found about 11%. Convective heat transfer coefficient for nanofluids was found as greater than that of the base liquid. Heat transfer enhancement increases with the particle volume concentration, but it is accompanied by increasing wall shear stress values. Higher heat transfer coefficients and lower shear stresses were detected in the case of temperature dependents models. The heat transfer always improves, as Reynolds number increases.

Xu et al. (2008) considered liquid flow in 30–344 μm (hydraulic diameter) channels at Reynolds numbers varies from 20 to 4000. Their results showed that characteristics of flow in micro channels agree well with conventional behavior predicted by Navier–Stokes equations.

They have suggested that deviations from classical behavior reported in earlier studies may have resulted from errors in the measurement of micro channel dimensions, rather than any micro scale effects .

Sabbah et al. (2008) observed that the prediction of heat transfer in micro-channels becomes difficult with increase in complicacy of the geometry of the micro-channels, requiring three-dimensional analysis of heat transfer in both solid and liquid phases. Computational Fluid Dynamics (CFD) models were implemented in order to study and optimize the thermal and hydraulic performance of micro channel heat sinks. Despite the small width of the channels, the conventional Navier Stokes and energy conservation equations still apply to the MCHE flow due to the continuum of the working fluid where the channel width is many times larger than the mean free path of liquid molecules (water). The microchannel is characterized by the laminar flow in it, due to the small hydraulic diameter of the channel which results in low Reynolds numbers

Oztop et al. (2008) has carried out CFD study on heat transfer and fluid flow due to buoyancy forces in a partially heated rectangular enclosure filled with nanofluids. The temperature of the right vertical wall kept lower than that right wall while other two walls are insulated. The finite volume technique is used to solve the governing equations. Different types of nanoparticles were tested. An increase in mean Nusselt number was found with the volume fraction of nanoparticles for the whole range of Rayleigh number. Heat transfer also increases with increasing of height of heater. It was also found that the heater location affects the flow and temperature fields when using nanofluids.

Mokrani et al. (2009) developed a reliable experimental device and adequate methodology to characterize the flow and convective heat transfer in flat micro channels. The study was concerned with measurement of pressure drop and heat transfer by a Newtonian fluid flow inside a flat micro channel of rectangular cross-section whose aspect ratio is sufficiently high that the flow can be considered two dimensional They considered the hydraulic diameter as twice of the channel height. The mathematical model used to describe the convective heat transfer between the walls and the fluid takes into account the whole field (solid wall and fluid layer) and the coupling between the conduction and the convection modes. Finally they concluded that the conventional laws and correlations describing the flow and convective heat transfer in ducts of large dimension are directly applicable to the micro channels of heights between 500 and 50 microns

Muthtamilselvan et al. (2009) has conducted a numerical study to investigate the transport mechanism of mixed convection in a lid-driven enclosure filled with nanofluids. The two vertical walls of the enclosure were kept insulated while the horizontal walls were at constant temperatures with the top surface moving at a constant speed. The model equations were discretized by finite volume technique with a staggered grid arrangement. The SIMPLE algorithm is used for handling the pressure velocity coupling. Numerical solutions are obtained for a wide range of parameters and copper-water nanofluid was used with Pr = 6.2. The streamlines, isotherm plots and the variation of the average Nusselt number at the hot wall have been presented and discussed. The variation of the average Nusselt number was observed linear with solid volume fraction.

In one of the recent studies by **Al-Nmir et al. (2009)**, an investigation of the hydrodynamic and thermal behavior of the flow in parallel plate micro heat exchanger was performed numerically, by adopting a combination of both the continuum approach and the possibility of slip at the boundaries. In their work, both viscous dissipation and internal heat generation were neglected. Fluent analysis was made based on solving continuum and slip boundary condition equations. Effects of different parameters; such as, Knudsen number (Kn), heat capacity ratio (Cr), effectiveness (ε), and number of transfer units (NTU) were examined. The study showed that both the velocity slip and the temperature jump at the walls increase with increasing Kn. The increase of the slip conditions reduce the frictional resistance of the wall against the flow, and under the same pressure gradient, pumping force leads to that the fluid flows much more in the heat exchanger.

Very recently, **Mathew and Hegab (2009)** theoretically analyzed the thermal performance of parallel flow micro heat exchanger subjected to constant external heat transfer. The model equations predicts temperature distributions as well as effectiveness of the heat exchanger. Moreover, the model can be used when the individual fluids are subjected to either equal or unequal amounts of external heat transfer.

One of the comprehensive studies in counter flow micro channel heat exchanger area was done by Hasan et al. 2009. In this work, numerical simulations were made to study the effect of the size and shape of channels; such as circular, square, rectangular, iso-triangular, and trapezoidal, in counter flow exchanger. The results show that for the same volume of heat exchanger, increasing the number of channels leads to an increase in both effectiveness and pressure drop. Also circular channels give the best overall performance (thermal and hydraulic) among various channel shapes.

Kang and Tseng (2007) theoretically modeled thermal and fluidic characteristics of a cross-flow micro heat exchanger assuming that flows in rectangular channels, where fin height and width are 32 μm and 200 μm respectively, are incompressible, steady, and laminar. The simulated results were validated with the experimental data. The effects of change of material from cupper to silicon and dimensions on its performance were investigated. The study shows that under the same effectiveness value, a small rise in the temperatures of working fluids results in an increase of the heat transfer rate, but a decrease in pressure drop occurs.

Foli et al. (2006) introduced multi-objective genetic algorithms for determining the optimal geometric parameters of the microchannels heat exchanger to maximize the heat transfer rate under specified design constraints. CFD analysis with an analytical method of calculating the optimal geometric parameters was also performed. This paper is important and a good work, because there is limited published literature on attempts at designing the exchanger for optimal performance.

Tsuzuki et al. (2009) proposed a new flow configuration, named S-shaped fin configuration to reduce the micro channel heat exchanger pressure drop. A numerical study using a 3D-CFD code, FLUENT, was performed to find Nusselt number correlations for the exchanger. The copper heat exchanger, whose dimensions are 1240 x 68 x 4.75 mm3, comprises cold water channels and hot CO2 channels. For both hot and cold sides, simulations were done to attain accurate empirical correlations for different temperatures.

Rebrov et al. (2011) has reviewed the experimental and numerical results on fluid flow distribution, heat transfer and combination thereof, available in the open literature. They have found that the experiments with single channels are in good agreement with predictions using the published correlations. The accuracy of multichannel experiments is lower due to flow maldistribution. Special attention was devoted to theoretical and experimental studies on the effect of a flow maldistribution on the thermal micro reactors. The review consists of two parts. In the first, the main methods to control flow distribution were reviewed. Several different designs of inlet/outlet chambers were presented together with corresponding models used for optimization of flow distribution. In the second part, recent achievements in understanding of heat transfer in micro channels are presented

Bachok et al (2011) has studied numerically a steady flow of an incompressible viscous fluid due to a rotating disk in a nanofluid. The transformed boundary layer equations have been solved numerically by a finite difference scheme, namely the Keller-box method. Numerical results for the flow and heat transfer characteristics were obtained for various values of the

nanoparticle volume fraction and suction/injection parameter. Two models for the effective thermal conductivity of the nanofluid, namely the Maxwell–Garnett model and the Patel model, were considered. It was found that for the Patel model, the heat transfer rate at the surface increases for both suction and injection, where as different behaviours were observed for the Maxwell–Garnett model.

Allen (2007) had investigated fluid flow and heat transfer in microchannels experimentally and numerically. Fluid flow and heat transfer experiments were conducted on a copper micro channel heat exchanger with constant surface temperature. The experimentally obtained friction factor were found fairly well agreement with theoretical correlations and moreover the experimental Nusselt number results agreed with theory very well in the transition/turbulent regime, but the results show a higher Nusselt number in the laminar regime than predicted by theoretical correlations. Philips created a CFD model to simulate the fluid in the inlet plenum and the microchannels. The results from these simulations showed good agreement with the experimental data in the transition/turbulent regime as well as with theoretical correlations for laminar and turbulent flow.

2.3 NANOFLUIDS AS HEAT ENHANCER

A nanofluid is a suspension of ultrafine particles in a conventional base fluid which tremendously enhances the heat transfer characteristics of the original fluid [**Somchai et al. 2007]**. Furthermore, nanofluids are expected to be ideally suited in practical applications as their use incurs little or no penalty in pressure drop because the nanoparticles are ultrafine, therefore, appearing to behave more like a single-phase fluid than a solid–liquid mixture. The nanoparticles were used to produce nanofluids in the reviewed literature are: aluminum oxide (Al2O3), copper (Cu), copper oxide (CuO), gold (Au), silver (Ag), silica nanoparticles and carbon nanotube [**Trisaksria and Somchai 2007**]. The base fluids used were water, oil, acetone, decene and ethylene glycol. Nanoparticles can be produced from several processes such as gas condensation, mechanical attrition or chemical precipitation techniques [**Le et al. 1999**]. The main reasons for the heat transfer enhancement of the nanofluids may roughly be listed as follows: the suspended nanoparticles increase the thermal conductivity of the fluids, and the chaotic movement of ultrafine particles increases fluctuation and turbulence of the fluids which accelerates the energy exchange process .

Many experimental studies have shown that nanofluids have much higher thermal conductivities than those predicted by macroscopic models (Masuda et al., 1993; Choi, 1995; Eastman et al., 1996; Eastman et al., 2001; Lee et al., 1999; Xuan and Li, 2000; Xie et al., 2002; Wang et al., 2003; Wen and Ding, 2004a; Hong et al., 2005). Choi et al. (1995) at Argonne National Laboratory proposed the use of nanoparticles to enhance the thermal conductivity of liquids, and coined the term 'nanofluids' for the resulting mixtures They have prepared it by suspending colloidal materials such as alumina, gold, silver, copper, copper oxide, etc., in liquids such as water, ethylene glycol, oil, radiator fluids, etc. The suspended nanoparticles can change the properties of the base fluid, leading to great potential for heat transfer enhancement. Later studies experimentally demonstrated this enhancement effect .

Lee et al. (1999) have used 50 nm or smaller Al_2O_3 and CuO particles to enhance the thermal conductivity of their nanofluids. They attributed the enhancement of heat transfer to the increased thermal dispersion resulting from the chaotic movements of nanoparticles, which accelerates the exchange of energy. They have showed the percentage enhancement in thermal conductivity was not only function of concentration and conductivities of the particle material and liquid, but particle size and shape as well [21].

Wang et al. (1999) have measured the effective thermal conductivity of nanofluids by a steady-state parallel-plate technique. The base fluids (water, ethylene glycol, vacuum pump oil and engine oil) contained suspended Al_2O_3 and CuO nanoparticles of 28 and 23 nm of average diameters, respectively. Experimental results demonstrated that the thermal conductivities of all nanofluids were higher than those of their base fluids. Also, comparison with various data indicated that the thermal conductivity of nanofluids increases with decreasing particles size.

Results demonstrated 12% improvement of the effective thermal conductivity at 3 vol% of nanoparticles

Mujumdar et al. (2007) have summarized recent research on fluid flow and heat transfer characteristics of nanofluids in forced and free convection flows and identified opportunities for future research. Convective heat transfer can be enhanced passively by changing flow geometry, boundary conditions, or by enhancing thermal conductivity of the fluid. Various techniques have been proposed to enhance the heat transfer performance of fluids. Alumina (Al_2O_3) and copper oxide are the most common and inexpensive nanoparticles used by many researchers in their experimental investigations. All the experimental results had demonstrated the enhancement of the thermal conductivity by addition of nanoparticles [23].

Das et al (2009) had numerically analyzed turbulent flow and heat transfer of three different nanofluids (CuO, Al_2O_3 and SiO_2) in an ethylene glycol and water mixture flowing through a circular tube under constant heat flux condition. They have developed new viscosity correlations for nanofluids as a function of volume concentration and temperature. Computed results are validated with existing well established correlations. It was found that nanofluids containing smaller diameter nanoparticles have higher viscosity and Nusselt number. Heat transfer coefficient of nanofluids increases with increase in the volume concentration of nanofluids and Reynolds number. Pressure loss was observed to increase with increase in the volume concentration of the nanofluids.

There are many inconsistent reports on nanofluids behaviour under other heat transfer conditions. For forced convective heat transfer, Pak and Cho (1999) found that the Nusselt number of Al2O3/water and TiO2/water nanofluids increased with increasing volume fraction of suspended nanoparticles and Reynolds number. However, the convective heat transfer coefficient for nanofluids with a volume fraction of 0.03 was found to be 12% lower than that of pure water. Similar observation has also been reported by Yang et al. (2005) for graphite nanofluids in laminar flow regime. The increase of experimental heat transfer coefficients was found to be lower than the enhancement of the effective thermal conductivity. Many other researchers, however, have reached opposite conclusions (i.e., Lee and Choi (1996); Xuan and Li, 2003; Wen and Ding, 2005). Xuan and Li (2003) studied Cu/water nanofluids heat transfer under turbulent flow conditions and showed substantial heat transfer enhancement. Wen and Ding (2004b) investigated heat transfer of Al2O3/H2O nanofluids under laminar flow conditions and showed that presence of nanoparticles did enhance the convective heat transfer. The enhancement was shown to be much higher than the increase of the effective thermal conductivity, especially in the entrance region. Controversial experimental results have also been observed for nanofluids heat transfer under pool boiling conditions. Das et al. (2003) investigated nucleate pool boiling heat transfer of Al2O3/H2O nanofluids using cylindrical cartridge heaters. The presence of nanoparticles was found to deteriorate boiling performance and the degradation was found to increase with nanoparticle concentrations. Deteriorated pool boiling heat transfer was also observed by Li et al. (2003) for CuO/H2O nanofluids, which was thought to be the decreasing of active nucleation sites from nanoparticle sedimentation. To the other side, however, significant pool boiling heat transfer enhancement was observed for Al2O3/H2O nanofluids (Tu et al., 2004) and for gold–water nanofluids (Witharana, 2003). For pool boiling at high heat fluxes,

remarkable increase in the critical heat flux was also reported (You et al., 2003; Vassallo et al., 2004). Taylor and Phelan (2009) have published a comprehensive review paper on pool boiling of nanofluids along with a few new set of data. They have shown that the surface condition is responsible for varying results of pool boiling. The study also explored that the boiling nanofluids under sub-cooled conditions led to a degradation of heat transfer, relative to saturated pool boiling of pure water. Daungthongsuk and Wongwises (2007) have discussed the method of calculation of heat transfer coefficient in case of micro channel heat exchanger using nanofluids. The heat transfer coefficient of the nanofluids is calculated from the following equations

$$Nu_{nf} = \frac{h_{nf} D}{k_{nf}} \tag{1}$$

$$h_{nf} = \frac{q}{T_w - T_f} \tag{2}$$

Where subscript nf indicates nanofluids, and T_W and T_f are the average wall and fluid temperatures. They also have developed the correlations for Nusselt number, Nu as a function of Reynolds number, Re, Peclet number, Pe and Prandtl number, Pr, and the correlatiuons are as follows:

For laminar flow $Nu_{nf} = 0.4328\left(1.0 + 11.285\phi^{0.754} Pe_d^{0.218}\right)\mathrm{Re}_{nf}^{0.333}\ \mathrm{Pr}_{nf}^{0.4}$ (3)

For turbulent flow $Nu_{nf} = 0.0059\left(1.0 + 7.6286\phi^{0.6886} Pe_d^{0.001}\right)\mathrm{Re}_{nf}^{0.9238}\ \mathrm{Pr}_{nf}^{0.4}$ (4)

Ding et al., 2007 has studied on forced convective heat transport characteristics experimentally using aqueous and ethylene glycol-based spherical titania nanofluids, and aqueous-based titanate nanotubes, carbon nanotubes and nano-diamond nanofluids. All the formulated nanofluids show a higher effective thermal conductivity than that predicted by the conventional theories. Except for the ethylene glycol-based titania nanofluids, all other nanofluids are found to be non-Newtonian. For aqueous-based titania and carbon and titanate nanotube nanofluids, the convective heat transfer coefficient enhancement exceeds, by a large margin, the extent of the thermal conduction enhancement. However, deterioration of the convective heat transfer is observed for ethylene glycol-based titania nanofluids at low Reynolds numbers and aqueous-based nano-diamond nanofluids. Possible mechanisms for the observed controversy are discussed from both microscopic and macroscopic viewpoints.

Khandekar et al. 2008 has studied the overall thermal resistance of closed two-phase thermosyphon using pure water and various water based nanofluids (of Al2O3, CuO and

laponite clay) as working fluids. It was observed that all these nanofluids show inferior thermal performance than pure water. Furthermore, it was found that the wettability of all nanofluids on copper substrate, having the same average roughness as that of the thermosyphon container pipe, is better than that of pure water. A scaling analysis was presented which shows that the increase in wettability and entrapment of nanoparticles in the grooves of the surface roughness cause decrease in evaporator side Peclet number that finally leads to poor thermal performance.

Gherasim et al. (2009) has presented an experimental investigation of the use of an Alumina/water nanofluid inside a radial flow cooling system. Results show that heat transfer is enhanced with the use of this type of nanofluid. Mean Nusselt number was found to increase with particle volume fraction, Reynolds number and a decrease in disk spacing.

CHAPTER 3

COMPUTATIONAL FLUID DYNAMICS MODEL EQUATIONS

In this study the both the single phase models and multiphase models are used for solving the respective category problems. This model will calculate one transport equation for the momentum and one for continuity for each phase, and then energy equations are solved to study the thermal behaviour of the system. The theory for this model is taken from the ANSYS Fluent 12.0.

3.1 SINGLE PHASE MODELING EQUATIONS

The single phase model equations include the equation of continuity, momentum equation and energy equation (ANSYS Fluent 12.0). The continuity and momentum equations are used to calculate velocity vector. The energy equation is used to calculate temperature distribution and wall heat transfer coefficient. The equation for conservation of mass, or continuity equation, can be written as follows:

3.1.1 Mass Conservation Equation

The equation for conservation of mass, or continuity equation, can be written as follows:

$$\frac{\partial \rho}{\partial t} + \nabla.(\rho \vec{\upsilon}) = S_m \tag{3.1}$$

Equation (3.1) is the general form of the mass conservation equation, and is valid for both incompressible compressible flows. The source S_m is the mass added to the continuous phase from the dispersed second phase (e.g., due to vaporization of liquid droplets) and any user-defined sources.

3.1.2 Momentum Conservation Equation

Conservation of momentum in an inertial (non-accelerating) reference frame is described by

$$\frac{\partial}{\partial t}(\rho \vec{\upsilon}) + \nabla.(\rho \vec{\upsilon} \vec{\upsilon}) = -\nabla p + \nabla.(\bar{\bar{\tau}}) + \rho \vec{g} + \vec{F} \tag{3.2}$$

Where p is the static pressure, $\bar{\bar{\tau}}$ is the stress tensor (described below), and $\rho\vec{g}$ and $\vec{F}$ are the gravitational body force and external body forces (e.g., that arise from interaction with the dispersed phase), respectively. $\vec{F}$ also contains other model-dependent source terms such as porous-media and user-defined sources.

The stress tensor $\bar{\bar{\tau}}$ is given by

$$\bar{\bar{\tau}} = \mu\left[(\nabla\vec{\upsilon} + \nabla\vec{\upsilon}^{\mathrm{T}}) - \frac{2}{3}\nabla.\vec{\upsilon}I\right] \tag{3.3}$$

Where μ is the molecular viscosity, I is the unit tensor, and the second term on the right hand side is the effect of volume dilation.

3.1.3 Energy equation

ANSYS FLUENT solves the energy equation in the following form:

$$\frac{\partial}{\partial t}(\rho E) + \nabla.\left(\vec{\upsilon}\left(\rho E + p\right)\right) = \nabla.\left(\kappa_{eff}\nabla T - \sum_{j} h_j\overrightarrow{J_j} + \left(\bar{\bar{\tau}}_{eff}.\vec{\upsilon}\right)\right) + S_h \tag{3.4}$$

Where κ_{eff} is the effective conductivity ($\kappa + \kappa_t$, where κ_t is the turbulent thermal conductivity, defined according to the turbulence model being used), and $\vec{J}_j$ is the diffusion flux of species J. The first three terms on the right-hand side of Equation represent energy transfer due to conduction, species diffusion, and viscous dissipation, respectively. S_h includes the heat of chemical reaction, and any other volumetric heat sources.

In Eq. (3.4)

$$E = h - \frac{p}{\rho} + \frac{\upsilon^2}{2} \tag{3.5}$$

Where sensible enthalpy h is defined for ideal gases as

$$h = \sum_{j} Y_j h_j \tag{3.6}$$

Y_j is the mass fraction of species j.

$$h_j = \int_{T_{ref}}^{T} c_{p,j}\, dT \tag{3.7}$$

T_{ref} is used as 298.15 K.

3.2 TWO PHASE MODELING EQUATIONS

A large number of flows encountered in nature and technology are a mixture of phases. Physical phases of matter are gas, liquid, and solid, but the concept of phase in a multiphase flow system is applied in a broader sense. In multiphase flow, a phase can be defined as an identifiable class of material that has a particular inertial response to and interaction with the flow and the potential field in which it is immersed. Currently there are two approaches for the numerical calculation of multiphase flows: the Euler-Lagrange approach and the Euler-Euler approach.

Euler-Lagrange approach

The Lagrangian discrete phase model in ANSYS FLUENT follows the Euler-Lagrange approach. The fluid phase is treated as a continuum by solving the Navier-Stokes equations, while the dispersed phase is solved by tracking a large number of particles, bubbles, or droplets through the calculated flow field. The dispersed phase can exchange momentum, mass, and energy with the fluid phase.

Euler-Euler approach

In the Euler-Euler approach, the different phases are treated mathematically as interpenetrating continua. Since the volume of a phase cannot be occupied by the other phases, the concept of phase volume fraction is introduced. These volume fractions are assumed to be continuous functions of space and time and their sum is equal to one.

In ANSYS FLUENT, three different Euler-Euler multiphase models are available: the volume of fluid (VOF) model, the mixture model, and the Eulerian model.

The VOF model is a surface-tracking technique applied to a fixed Eulerian mesh. It is used for two or more immiscible fluids where the position of the interface between the fluids is of interest. In the VOF model, a single set of momentum equations is shared by the fluids, and the volume fraction of each of the fluids in each computational cell is tracked throughout the domain.

The mixture model is designed for two or more phases (fluid or particulate). As in the Eulerian model, the phases are treated as interpenetrating continua. The mixture model solves for the mixture momentum equation and prescribes relative velocities to describe the dispersed phases.

3.2.1 Volume of Fluid (VOF) Model

The VOF formulation in ANSYS FLUENT is generally used to compute a time-dependent solution, but for problems in which concerned are only with a steady-state solution; it is possible to perform a steady-state calculation.

3.2.1.1 Volume Fraction Equation

The tracking of the interface(s) between the phases is accomplished by the solution of a continuity equation for the volume fraction of one (or more) of the phases. For the q^{th} (fluid's volume fraction) phase, this equation has the following form:

$$\frac{1}{\rho_q}\left[\frac{\partial}{\partial t}\left(\alpha_q \rho_q\right)+\nabla.\left(\alpha_q \rho_q \vec{\upsilon}_q\right)=S_{\alpha_q}+\sum_{p=1}^{n}\left(\dot{m}_{pq}-\dot{m}_{qp}\right)\right] \tag{3.8}$$

Where $\dot{m}_{qp}$ is the mass transfer from phase q to phase p and $\dot{m}_{pq}$ is the mass transfer from phase p to phase q. By default, the source term on the right-hand side of Eq. 3.8, S_{α_q} is zero, but we can specify a constant or user-defined mass source for each phase. The volume fraction equation will not be solved for the primary phase; the primary-phase volume fraction will be computed based on the following constraint:

$$\sum_{p=1}^{n}\alpha_q = 1 \tag{3.9}$$

3.2.1.2 Material Properties

The properties appearing in the transport equations are determined by the presence of the component phases in each control volume. In a two-phase system, for example, if the phases are represented by the subscripts 1 and 2, and the mixture density in each cell is given by

$$\rho = \alpha_2 \rho_2 + \left(1-\alpha_2\right)\rho_1 \tag{3.10}$$

In general, for n phase system, the volume-fraction-averaged density takes on the following form:

$$\rho = \sum \alpha_q \rho_q \tag{3.11}$$

All other properties (e.g., viscosity) are also computed in this manner.

3.2.1.3 Momentum Equation

A single momentum equation is solved throughout the domain, and the resulting velocity field is shared among the phases. The momentum equation, shown below, is dependent on the volume fractions of all phases through the properties ρ and μ.

$$\frac{\partial}{\partial t}(\rho\vec{v}) + \nabla.(\rho\vec{v}\vec{v}) = -\nabla p + \nabla.\left[\mu\left(\nabla\vec{v} + \nabla\vec{v}^T\right)\right] + \rho\vec{g} + \vec{F} \tag{3.12}$$

One limitation of the shared-fields approximation is that in cases where large velocity differences exist between the phases, the accuracy of the velocities computed near the interface can be adversely affected.

3.2.1.4 Energy Equation

The energy equation, also shared among the phases, is shown below

$$\frac{\partial}{\partial t}(\rho E) + \nabla.\left(\vec{v}\left(\rho E + p\right)\right) = \nabla.\left(k_{eff}\nabla T\right) + S_h \tag{3.13}$$

The VOF model treats energy, E, and temperature, T, as mass-averaged variables:

$$E = \frac{\sum_{q=1}^{n} \alpha_q \rho_q E_q}{\sum_{q=1}^{n} \alpha_q \rho_q} \tag{3.14}$$

Where E_q for each phase is based on the specific heat of that phase and the shared temperature.

The properties ρ and k_{eff} (effective thermal conductivity) are shared by the phases. The source term, S_h, contains contributions from radiation, as well as any other volumetric heat sources.

3.2.2 Mixture Model

The mixture model is a simplified multiphase model that can be used in different ways. The mixture model allows us to select granular phases and calculates all properties of the granular phases. This is applicable for liquid-solid flows.

3.2.2.1 Continuity Equation

$$\frac{\partial}{\partial t}(\rho_m) + \nabla.(\rho_m \vec{\upsilon}_m) = 0 \tag{3.15}$$

Where $\vec{\upsilon}_m$ is the mass-averaged velocity:

$$\vec{\upsilon}_m = \frac{\sum_{k=1}^{n} \alpha_k \rho_k \vec{\upsilon}_k}{\rho_m} \tag{3.16}$$

and ρ_m is the mixture density:

$$\rho_m = \sum_{k=1}^{n} \alpha_k \rho_k \tag{3.17}$$

α_k is the volume fraction of phase k

3.2.2.2 Momentum Equation

The momentum equation for the mixture can be obtained by summing the individual momentum equations for all phases. It can be expressed as:

$$\frac{\partial}{\partial t}(\rho_m \vec{\upsilon}_m) + \nabla.(\rho_m \vec{\upsilon}_m \vec{\upsilon}_m) = -\nabla p + \nabla.\left[\mu_m\left(\nabla \vec{\upsilon}_m + \nabla \vec{\upsilon}_m{}^T\right)\right] + \rho_m \vec{g} + \vec{F} + \nabla.\left(\sum_{k=1}^{n} \alpha_k \rho_k \vec{\upsilon}_{dr,k} \vec{\upsilon}_{dr,k}\right) \tag{3.18}$$

Where n is the number of phases, $\vec{F}$ is a body force, and μ_m is the viscosity of the mixture and defined as

$$\mu_m = \sum \alpha_k \mu_k \tag{3.19}$$

$\vec{\upsilon}_{dr,k}$ is the drift velocity for secondary phase k :

$$\vec{\upsilon}_{dr,k} = \vec{\upsilon}_k - \vec{\upsilon}_m \tag{3.20}$$

3.2.2.3 Energy Equation

The energy equation for the mixture takes the following form:

$$\frac{\partial}{\partial t}\sum_{k=1}^{n}\left(\alpha_k \rho_k E_k\right) + \nabla.\sum_{k=1}^{n}\left(\alpha_k \vec{\upsilon}_k \left(\rho_k E_k + p\right)\right) = \nabla.\left(k_{eff}\nabla T\right) + S_E \tag{3.21}$$

Where k_{eff} is the effective conductivity $\left(\sum \alpha_k (k_k + k_t)\right)$, where k_t is the turbulent thermal conductivity, defined according to the turbulence model being used). The first term on the right-hand side of Eq. 3.21 represents energy transfer due to conduction. S_E include any other volumetric heat sources. In Eq. 3.21

$$E_k = h_k - \frac{p}{\rho_k} + \frac{v_k^2}{2} \tag{3.22}$$

for a compressible phase, and $E_k = h_k$ for an incompressible phase, where h_k is the sensible enthalpy for phase k .

3.2.2.4 Volume Fraction Equation for the Secondary Phases

From the continuity equation for secondary phase p , the volume fraction equation for secondary phase p can be obtained:

$$\frac{\partial}{\partial t}\left(\alpha_p \rho_p\right) + \nabla.\left(\alpha_p \rho_p \vec{\upsilon}_m\right) = -\nabla.\left(\alpha_p \rho_p \vec{\upsilon}_{dr,p}\right) + \sum_{q=1}^{n}\left(\dot{m}_{qp} - \dot{m}_{pq}\right) \tag{3.23}$$

Chapter 4

SIMULATION OF SINGLE PHASE FLUID FLOW IN A CIRCULAR MICRO CHANNEL

It is well known that nanoparticles have very high thermal conductivity compared to commonly used coolant. Thus, the thermal conductivity and other fluid properties are changed by mixing the particle in fluid. The changed properties of the nanofluids determine the heat transfer performance of the microchannel heat exchanger with nanofluids. This point is illustrated in this chapter by doing the computational fluid dynamics (CFD) analysis of the hydrodynamics and thermal behaviour of the single phase flow through a circular micro channel (Lee and Mudawar, 2007).

4.1 SPECIFICATION OF PROBLEM

Consider a steady state fluid flowing through a circular micro channel of constant cross-section as shown in Fig. 4.1 (Lee and Mudawar, 2007). The diameter and length of circular micro channel are 0.0005m and 0.1m respectively. The inlet velocity is *u (*m/s), which is constant over the inlet cross-section. The fluid exhausts into the ambient atmosphere which is at a pressure of 1 atm.

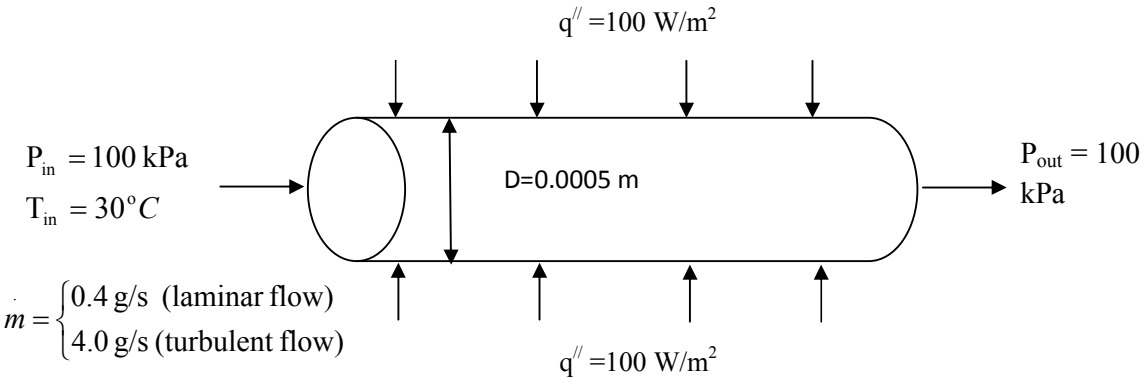

Figure 4.1: Fluid flow through a circular micro channel of constant cross-section

As fluid flows through in a pipe at both hydraulic and thermally fully developed condition, the Nusselt number is constant for laminar flow and it follows the Dittius-Boelter equation for turbulent flow.

$$Nu = 4.36 \qquad \text{for laminar flow} \tag{4.1}$$

$$\text{i.e. } \frac{hD}{k} = 4.36 \quad \Rightarrow \quad h \approx \kappa \tag{4.2}$$

And

$$Nu = 0.023\,\mathrm{Re}^{0.8}\,\mathrm{Pr}^{0.4} \qquad \text{for turbulent flow} \tag{4.3}$$

$$\text{i.e. } \frac{hD}{k} = 0.023\left(\frac{Dv\rho}{\mu}\right)^{0.8}\left(\frac{C_p\mu}{k}\right)^{0.4} \quad \Rightarrow h \approx \kappa^{0.6}\upsilon^{0.8}\mu^{-0.4} \tag{4.4}$$

From Eq. 4.2 and Eq. 4.4 it is clear that thermal conductivity has greater effect on heat transfer coefficient for laminar flow as compared to turbulent flow. This implies the enhancement effect due to the increased thermal conductivity of nanofluids is significantly weaker for turbulent flow than for laminar. The enhancement in turbulent flow is also dependent on flow rate in addition to viscosity and specific heat. Since $h \approx \kappa^{0.6}\mu^{-0.4}C_p^{0.4}$ and because increased nanoparticle concentration enhances viscosity and degrades specific heat, the enhancement effect of nanoparticles in turbulent flow is further reduced compared to thermal conductivity alone.

4.2 GEOMETRY IN ANSYS WORKBENCH

The Computational domain of circular micro channel is represented in two dimensional (2D) form by a rectangle and displayed in Fig. 4.2. The geometry consists of a wall, a centerline, and an inlet and outlet boundaries. The radius, R and the length, L of the pipe are specified in the figure.

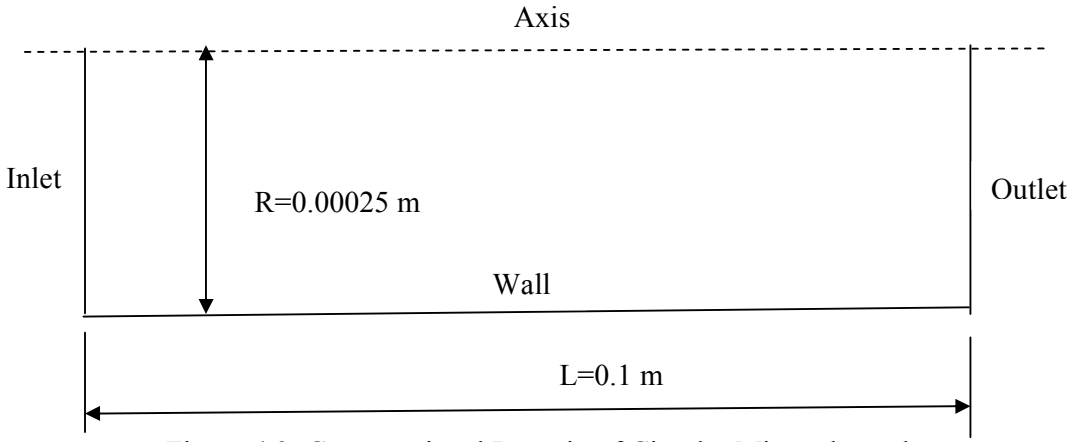

Figure 4.2: Computational Domain of Circular Micro channel

4.3 MESHING OF GEOMETRY

Structured meshing method done in ANSYS Workbench was used for meshing the geometry. 100×10 nodes were created. The 2D geometry of circular micro channel with structured mesh is shown in Fig. 3.

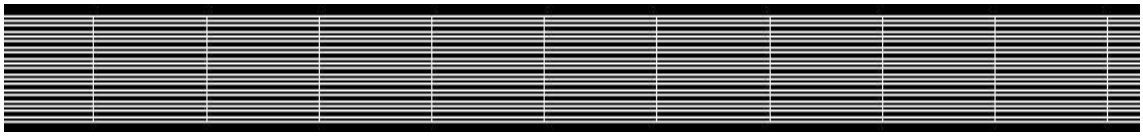

Figure 4.3: Two dimensional geometry of circular micro channel with structured mesh

4.4 PHYSICAL MODELS

Based on the Reynolds number, $\mathrm{Re} = Du\rho/\mu$, either viscous laminar model or standard $\kappa - \varepsilon$ model is used for laminar and turbulent flow respectively. The choice of the model is shown in Table 4.1. D is the diameter of the microchannel, ρ and μ are the density and viscosity of the fluid.

Table 4.1: Choice of model based on Reynolds number

Reynolds no. (Re)	Flow (Model)
< 2000	Laminar
> 2000	$\kappa - \varepsilon$ Model

4.5 MATERIAL PROPERTIES

Pure water is used as base working fluid and Alumina (Al_2O_3) is taken as nanoparticles. The density, heat capacity and thermal conductivity of alumina are 3,600 kg/m^3, 765 J/kgK and 36 W/mK respectively. The properties of nanofluids (nf) are given in Table 4.2 at 30^{o}C temperature and 100 kPa pressure.

Table 4.2 Water base fluid properties with different concentration of alumina nanoparticles (Lee and Mudawar, 2007)

	ϕ=0%	ϕ=1%	ϕ=2%	ϕ=3%	ϕ=4%	ϕ=5%
k_{nf} (W/mK)	0.603	0.620	0.638	0.656	0.675	0.693
ρ_{nf} (kg/m^3)	995.7	1021.7	1047.7	1073.8	1099.8	1125.9
μ_{nf} (kg/m s)	7.97X10^{-4}	8.17X10^{-4}	8.376X10^{-4}	8.576X10-^{4}	8.775X10^{-4}	8.974X10-^{4}
$C_{p,nf}$ (kJ/kg K)	4.183	4.149	4.115	4.081	4.046	4.012

4.6 GOVERNING EQUATIONS

For 2D axis symmetric geometries, the continuity equation is given by (ANSYS Fluent 12.0).

$$\frac{\partial \rho}{\partial t}+\frac{\partial}{\partial x}\left(\rho \upsilon_x\right)+\frac{\partial}{\partial r}\left(\rho \upsilon_r\right)+\frac{\rho \upsilon_r}{r}=0 \tag{4.5}$$

Where x represents axial coordinate in the direction of flow, r is the radial coordinate i.e. transverse direction, υ_x is the axial velocity, and υ_r is the radial velocity components. For 2D axis symmetric geometries, the axial and radial momentum conservation equations are given by (ANSYS Fluent 12.0)

$$\frac{\partial}{\partial t}(\rho \upsilon_x)+\frac{1}{r}\frac{\partial}{\partial x}\left(r\rho \upsilon_x \upsilon_x\right)+\frac{1}{r}\frac{\partial}{\partial r}\left(r\rho \upsilon_r \upsilon_x\right)=-\frac{\partial p}{\partial x}$$
$$+\frac{1}{r}\frac{\partial}{\partial x}\left[r\mu\left(2\frac{\partial \upsilon_x}{\partial x}-\frac{2}{3}\left(\nabla .\vec{\upsilon}\right)\right)\right]+\frac{1}{r}\frac{\partial}{\partial r}\left[r\mu\left(\frac{\partial \upsilon_x}{\partial r}+\frac{\partial \upsilon_r}{dv_x}\right)\right]+F_x \tag{4.6}$$

And

$$\frac{\partial}{\partial t}\left(\rho \upsilon_r\right)+\frac{1}{r}\frac{\partial}{\partial x}\left(r\upsilon_x \upsilon_r\right)+\frac{1}{r}\frac{\partial}{\partial r}\left(r\upsilon_r \upsilon_r\right)=-\frac{\partial p}{\partial r}+\frac{1}{r}\frac{\partial}{\partial x}\left[r\mu\left(\frac{\partial \upsilon_r}{\partial x}+\frac{\partial \upsilon_x}{\partial r}\right)\right]$$
$$+\frac{1}{r}\frac{\partial}{\partial r}\left[r\mu\left(2\frac{\partial \upsilon_r}{\partial r}-\frac{2}{3}\left(\nabla .\vec{\upsilon}\right)\right)\right]-2\mu\frac{\upsilon_r}{r^2}+\frac{2}{3}\frac{\mu}{r}\left(\nabla .\vec{\upsilon}\right)+\rho\frac{\upsilon_z^2}{r}+F_r \tag{4.7}$$

Where,

$$\nabla.\vec{\upsilon} = \frac{\partial \upsilon_x}{\partial x} + \frac{\partial \upsilon_r}{\partial r} + \frac{\upsilon_r}{r} \tag{4.8}$$

Since the microchannel with small radial thickness is horizontally placed, the external body force F is taken as zero.

Turbulent flows are characterized by fluctuating velocity fields. These fluctuations mix transported quantities such as momentum, energy, and species concentration, and cause the transported quantities to fluctuate as well. Since these fluctuations can be of small scale and high frequency, they are too computationally expensive to simulate directly in practical engineering calculations. Instead, the instantaneous (exact) governing equations can be time-averaged, ensemble-averaged, resulting in a modified set of equations that are computationally less expensive to solve. However, the modified equations contain additional unknown variables, and turbulence models are needed to determine these variables in terms of known quantities.

The standard $k-\varepsilon$ model (ANSYS Fluent 12.0) is used to model single phase turbulent flow in circular micro channel. The turbulence kinetic energy, k, and its rate of dissipation, ε, are obtained solving the following transport equations:

$$\frac{\partial}{\partial t}(\rho k) + \frac{\partial}{\partial x_i}(\rho k \upsilon_i) = \frac{\partial}{\partial x_j}\left[\left(\mu + \frac{\mu_t}{\sigma_k}\right)\frac{\partial k}{\partial x_j}\right] + G_k + G_b - \rho\varepsilon - Y_M + S_k \tag{4.9}$$

And

$$\frac{\partial}{\partial t}(\rho\varepsilon) + \frac{\partial}{\partial x_i}(\rho\varepsilon \upsilon_i) = \frac{\partial}{\partial x_j}\left[\left(\mu + \frac{\mu_t}{\sigma_\varepsilon}\right)\frac{\partial \varepsilon}{\partial x_j}\right] + C_{1\varepsilon}\frac{\varepsilon}{k}(G_k + C_{3\varepsilon}G_b) - C_{2\varepsilon}\rho\frac{\varepsilon^2}{k} + S_\varepsilon \tag{4.10}$$

In these equations, G_k represents the generation of turbulence kinetic energy due to the mean velocity gradients. G_b is the generation of turbulence kinetic energy due to buoyancy. Y_M represents the contribution of the fluctuating dilatation in compressible turbulence to the overall dissipation rate. $C_{1\varepsilon}$, $C_{2\varepsilon}$ and $C_{3\varepsilon}$ are constants. σ_k and σ_ε are the turbulent Prandtl numbers for k and ε, respectively. S_k and S_ε are user-defined source terms.

Modelling the Turbulent Viscosity

The turbulent (or eddy) viscosity μ_t is computed by combining k and ε as follows:

$$\mu_t = \rho C_\mu \frac{k^2}{\varepsilon} \tag{4.11}$$

Model Constants

The model constant $C_{1\varepsilon}.C_{2\varepsilon}$, $C_{3\varepsilon}$ σ_k and σ_ε have the following default values $C_{1\varepsilon} = 1.44$, $C_{2\varepsilon} = 1.92$, $C_\mu = 0.09$, $\sigma_k = 1.0$ and $\sigma_\varepsilon = 1.3$

The governing equation for energy is same as represented in Eq. 3.4.

The bulk mean temperature, $T_{m,x}$ and wall temperature, $T_{w,x}$ with distance x from the microchannel entrance can be obtained by doing the thermal energy balance around the microchannel as shown in Fig. 1. The equations are Eq. 4.12 and Eq. 4.13. .

$$T_{m,x} = T_{in} + \frac{q'' \pi D x}{\dot{m} C_{p,nf}} \tag{4.12}$$

$$T_{w,x} = T_{m,x} + \frac{q''}{h} \tag{4.13}$$

Where, T_{in} (303.15 K), is the specified inlet temperature. q'' and h are the heat flux and heat transfer coefficient respectively.

To characterize the effect of fluid flow on the thermal behaviour of the microchannel heat exchanger Peclet number, Pe is defined as

$$Pe = \frac{\rho_f C_{p,f} u}{\frac{k}{L}} = \frac{Convective\ \ Flux}{Conductive\ \ Flux} \tag{4.14}$$

4.7 BOUNDARY CONDITIONS

A no slip boundary condition was assigned for the non porous wall surfaces, where both velocity components were set to zero at that boundary i.e. $\upsilon_x = \upsilon_r = 0$. A constant heat flux (100 W/m2) is applied on the channel wall. Axis symmetry was assigned at centerline. A uniform mass flow inlet and a constant inlet temperature were assigned at the channel inlet. At the exit, pressure was specified.

4.8 METHOD OF SOLUTIONS

There are two ways to solve the problem stated above: (i) analytical method and (ii) CFD method. Lee and Mudwar, 2007 have used analytical method. The method consists of calculation of heat transfer coefficient (h) from either of Eq. 4.3 or Eq. 4.4 depending on whether flow is laminar or turbulent, calculation of bulk mean temperature of fluid using Eq. 4.12 followed by the calculation of wall temperature using eq. 4.13. The results given by Lee and Mudwar, 2007 are having errors in wall temperature and mean temperature calculation at the given inlet mass flow rate. Hence, in the present study, the analytical values of heat transfer coefficients are calculated using Eq. 4.3 / Eq. 4.4. The heat transfer coefficients are also obtained using CFD methods and then both the values are compared.

The CFD method follows the use of commercial software ANSYS Fluent 12.0 to solve the problem. The specified solver in Fluent uses a pressure correction based iterative SIMPLE algorithm with 1st order upwind scheme for discretising the convective transport terms. The convergence criteria for all the dependent variables are specified as 0.001. The default values of under-relaxation factor as shown in Table 4.3 are used in the simulation work.

Table 4.3 Relaxation factor

Factors	Value
Pressure	0.3
Density	1.0
Body force	1.0
Momentum	0.7
Energy	1.0

Using the CFD computed wall temperatures and mean temperature from Eq. 4.12; heat transfer coefficients can be calculated by Eq. 4.13.

4.9 RESULTS AND DISCUSSIONS

The hydrodynamics behaviour of the channel can be studied in terms velocity distribution within the channel. The value of Re is 1278.0 for inlet mass flow rate 0.4 gm/s and it becomes 12780.0 for 4.0 gm/s inlet mass flow rate. Thus the flow is laminar and turbulent for 0.4 gm/s and 4.0 gm/s inlet mass flow rates respectively. The variation of centreline velocity at laminar state with axial position (X) for water and its nanofluid are displayed in Fig. 4.4. The figure shows that for all the fluids the entrance lengths i.e. the length required to reach fully developed state are the same. The density and viscosity of nanofluids increases with increase in the nanoparticles concentration in water. Thus, the velocity at any axial position decreases with increase in the nanoparticles concentration as found in Fig. 4. The same is shown at turbulent state in Fig. 4.5. It is also observed here that the axial velocity decreases with increase in nanofluid concentrations. Unlike laminar flow, the entrance lengths are found different in turbulent flow condition.

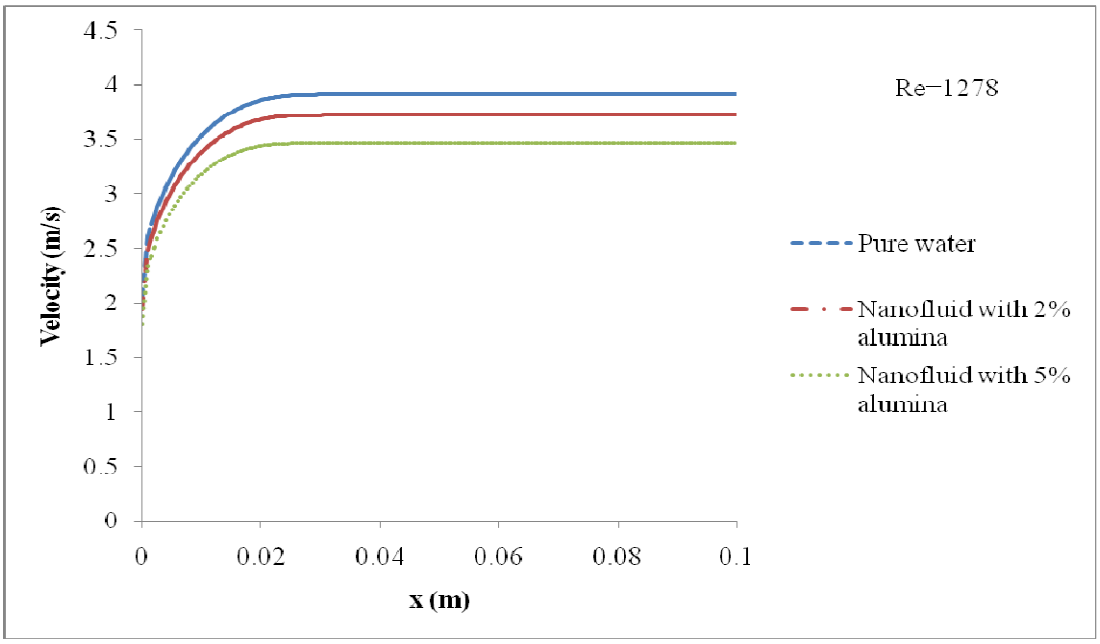

Figure 4.4: Velocity profile at centerline in the circular micro channel at Re =1278. Pr_{Water} =5.53 , $Pr_{2\%}$ = 5.40, $Pr_{5\%}$ = 5.20.

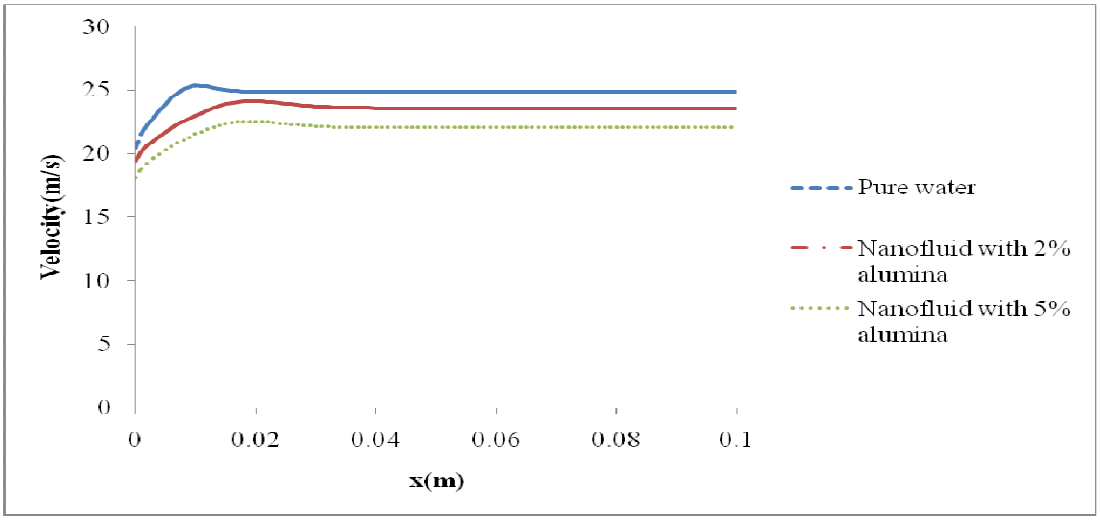

Figure 4.5: Velocity profile at centerline in the circular micro channel at Re =12780. Pr_{Water} =5.53 , $Pr_{2\%}$ =5.40 , $Pr_{5\%}$ =5.20.

Comparison of analytical and computational heat transfer coefficient for laminar (Re = 1278.0) and turbulent flow (Re = 12780.0) of water and its nanofluids (with 2% and 5% alumina) are shown in Table 4.4 and 4.5 respectively. The same comparison is also displayed in Fig. 4.6 and 4.6. The comparison shows that the CFD results can well predict the analytical heat transfer coefficient. The heat transfer data shows that inclusion of nanoparticles in water increases the heat transfer coefficient. More nanoparticle concentration more is the heat transfer coefficient. In case of laminar flow, both the analytical and CFD results show that heat transfer coefficient increases approximately by 15% magnitude from pure water to 5% nanofluid. As expected, both the tabular data and figures show that heat transfer coefficients in turbulent flow are more than laminar values. Like laminar heat transfer coefficient, the values of heat transfer coefficients in turbulent flow also increases with increase in nanoparticles concentration. Both the analytical and CFD values of it increase by 12% magnitude from pure water to 5% nanofluid. Thus, the increase of heat transfer coefficient is more in laminar flow than turbulent flow. But the percentage increase in heat transfer coefficient in turbulent zone is not negligible. These results contradict the results obtained by Lee and Mudawar, (2007). The use of nanofluids favourable therefore favourable both in laminar and turbulent fluid flow regimes. The heat transfer coefficient values for both type of flow are found to be independent of axial position. It means that circular micro channel is at fully thermal developed condition in both cases.

Table 4.4 Comparison of analytical heat transfer coefficient with the present CFD results at laminar (Re == 1278.0) flow for water and nanofluid.

	Analytical Heat Transfer Coefficient($W/m^2.K$)			Computational Heat Transfer Coefficient($W/m^2.K$)		
Position (m)	Pure Water	Nanofluid with 2 % Alumina	Nanofluid with 5 % Alumina	Pure Water	Nanofluid with 2 % Alumina	Nanofluid with 5 % Alumina
0	5258.16	5563.36	6042.96	5263.16	5555.56	6044.21
0.02	5258.16	5563.36	6042.96	5263.16	5555.56	6044.21
0.04	5258.16	5563.36	6042.96	5263.16	5555.56	6044.21
0.06	5258.16	5563.36	6042.96	5263.16	5555.56	6044.21
0.08	5258.16	5563.36	6042.96	5263.16	5555.56	6044.21
0.1	5258.16	5563.36	6042.96	5263.16	5555.56	6044.21

Table 4.5 Comparison of analytical heat transfer coefficient with the present CFD results at turbulent (Re =12780.0) flow for water and nanofluid.

	Analytical Heat Transfer Coefficient($W/m^2.K$)			Computational Heat Transfer Coefficient($W/m^2.K$)		
Position (m)	Pure Water	Nanofluid with 2 % Alumina	Nanofluid with 5 % Alumina	Pure Water	Nanofluid with 2 % Alumina	Nanofluid with 5 % Alumina
0	106020.5	111111.9	118882.3	106097.2	111184.5	118893.5
0.02	106020.5	111111.9	118882.3	106097.2	111184.5	118893.5
0.04	106020.5	111111.9	118882.3	106097.2	111184.5	118893.5
0.06	106020.5	111111.9	118882.3	106097.2	111184.5	118893.5
0.08	106020.5	111111.9	118882.3	106097.2	111184.5	118893.5
0.1	106020.5	111111.9	118882.3	106097.2	111184.5	118893.5

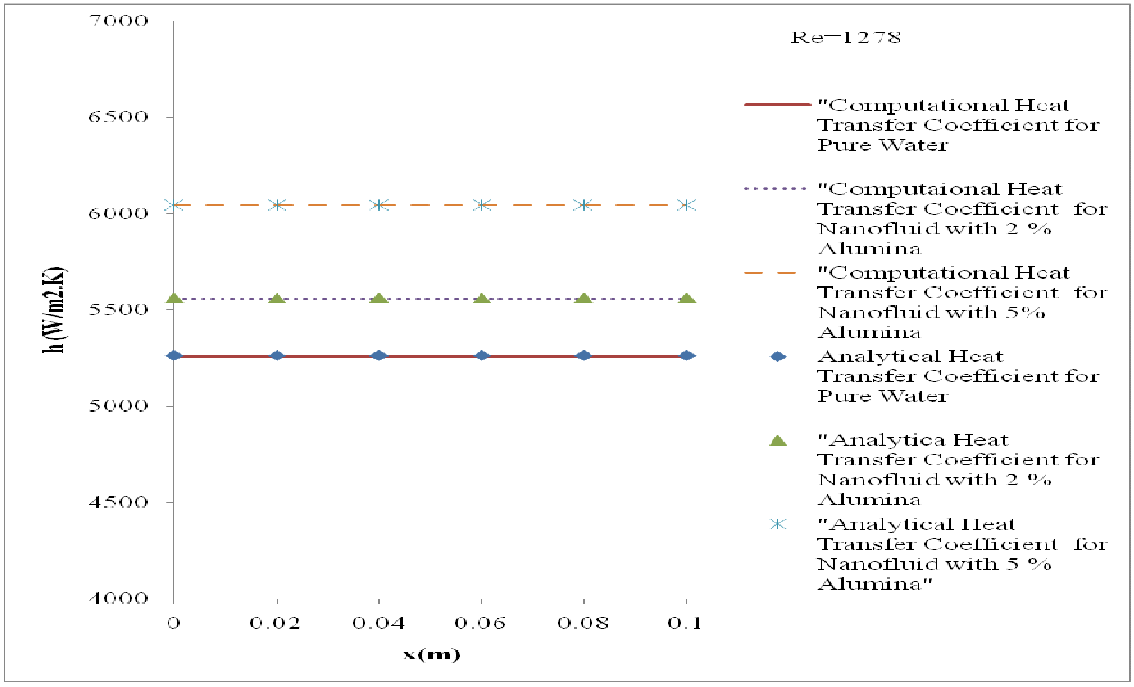

Figure 4.6: Variation heat transfer coefficient for laminar flow (Re =1278.0) in circular micro channel for water and its nanofluid

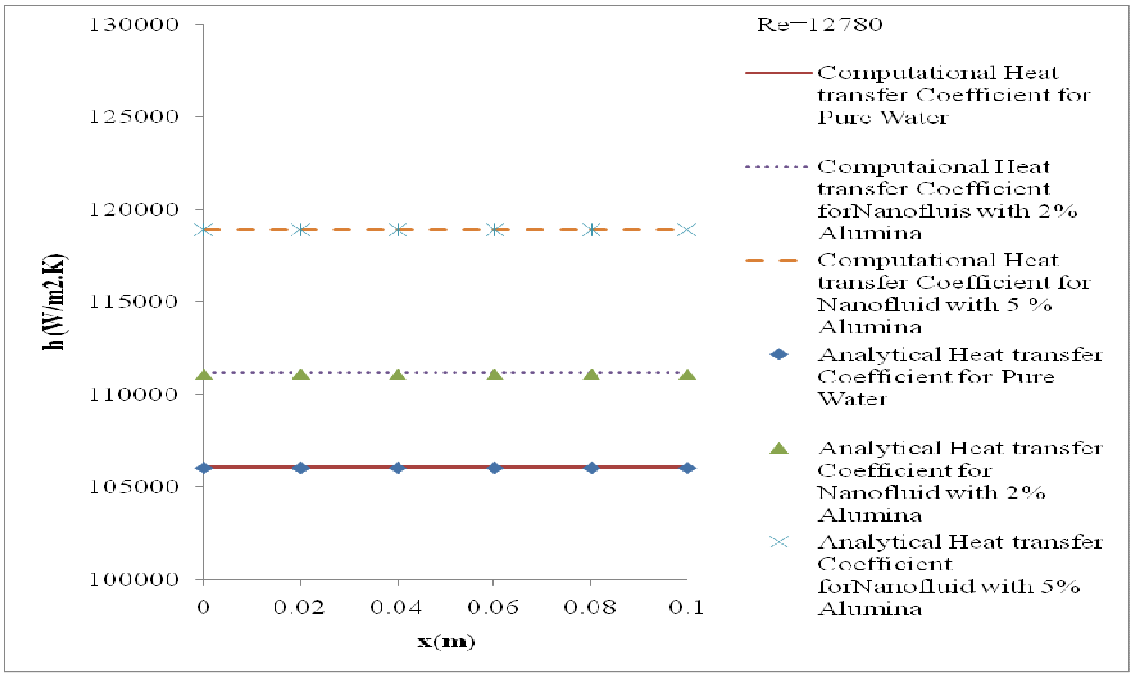

Figure 4.7: Variation heat transfer coefficient for turbulent flow (Re =12780.0) in circular micro channel for water and its nanofluid

In laminar flow $Nu = 4.36$ (i.e. $h \propto k$). To prove it, Table 4.6 shows the ratio of heat transfer coefficient of water to heat transfer coefficient of nanofluids at different values of Re. From Table it is clear that the ratio of heat transfer coefficient of water to heat transfer coefficient of nanofluids is equal to thermal conductivity of water to thermal conductivity its nanofluid. Hence, at laminar flow condition $h \propto k$.

Table 4.6: Validation of laminar flow model based on the relation between heat transfer coefficient and thermal conductivity of the fluid.

The variation of wall temperature with axial distant (X) is shown in Fig. 4.8, 4.9 and 4.10. The analytical wall temperature can be calculated from Eq. 4.13 using the anlytical values

Re	Heat Transfer Coefficient ($W/m^2.K$)	$\frac{k_{2\%}}{k_{0\%}} = 1.06$	$\frac{k_{5\%}}{k_{0\%}} = 1.15$	$\frac{k_{5\%}}{k_{2\%}} = 1.09$		
	$h_{0\%}$	$h_{2\%}$	$h_{5\%}$	$\frac{h_{2\%}}{h_{0\%}}$	$\frac{h_{5\%}}{h_{0\%}}$	$\frac{h_{5\%}}{h_{2\%}}$
0.1	558.65	591.06	642.1	1.058	1.149	1.09
5	3333.3	3533.3	3826.5	1.06	1.148	1.08
25	4545.4	4805.6	5227.1	1.058	1.151	1.09
50	5003	5284.2	5758.5	1.056	1.151	1.09

of heat transfer coefficiet. In Fig. 4.8 and 4.9 analytical wall temperatures are also compared with the wall temperatures obtained using CFD methods. It is oberved that both the ananltycal and compted wall temperatures are same at all position. The figures also depicts that the wall temperatures are equal to inlet temperatures over the axial distane of the channel. It happents both in the laminar and turbulent flow conditions. The value of Peclet number, Pe for both Re = 1278.0 and Re = 12780.0 are much much greater than 1.0, and hence temperature at all the point on axis becomes equal to inlet temperature. As Re decreass to 0.1 (very low value), the Pe value decreases substantially and also residenc time of the fluid in the channel increases due to decrease in inlet velocity of the fluid. Thus a substantial change in temperature from inlet to outlet of the channel is observed at

Re = 0.1 shown in Fig. 4.10. It is also noticed in Fig. 4.10 that the use of pure water results in more wall temperature than its nanofluids, and wall temperature at a particular axial position decreases with increase in nano particle concentrations. It might happen due to combined effect of density, viscosity and thermal conductivity.

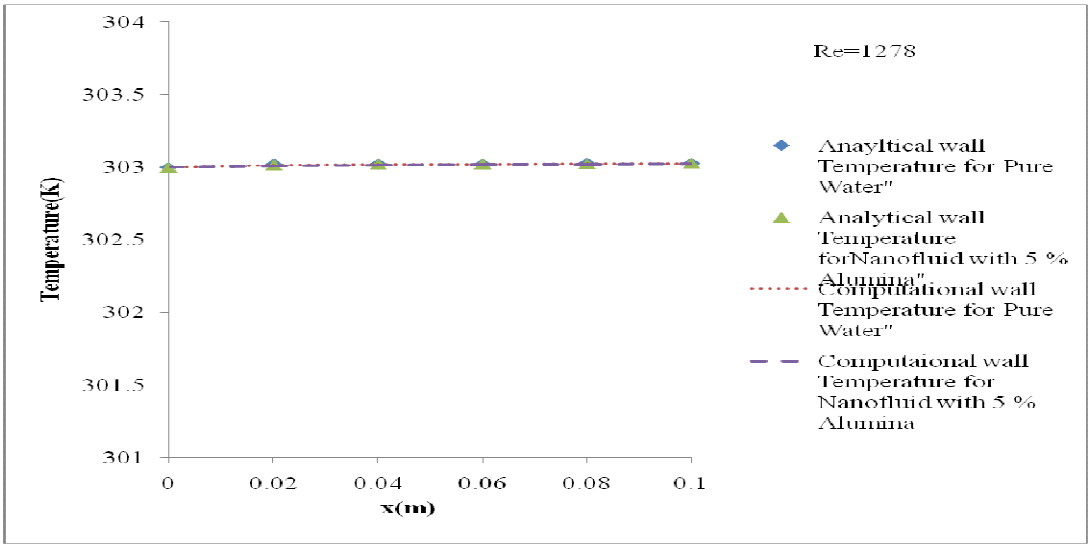

Figure 4.8: Variation wall temperature for laminar flow (Re =1278.0) in circular micro channel for water and its nanofluid

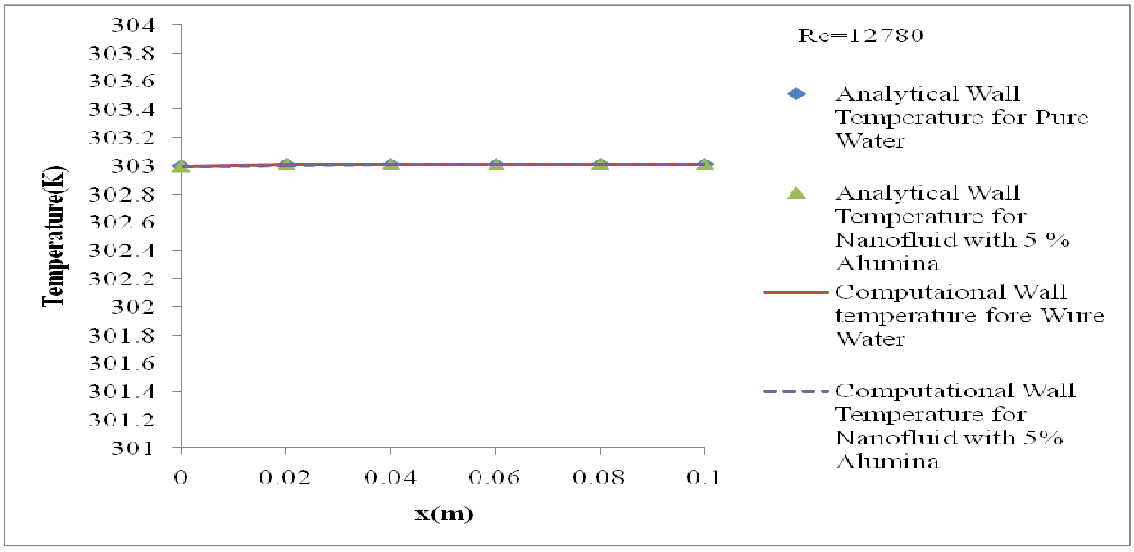

Figure 4.9: Variation wall temperature for turbulent flow (Re =12780.0) in circular micro channel for water and its nanofluid

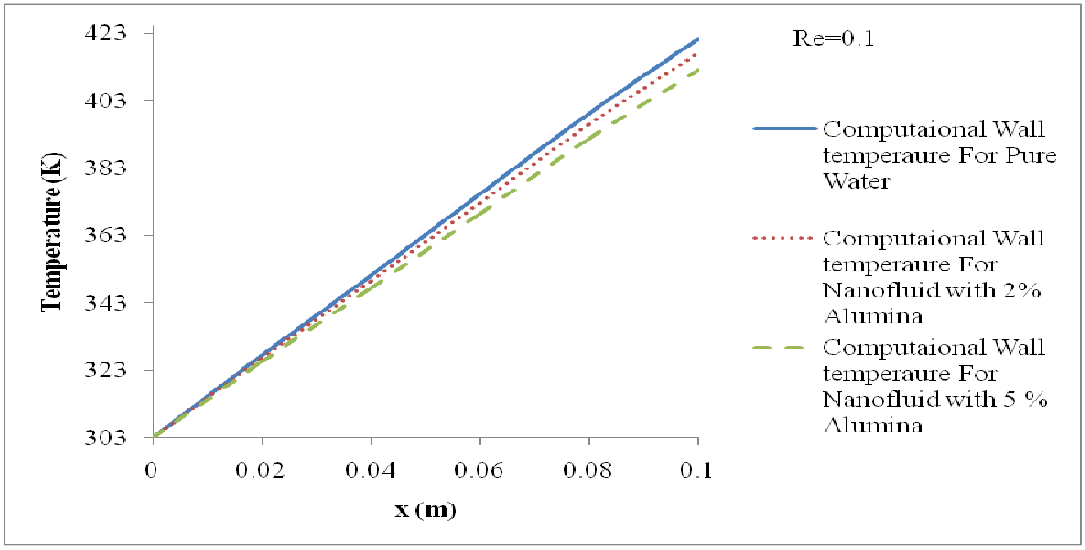

Figure 4.10: Variation wall temperature for Re = 0.1 in circular micro channel for water and its nanofluid

The study on variation of wall temperature using water as the heating medium in circular micro channel is done for different values of Reynolds number. These are tabulated in Table 4.7 and also depicted in Fig. 8. From the figure it is clear that there is less variation in wall temperature at higher Re than the lower one. The table and figure also depicts that effectively there is no change in temperature with distance as Re is greater than 1.0. The Peclet number, *Pe* increases with increase in Re. Thus the contribution of convective heat flux dominates over conductive heat flux at higher Re. The inlet temperature of the fluid penetrates more towards the outlet at higher *Pe* . Hence, it is expected that the variation of temperature reduces from inlet to outlet with increase in Re.

The effect of Reynolds number on the variation of wall temperature with axial position is represented in Table 4.8 and also in Fig. 4.11. It shows that as Re decreases the wall temperature increases more with axial position. It occurs due to decrease in Pe with the decrease in Re.

Table 4.7 Variation of wall temperature with axial distance at different values of Re

Wall Temperature K	Position (m)	Re=0.1	Re=1	Re=5	Re=10	Re=15	Re=25	Re=30	Re=50
	0	303.32	303.12	303.035	303.022	303.018	303.019	303.012	303.004
	0.02	327.239	305.47	303.511	303.265	303.183	303.117	303.101	303.068
	0.04	351.241	307.87	303.991	303.505	303.343	303.213	303.181	303.116
	0.06	375.24	310.27	304.471	303.745	303.503	303.309	303.261	303.164
	0.08	399.32	312.67	304.951	303.985	303.663	303.405	303.341	303.212
	0.1	421.42	315	305.419	304.219	303.819	303.499	303.419	303.258

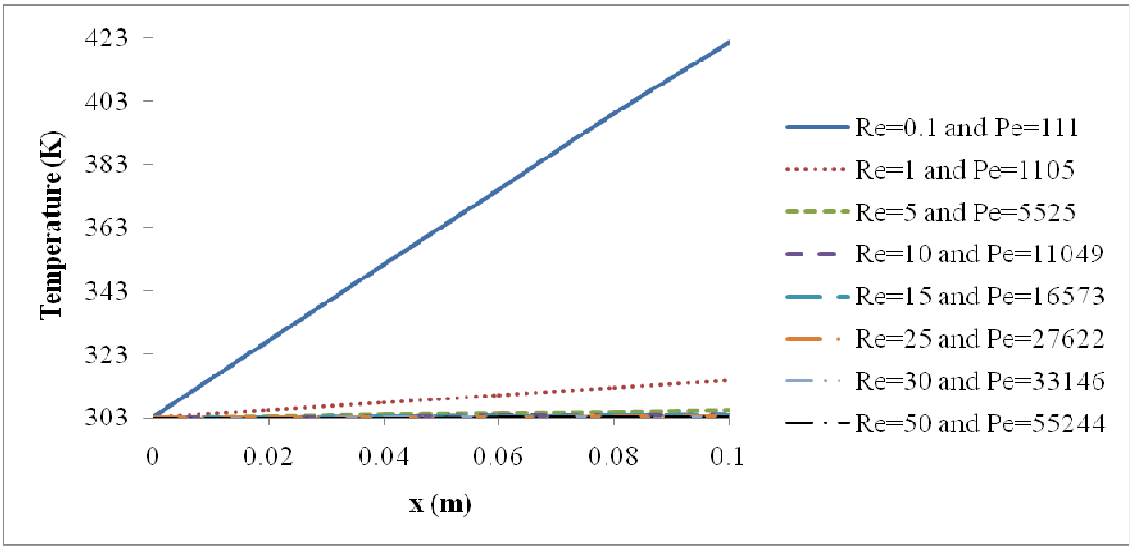

Figure 4.11: Variation of wall temperature with axial distant for different value of Reynolds number and Peclet number. Water is used as the fluid in the heat exchanger.

Varition of velocity of water with radius (Y) at different axial position (X) for diffrent values of Re is shown in Fig. 4.12. From the figure its is clear that velocity has no variation with X i.e. from inlet to exit the profiles are same. This indicates that ciruclar mirochannel is at fully developed flow condition.The same is true for all fluid flow with water as well as its nanofluid. One typical obsevation is made that with increasing Re, the velocity profile becomes more parabolic. The variation of velocity is found to be limited closer to the wall and around the center a flat profile is observed at Re = 0.1. This undeveloped velocity at lower Re results in domination of conductive heat transport compared to the higher Re case, and thus larger variation of temperatures are occuring at lower Re.

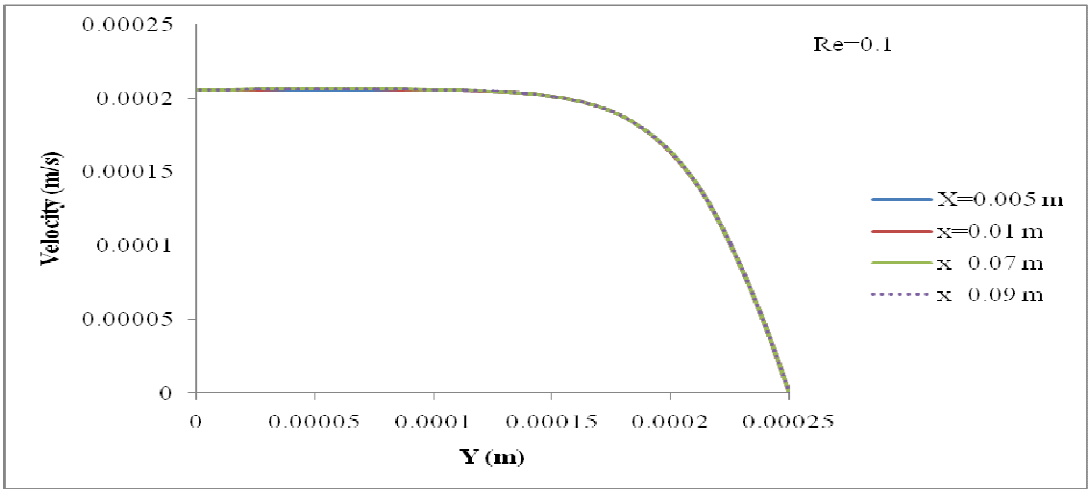

(a)

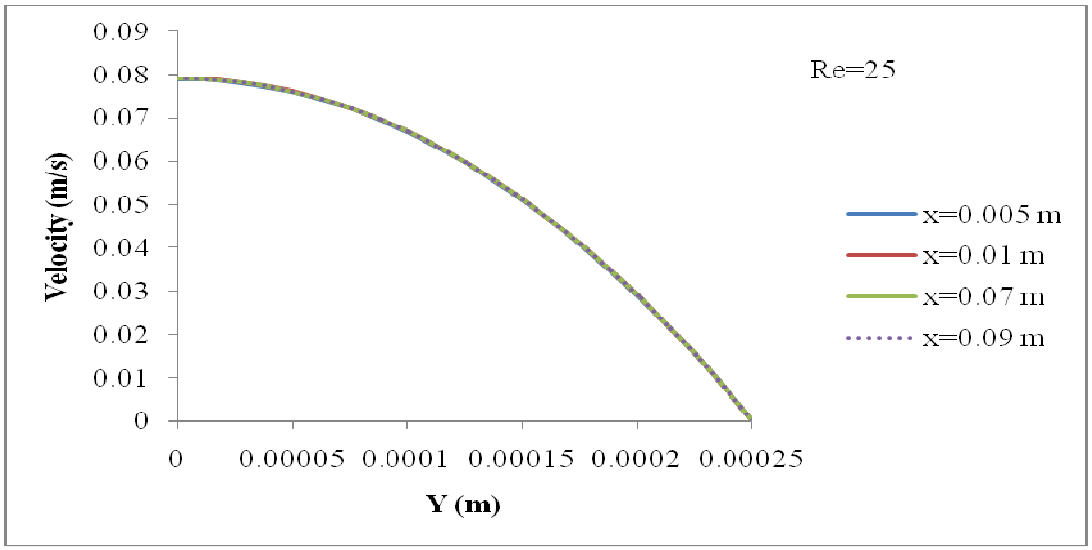

(b)

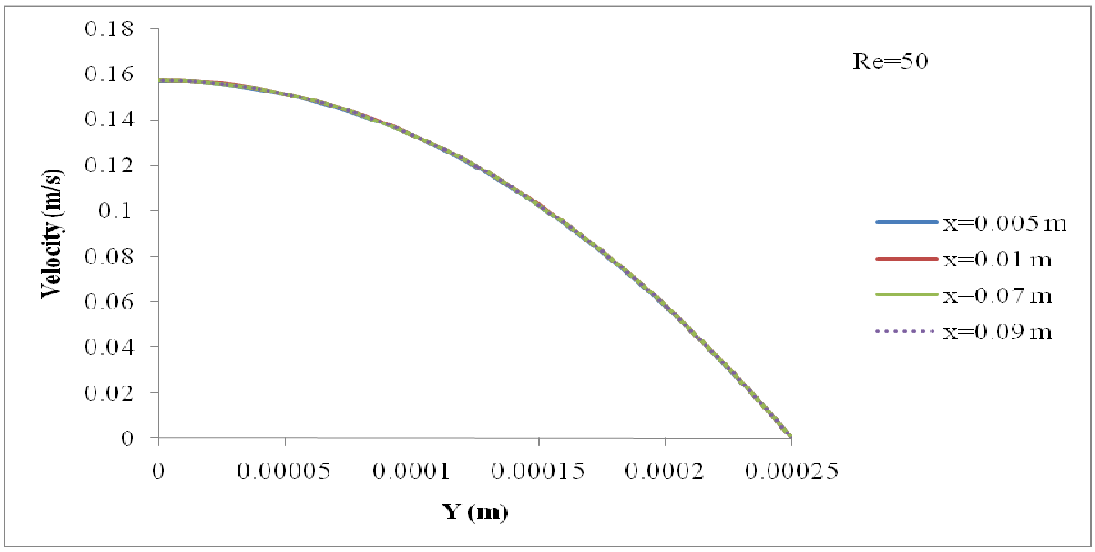

(c)

Figure 4.12: Variation of velocity of water in radial direction at different values of X for (a) Re = 0.1 (b) Re = 25 (c) Re = 50. Water is used as the fluid in the heat exchanger.

The varition of wall temperature of water with radial posititon (Y) at different values of X and at different values of Re is shown in Fig. 4.13. All the figure shows that there is no variation of temperature in Y direction. It happens because convective heat transfer rate dominates over conductive heat transfer rate even at Re = 0.1 for which also Pe >> 1. At Re = 0.1, temperature increases with the increase X, and the possible explanation is given while discussing the velocity profile of water in the exchanger. The relative comaprison of variation of temperature at different Re depicts that outlet temperature approaches inlet temperature with increase in Re. It occurs due to increase in Peclet number with Re. Fig. 4.13(c) represents the variation wall temperature with Y at different X at very low value of Re. In this case, Pe is much less than 1.0. Thus conductive heat transport dominitates over convective heat transfer here. But still there is no temperature distribution observed with radial position. It happens because the the diameter of the channel is very very less compared to the length.

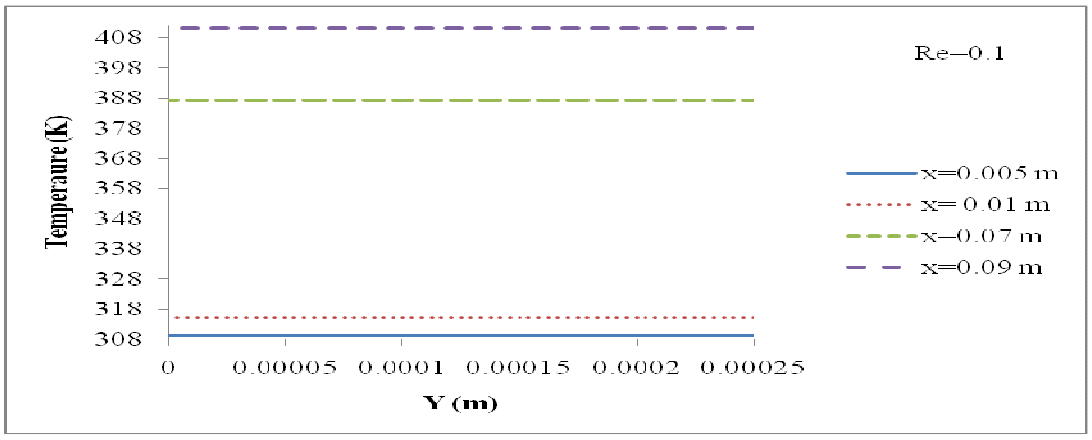

(a)

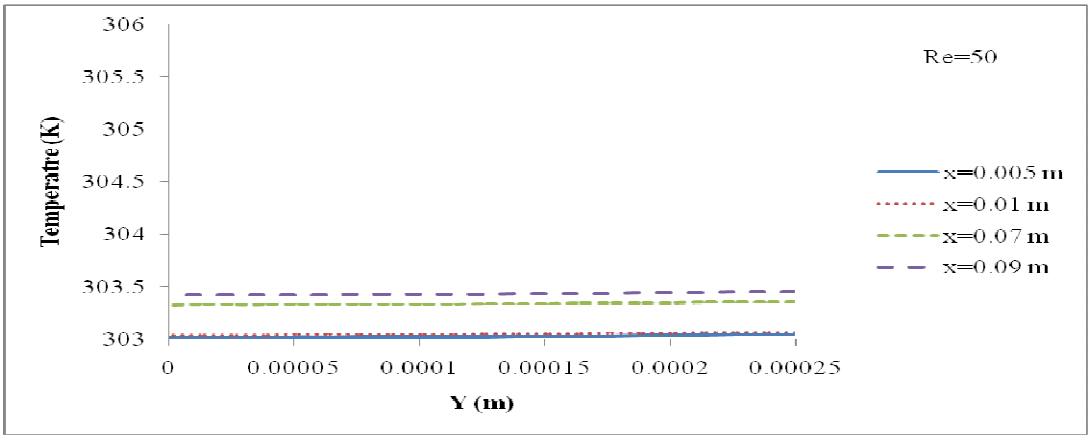

(b)

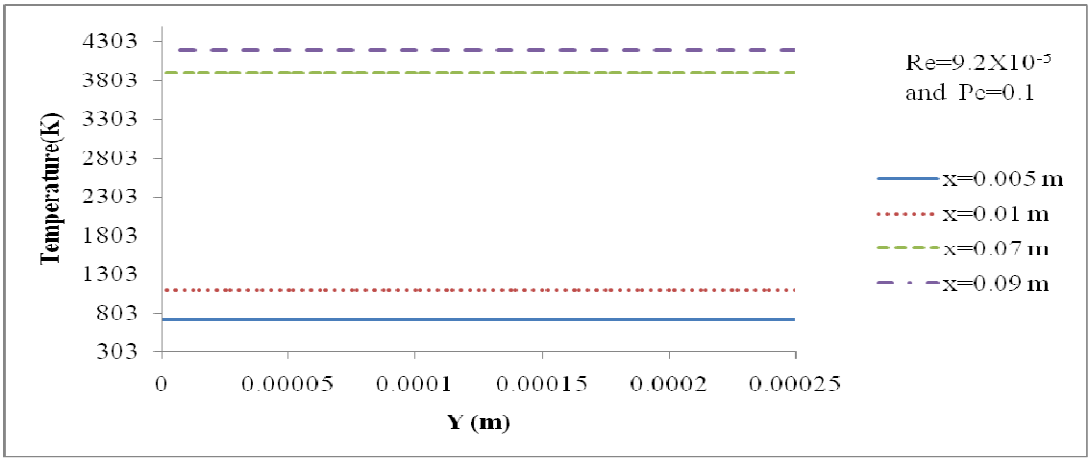

(c)

Figure 4.13: Temperature of pure water at different position in X direction for diffrent values of Re (a) Re = 0.1 (b) Re = 25 (c) Re = 50. Water is used as the fluid in the heat exchanger.

To see the entrance effect of circular micro channel on the velocity profile a velocity contours plot for differnt Reynolds are shown in Figs. 4.14 to 4.16. The figures show that the fluid rquires to travel certain distance in the flow direction called entrance length to get fully developed velocity profile. It is quite viscible in the figures that the entrance length as expected increases with increase in Reynolds number. The velocity contours at the exit also show that wall effect penetrates more towards the center and the thicknes of the zone with maximum velocity shrinks with increase in Re.

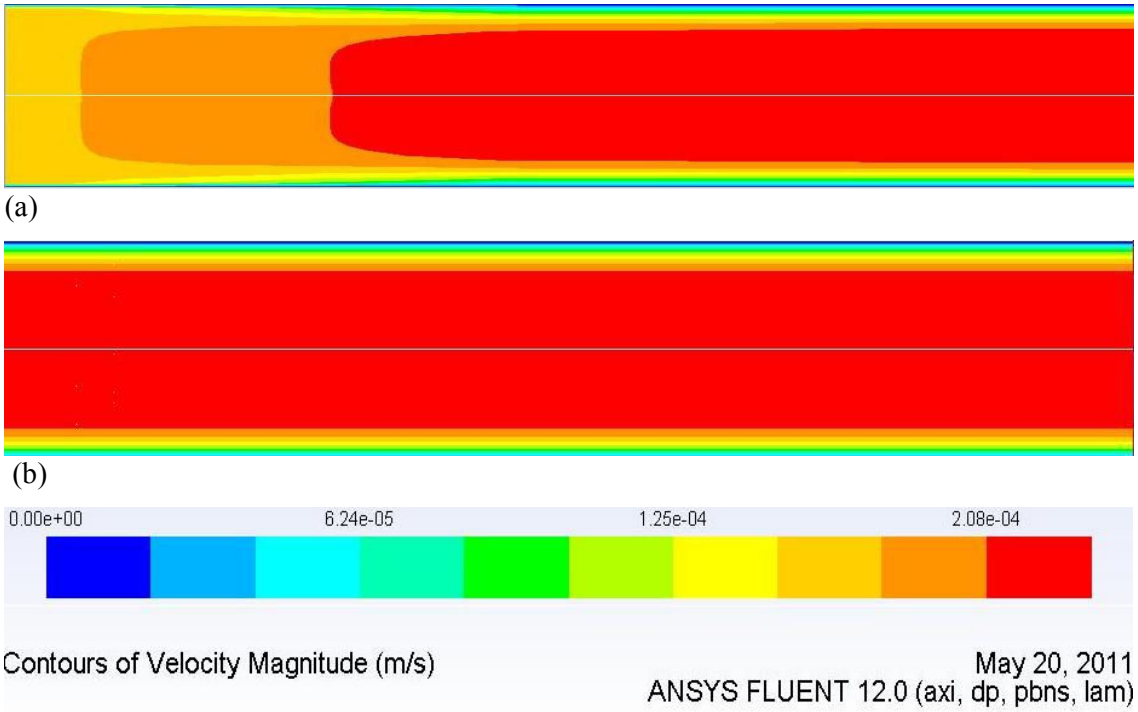

Figure 4.14: Water velocity contour plot at Re = 0.1 for water (a) Nearer to the entrance (b) Nearer to the exit

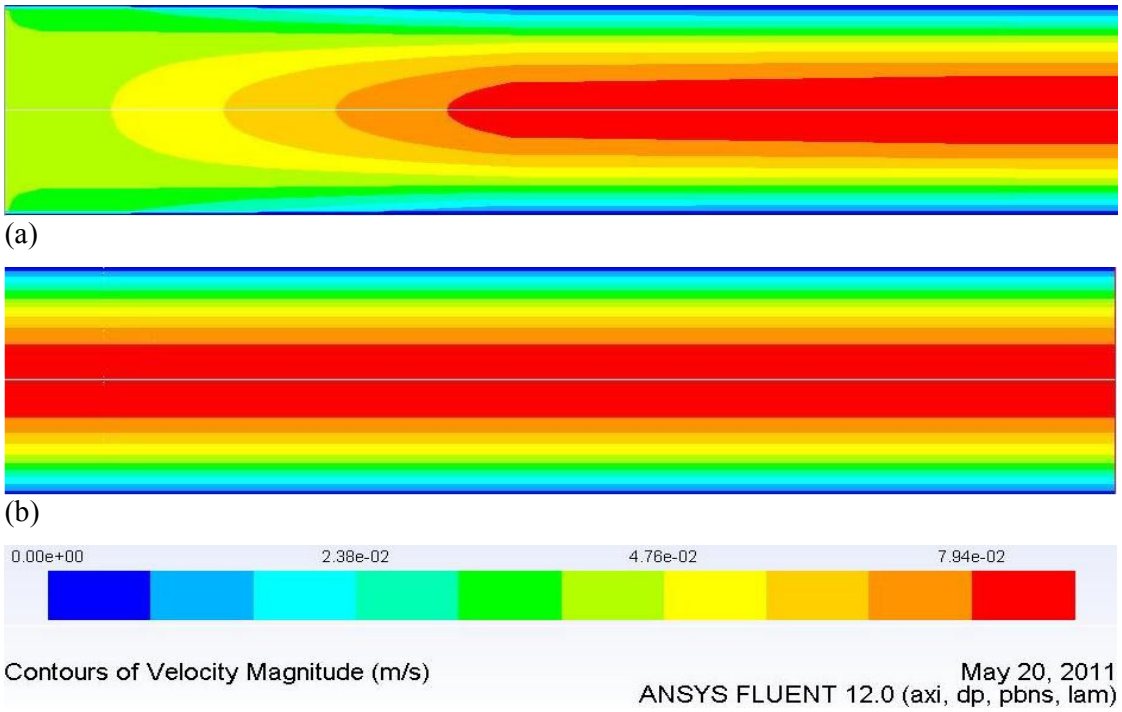

Figure 4.15: Water velocity contour plot at Re = 25 for water (a) Nearer to the entrance (b)Nearer to the exit. Water is used as the fluid in the heat exchanger.

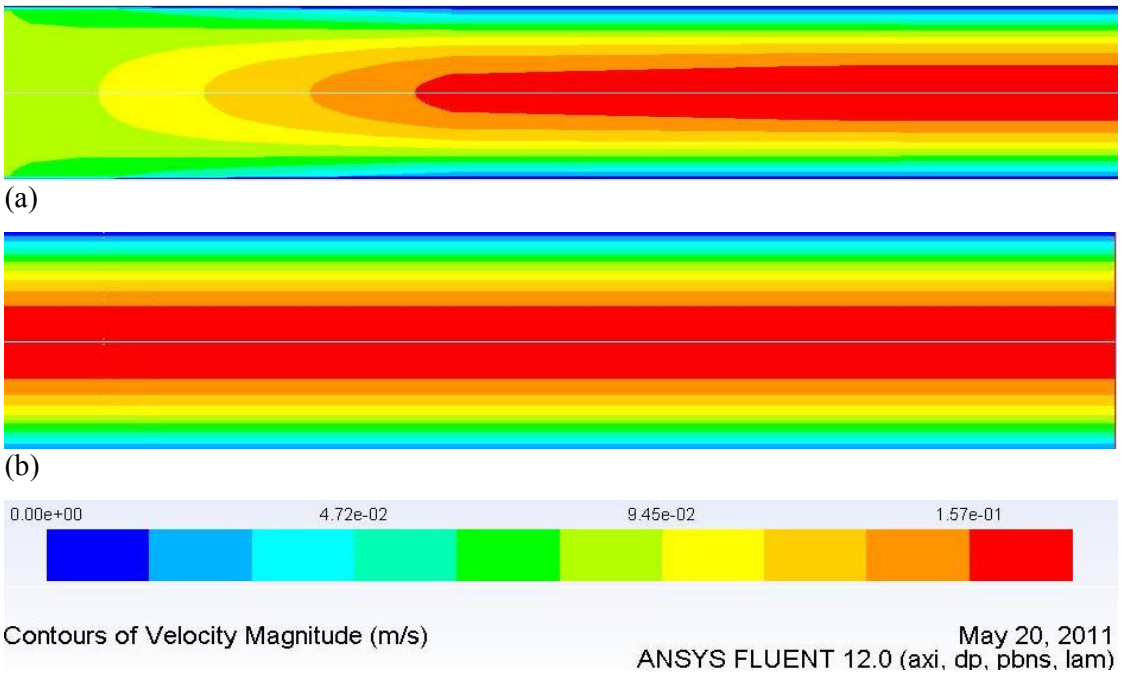

Figure 4.16: Velocity contour plot at Re = 50 for water (a) Nearer to the entrance (b)Nearer to the exit. Water is used as the fluid in the heat exchanger.

Temperature contour plots are shown in Figs. 4.17 and 4.18 for Re equal to 0.1 and 50 respectively. The contours support the different temperature profiles as discussed before. These also show that there is no variation of temperature in the radial direction.

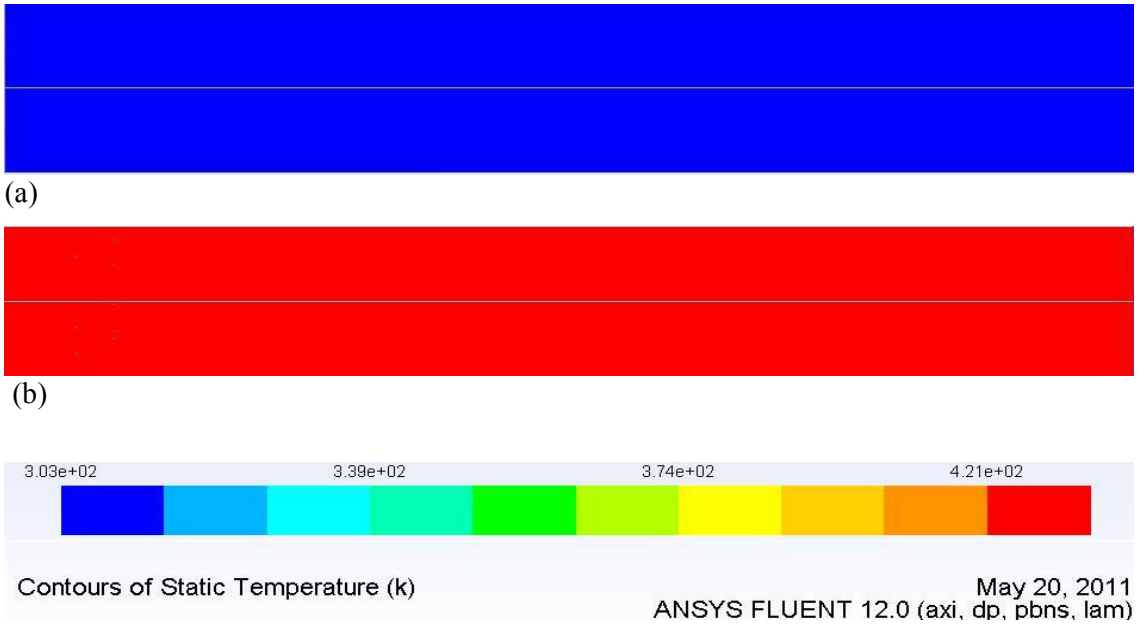

Figure 4.17 Temperature contour plot at Re = 0.1 (a) Nearer to the entrance (b) Nearer to the exit. Water is used as the fluid in the heat exchanger.

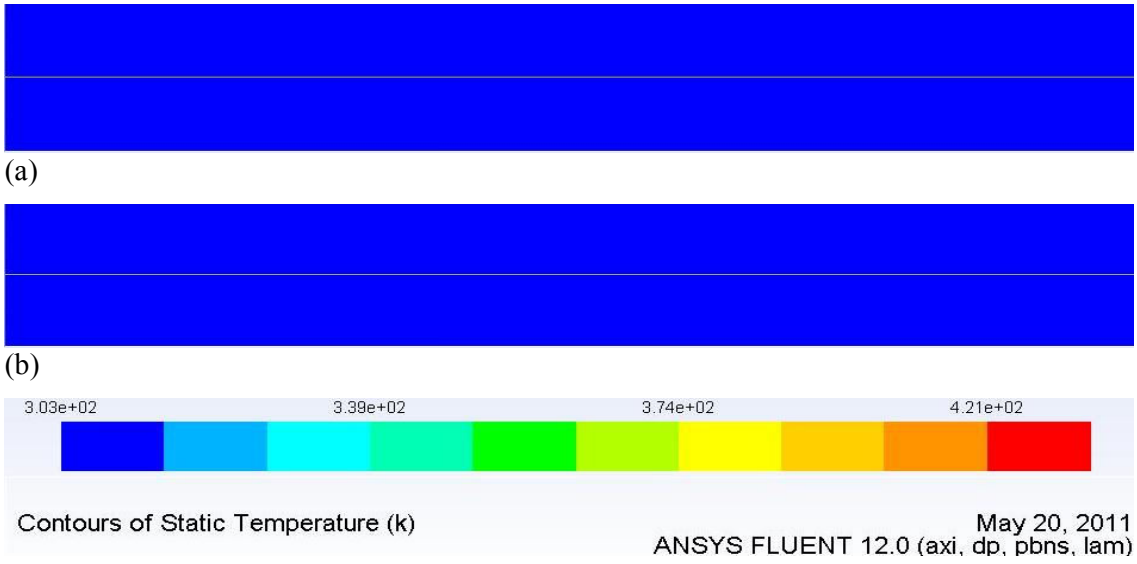

Figure 4.18: Temperature contour plot at Re = 50. (a) Nearer to the entrance (b)Nearer to the exit. Water is used as the fluid in the heat exchanger.

Pressure contour plots at different Reynolds no. for water are shown Figs. 4.19 to 4.21. From pressure contour it is clear that as Reynolds number. increases pressure drop increases. A linear variation of pressure is with axial distance at all Re. The same is observed with all nanofluids.

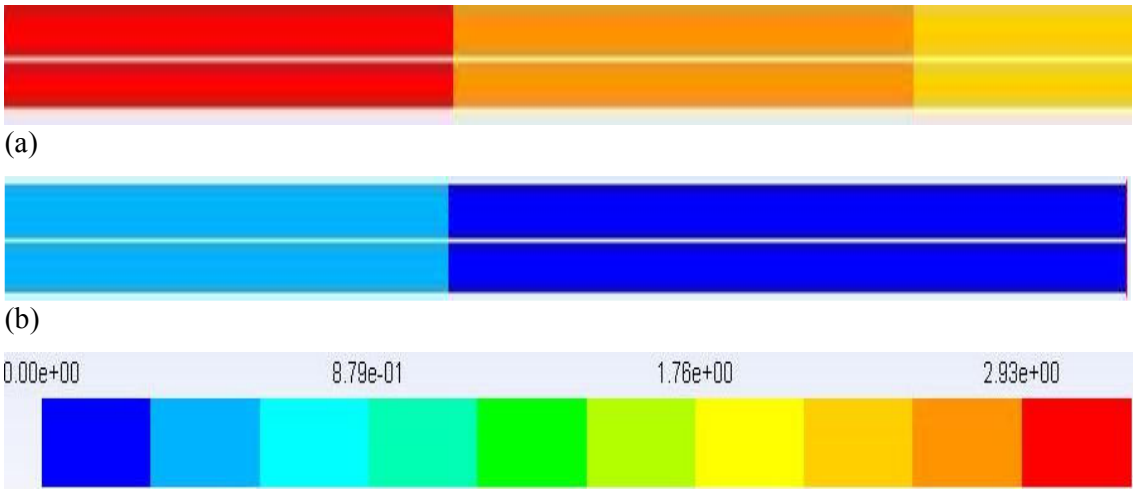

Figure 4.19: Pressure contour plots Re = 0.1 for water (a) Nearer to the entrace (b)Nearer to the exit. Water is used as the fluid in the heat exchanger.

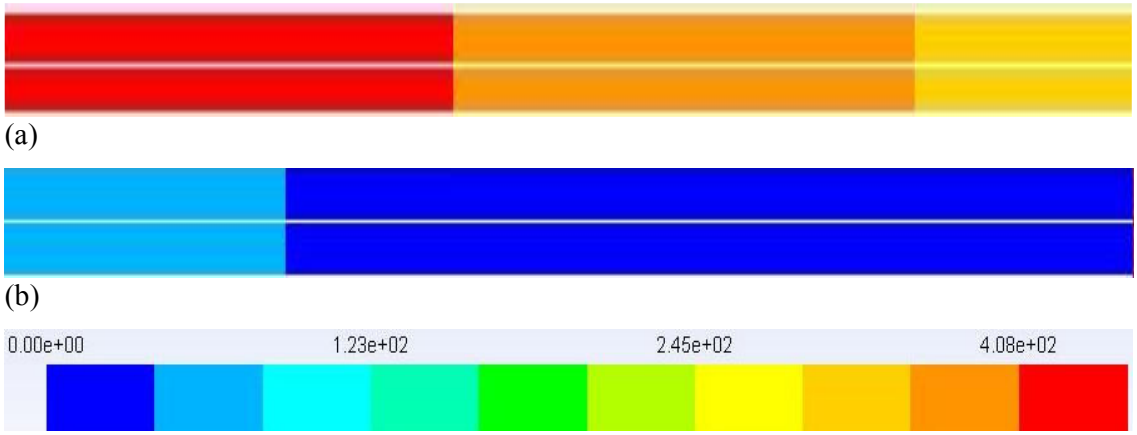

Figure 4.20: Pressure contour plots Re = 25 for water (a) Nearer to the entrace (b)Nearer to the exit. Water is used as the fluid in the heat exchanger.

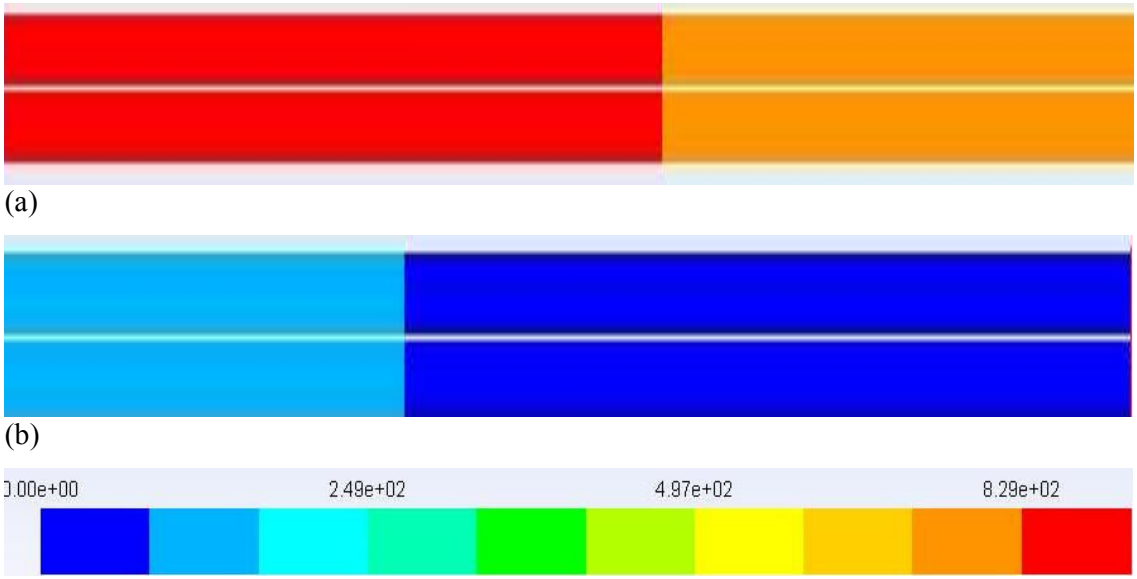

Figure 4.21: Pressure contour plots Re = 50 for water (a) Nearer to the entrace (b)Nearer to the exit. Water is used as the fluid in the heat exchanger.

4.10 CONCLUSIONS

A numerical study of single phase fluid flow in a circular micro channel is discussed. Water and its nanofluids are used as fluid medium. Key conclusion of this chapter can be summarized as follows.

- The computational results successfully validated the analytical data for circular micro channel.
- Heat transfer coefficient is constant throughout the circular micro channel due to its fully developed conditions
- As the concentration of nanoparticle increases heat transfer coefficient also increases
- The enhancement of heat transfer in laminar flow is greater as compared to turbulent flow and use of nanoparticles both in laminar and turbulent conditions are found beneficial.
- Wall temperature increase with in the flow direction of circular micro channel at very low Re.

- Wall temperature has negligible variation for higher Reynolds due to greater value of Peclet no.
- Pressure and temperature contours represent successfully the hydrodynamic and thermal behaviour of the system

Chapter 5

MODELING OF SINGLE PHASE FLUID FLOW IN RECTANGULAR MICRO CHANNEL

This chapter deals with simulation of single phase fluid flow in a rectangular micro channel embedded in a test module. The experimental setup with test module was developed by Qu and Mudawar (2007) as shown in Fig. 5.1. Construction of micro channel test module with thermocouple locations is shown in Fig. 5.2 (Qu and Mudawar, 2007). The micro channel is made of oxygen free copper.

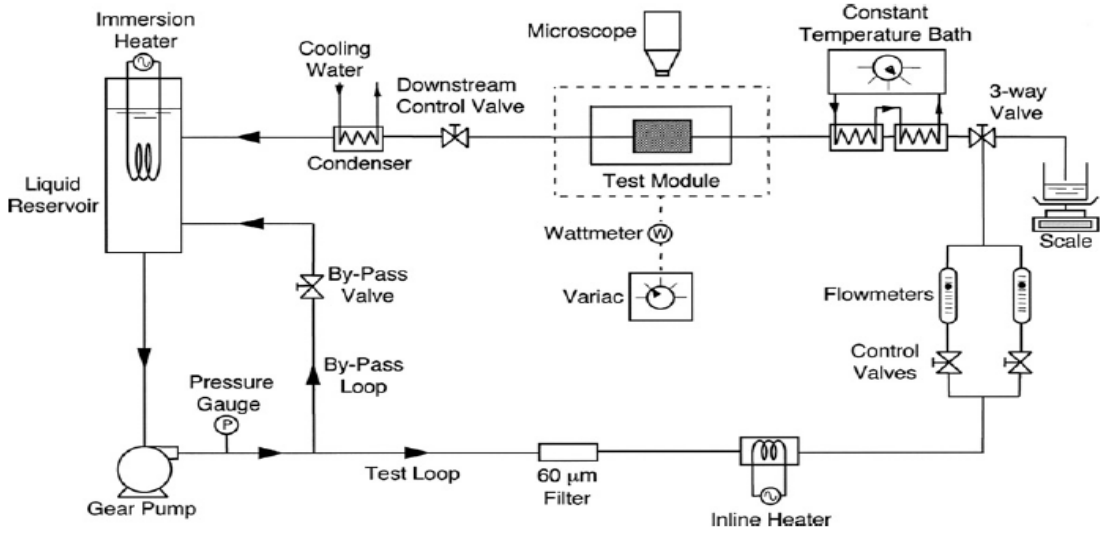

Figure 5.1 Experimental setup with micro channel test module

5.1 PROBLEM SPECIFICATION

The experimental work which was performed by Lee and Mudawar, (2007) on the test rig is simulated in the present study. Fluid is flowing through a rectangular micro channel embedded in a test module. There are 21 parallel rectangular micro-channels in the module. The dimension of each micro channel is 215 μm width, 821 μm depth and 4.48 cm length. The inlet velocity is u (m/s). The micro channel is made of oxygen free copper. The heating is provided by 12 cartridge heaters that are embedded in underside of test module. The top surface of micro channel is subjected to adiabatic conditions. Operating conditions for the study are as follows: The operating range of Reynolds

number based on the hydraulic diameter of the channel, $\mathrm{Re}_{Dh} = 140 - 941$,the power input range to the channel, $Q = 100 - 300$ W, the inlet temperature of fluid to the channel, $T_{in} = 30\,^{o}\mathrm{C}$, the range of inlet pressure, $P_{in} = 1.17 - 1.36$ bar, and the output pressure, $P_{out} = 1.12$ bar.

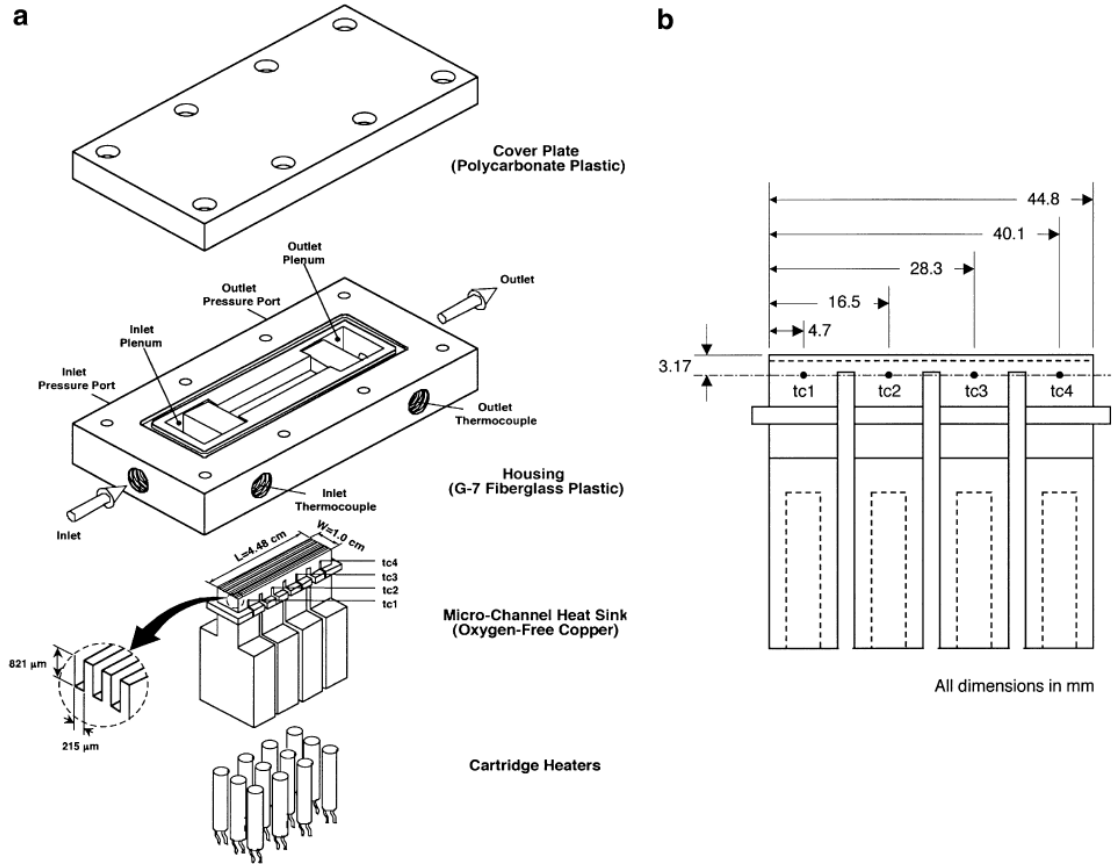

Figure 5.2 Construction of micro channel test module with thermocouple locations

5.2 GEOMETRY OF THE COMPUTATIONAL DOMAIN

In this study, a single micro channel out of 21 channels is considered as computational domain. Figure 5.3 represents the unit cell (computational domain) of micro channel heat sink with half of surrounding copper walls. Dimension of unit cell micro channel are shown in Table 5.1 (Qu and Mudawar 2004).

Table 5.1 Dimension of unit cell micro channel

$W_{w(}\,\mu m)$	$W_{ch(}\,\mu m)$	$H_{w1}(\,\mu m)$	$H_{ch}(\,\mu m)$	$H_{w2}(\,\mu m)$
125	215	12700	821	5637

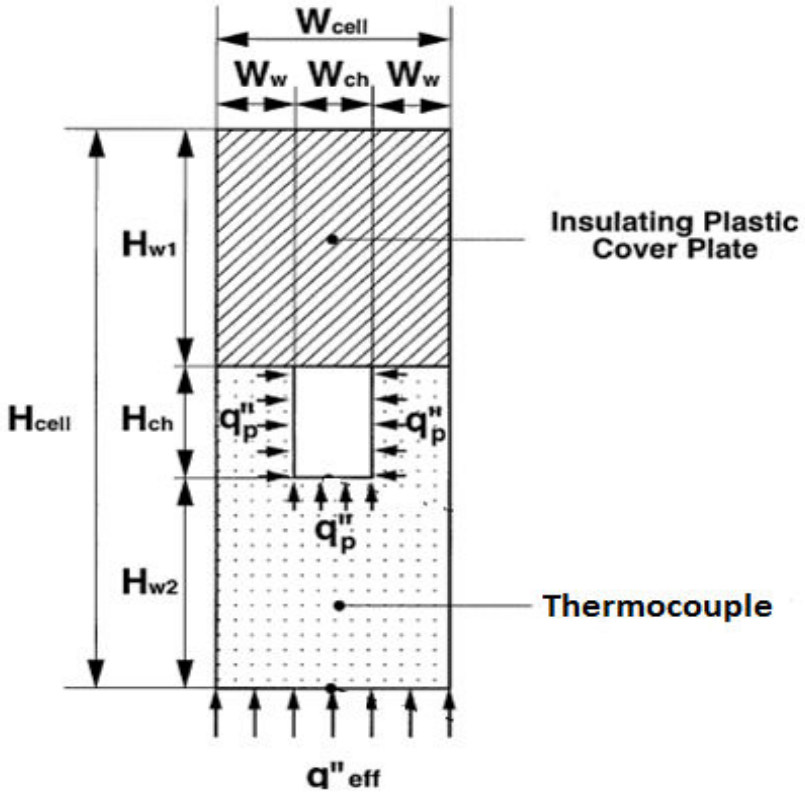

Figure 5.3 Computational domain of rectangular micro channel

5.3 MESHING OF THE COMPUTATIONAL DOMAIN

Structured mesh method was used for meshing the geometry as shown in Fig. 5.3. Nodes were created with element size of 0.0005 in all three dimensional coordinates. Fig. 5.4 represents three dimensional geometry of rectangular micro channel with structured mesh.

5.4 PHYSICAL MODEL

Physical model for simulation of single phase fluid flow is same as discussed in chapter 4.

5.5 FLUID PROPERTIES

Working fluid properties are same as discussed in Chapter 4. Here copper is considered as solid and its default properties as in ANYSYS (Fluent), density, heat capacity and thermal conductivity are 8978 kg/m^3, 381 J/kgK and 387.6 W/mK respectively.

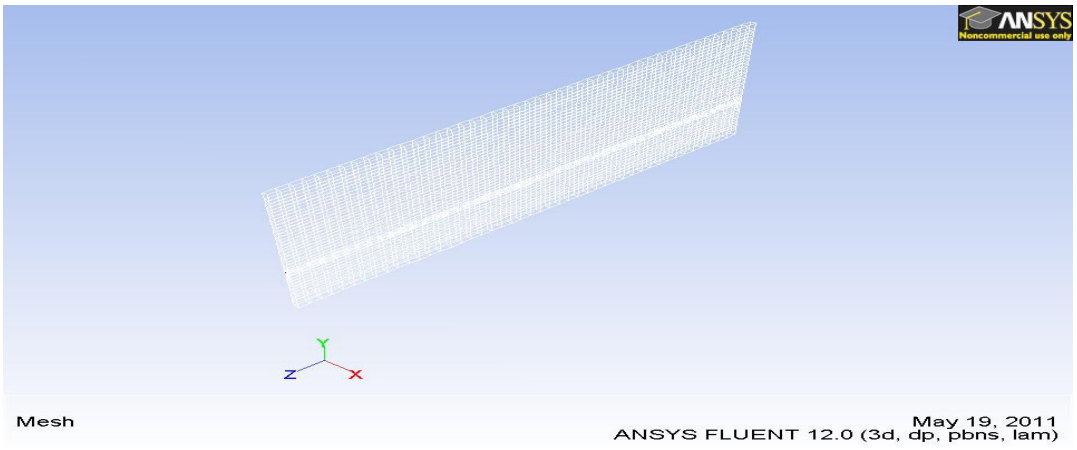

Figure 5.4 Three dimensional geometry of rectangular micro channel with structured mesh

5.6 ASSOCIATED EQUATIONS

The following equations were used in this chapter.

A single phase micro channel friction factor is determined from the pressure drop across the channel, Δp_{ch}.

$$f_{sp} = \frac{\Delta p_{ch} D_h}{2 L \rho_f u^2} \tag{5.1}$$

The heat flux for unit cell is given equation (Qu and Mudawar 2007):

$$q''_{eff} = \frac{P_W}{N A_{bot}} \tag{5.2}$$

Where N is no. of micro channel. $A_{bot} = W_{Cell} \times L$ is the bottom area of unit cell micro channel.

The heat flux to channel is given by (Qu and Mudawar 2004):

$$q''_p = \frac{q''_{eff} W_{cell}}{W_{ch} + 2H_{ch}} \tag{5.3}$$

Single phase heat transfer coefficient along micro channel defined as

$$h_{sp} = \frac{q''_p}{T_w - T_m} \tag{5.4}$$

Where T_W is the wall temperature, and mean fluid temperature is evaluated by energy balance around the channel.

5.7 BOUNDARY CONDITIONS

A no slip boundary condition was assigned for the surfaces, where both velocity components were set to zero at that boundary i.e. u = υ = 0. An uniform velocity inlet and a constant inlet temperature were assigned at the channel inlet. At the exit, Pressure was specified. At all wall surfaces heat flux was assigned. All the sink surfaces subjected to adiabatic conditions (heat flux is zero except bottom sink. Effective heat flux is assigned to channel bottom, channel left and channel right .Channel top is also subjected adiabatic conditions. The Continuum is assigned as solid in heat sink and fluid in channel. At different zone boundary condition defined as

Table 5.1a: Specification of zone type in ANSYS Workbench

Zone	Type
Inlet Sink	Wall
Outlet Sink	Wall
Bottom Sink	Wall
Left Sink	Wall
Wall	Wall
Top Sink	Wall
Channel Inlet	Velocity Inlet
Channel Outlet	Pressure Outlet
Channel Bottom	Wall
Channel Left	Wall
Channel Right	Wall
Channel top	Wall

5.8 SOLUTION METHODS

The specified solver uses a pressure correction based iterative SIMPLE algorithm with 1st order upwind scheme for discretisation of convective transport terms. The convergence criteria for all the dependent variables are specified as 0.001. The default values of under-relaxation factor as shown in Table 3 are used in the simulation work.

4.9 RESULTS AND DISCUSSIONS

The variation of velocity of water and its nanofluid (1% alumina and 2% alumina) with axial position (x) at Re=140 is shown in Fig. 5.5. Velocity is at centerline as indicted in figure 5.5. It is observed almost at the entrance velocity of all types of fluids got fully developed. The entrance length of all the fluids also found to be same.

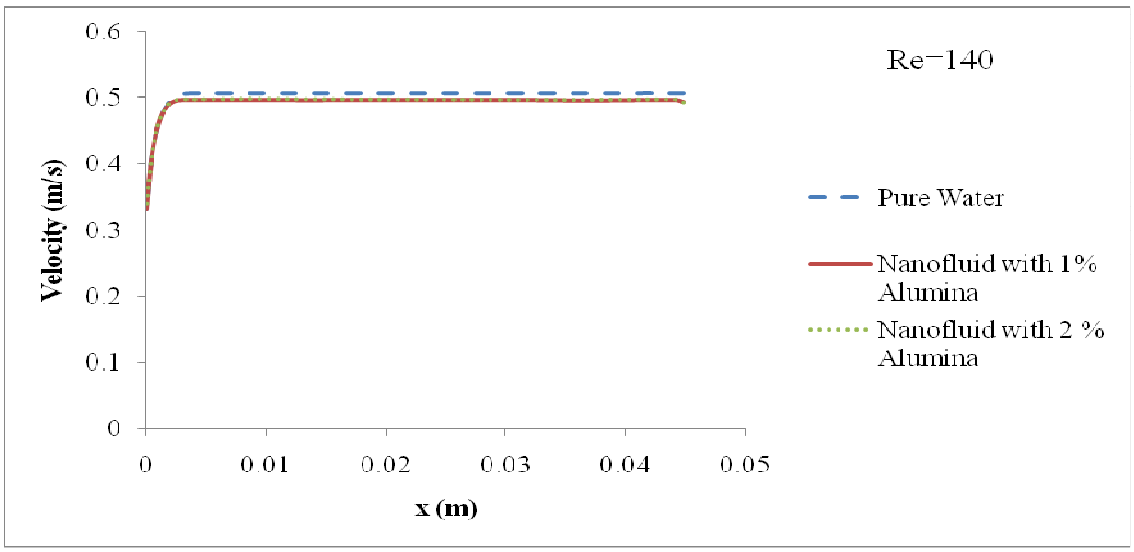

Figure 5.5: Velocity profile for water and its nonofluid at Re=140

Comparison of the present computed pressure drops and friction factors for water and its nano fluid at diffrenent Re 140-941 with experimental results (Lee and Mudawar, 2007) are depicted in Table 5.2, 5.3 and 5.4 respectively. The same is also shown in Fig. 5.6 to 5.8. These show that as Reynolds number increases pressure drop increases and friction factor decreases. Here one thing is noticeable that the pressure drop increases with increasing nanoparticle concentration at the same Reynolds number. For example at Reynolds number 200, pure water and its nanofluid with alumina (1% and 2% volume concentration) gives pressure drop across micro channel equal to 0.38 bar, 0.46 bar and 0.61 bar respectively.

Table 5.2 Comparison of computation pressure drop and friction factor of water with experimental values (Lee and Qudawar, 2007)

Reynolds No	Experimental		Computational	
	Pressure Drop	Friction Factor	Pressure Drop	Friction Factor
189.524	0.259653	0.022414	0.4496	0.038811
260.276	0.389479	0.017827	0.6135	0.028081
397.529	0.66536	0.013055	0.9491	0.018622
459.665	0.811415	0.011907	1.2572	0.018449
530.531	0.957469	0.010548	1.4409	0.015873
588.074	1.071	0.009603	1.588	0.014238
721.075	1.363	0.008128	1.9136	0.011412
840.98	1.655	0.007256	2.2304	0.009778
903.115	1.801	0.006847	2.3971	0.009113
941	1.85	0.006478	2.4962	0.008741

Table 5.4 Comparison of computation pressure drop and friction factor of 1% Alumina with experimental values (Lee and Mudawar, 2007)

Reynolds No.	Experimental		Computational	
	Pressure Drop (bar)	Friction Factor	Pressure Drop	Friction Factor
172.062	0.259653	0.026503	0.5681	0.057986
234.198	0.405707	0.022352	0.7041	0.038791
292.081	0.56799	0.020119	0.8505	0.030125
358.581	0.714045	0.016781	1.0219	0.024016
416.351	0.8601	0.014993	1.1641	0.020293
540.849	1.185	0.012241	1.4955	0.015449
656.388	1.477	0.010359	1.7888	0.012546
709.68	1.607	0.009642	1.9234	0.01154
821.081	1.931	0.008655	2.2218	0.009959
874.599	2.093	0.008268	2.3731	0.009375

Table 5.5 Comparison of computation pressure drop and friction factor of 2% Alumina with experimental values (Lee and Qudawar, 2007)

Reynolds No.	Experimental		Computational	
	Pressure Drop (bar)	Friction Factor	Pressure Drop	Friction Factor
146.551	0.357022	0.048986	0.5067	0.069522
212.824	0.470621	0.030618	0.6922	0.045034
266.342	0.632903	0.026291	0.8041	0.033403
328.591	0.795186	0.021702	0.9651	0.02634
435.287	1.071	0.016657	1.2454	0.019369
546.575	1.379	0.013602	1.5382	0.015173
604.685	1.574	0.012685	1.6989	0.013692
707.128	1.866	0.010997	1.9793	0.011665
756.168	2.012	0.010369	2.0973	0.010809
805.434	2.191	0.009953	2.2391	0.010171

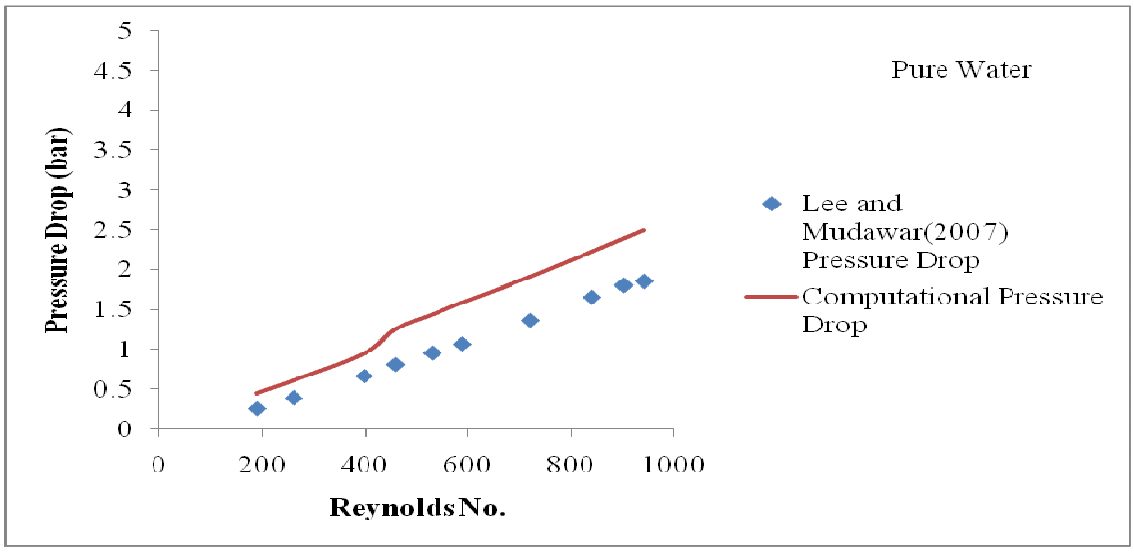

(a)

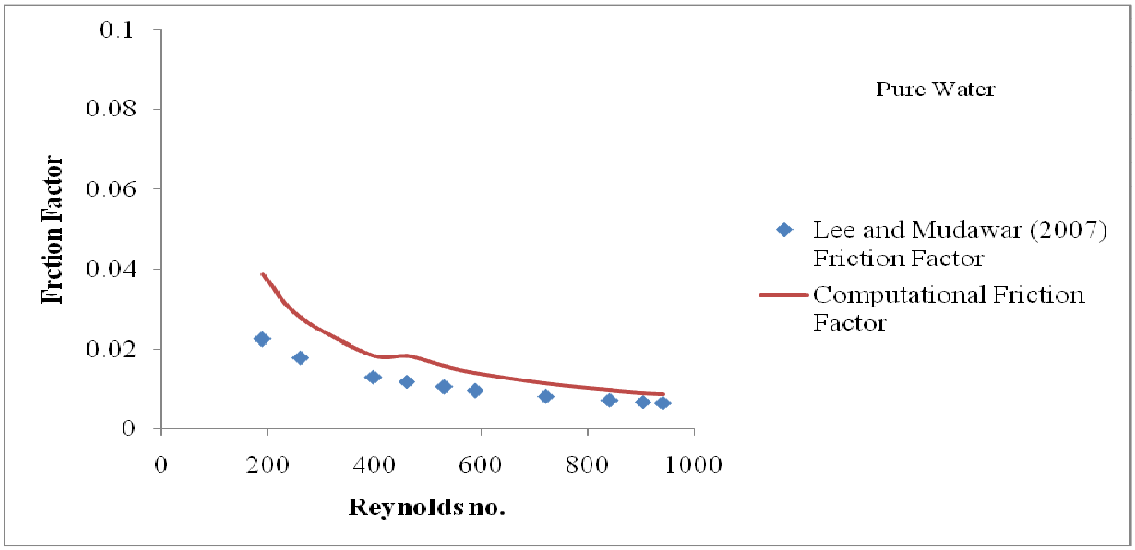

(b)

Figure 5.6: Variation of computational and experimental pressure drop and friction factor of water with Re. (a) Pressure drop (b) Friction factor

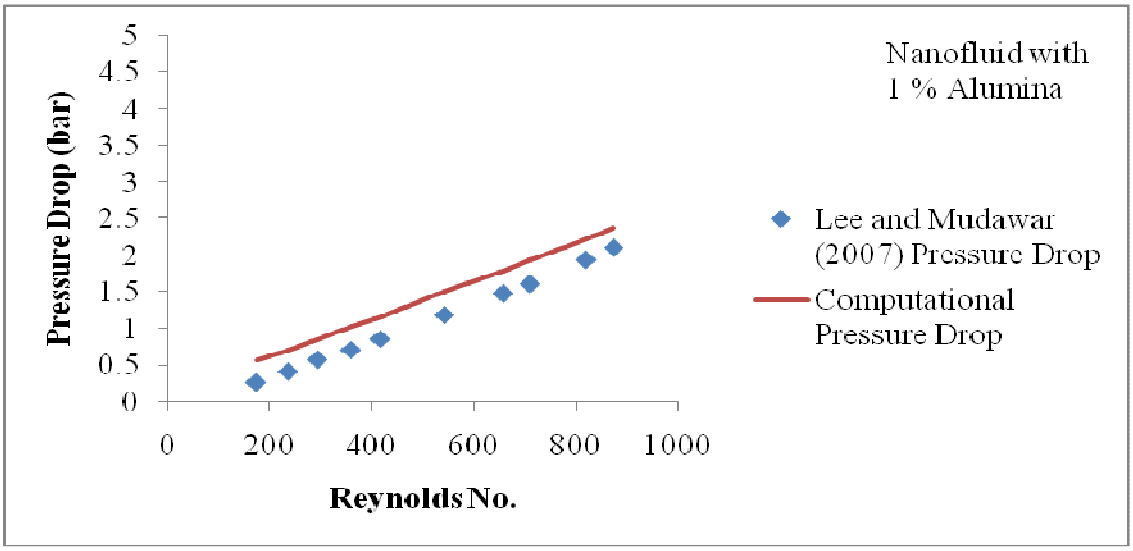

(a)

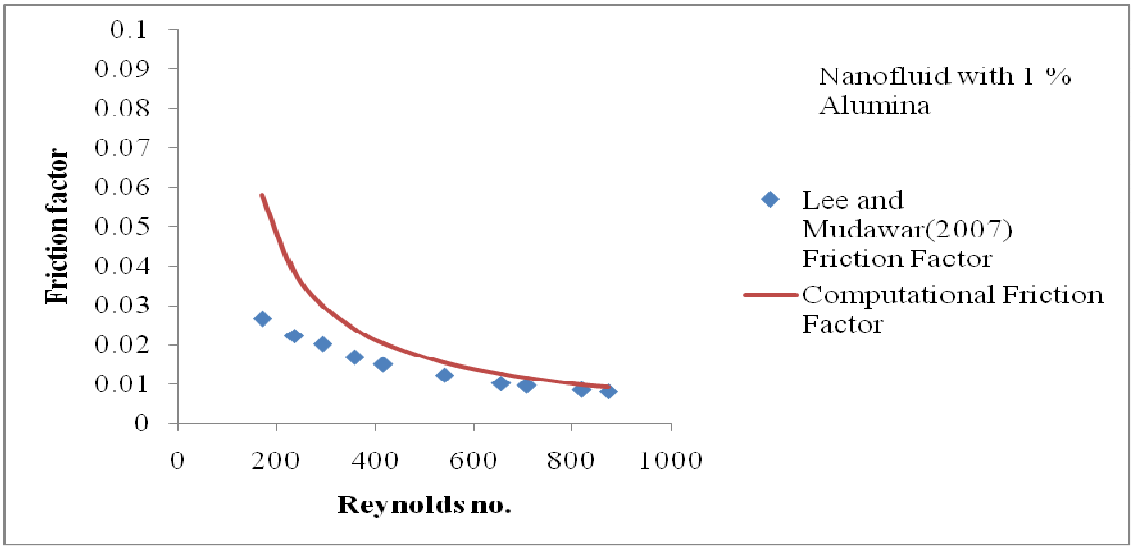

(b)

Figure 5.7: Variation of computational and experimental pressure drop and friction factor of 1% Alumina with Re. (a) Pressure drop (b) Friction factor

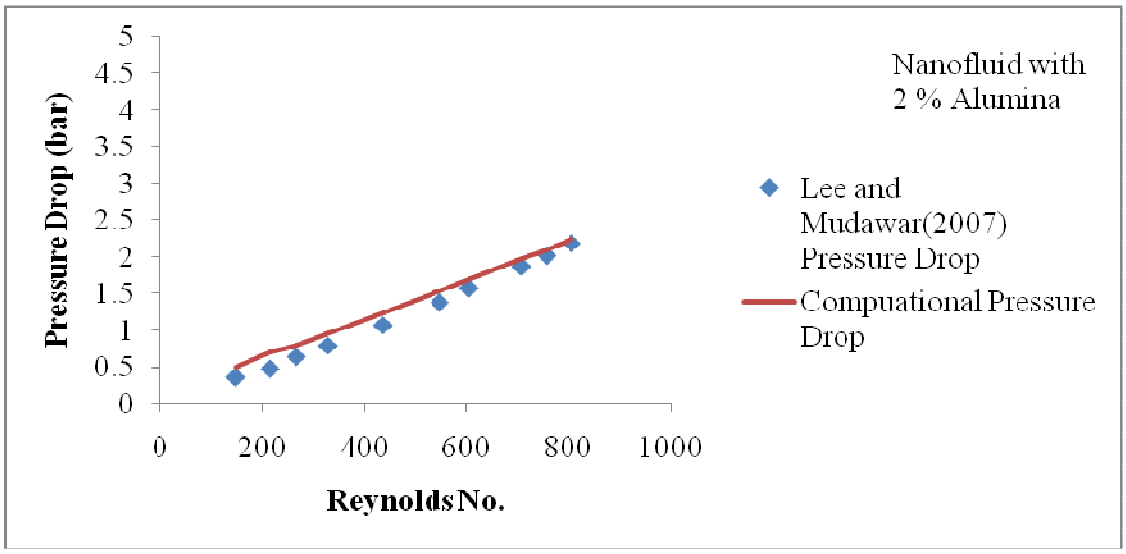

(a)

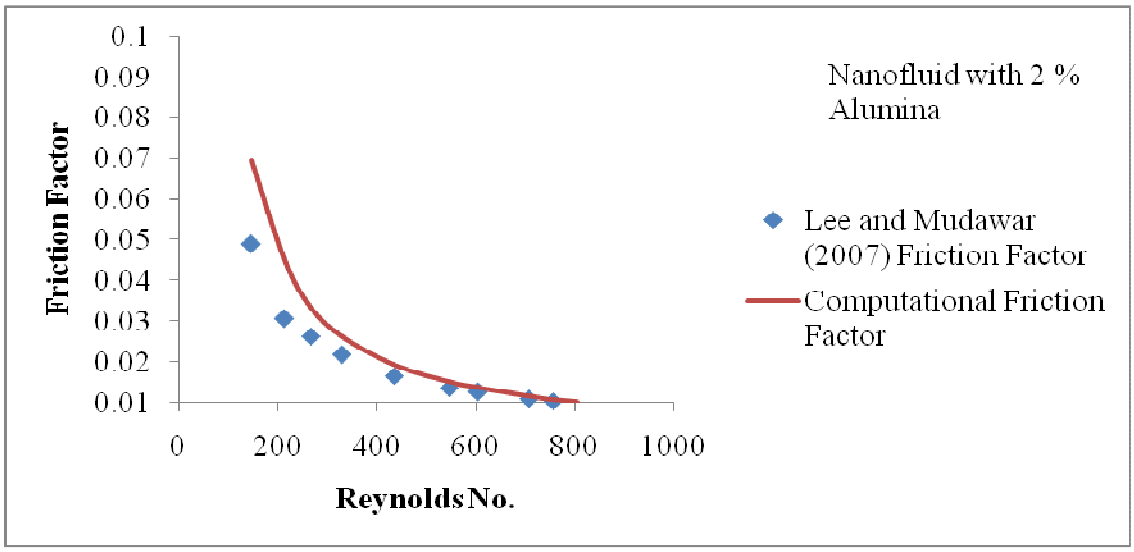

(b)

Figure 5.8: Variation of computational and experimental pressure drop and friction factor of 2% Alumina with Re. (a) Pressure drop (b) Friction factor

Variation of heat transfer coefficient on the bottom wall along micro channel at different power inputs for water and its nanofluids (1% and 2% alumina) are shown in Figs. 5.9 to 5.11 respectively. A decreasing trend of the heat coefficient values in the flow direction are observed in all the cases. Higher values of heat transfer coefficient are obtained at entry region of micro channel where as lower values are obtained at the exit region for all fluid properties. For example heat transfer coefficient at entry region and exit region are 16,837 $W/m^2.K$ and 5,811 $W/m^2.K$ respectively at 100 W heat input for pure water. Here one noticeable thing is that increasing the heat flux has a very weak effect on the heat

transfer coefficient of pure water and its nanofluids and the observation matches with Lee and Mudawar, 2007 observations.

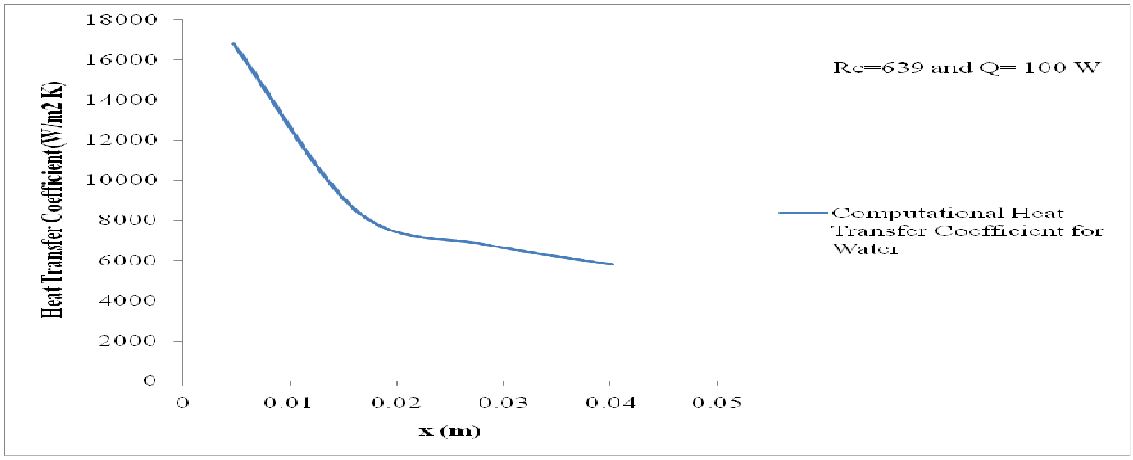

(a)

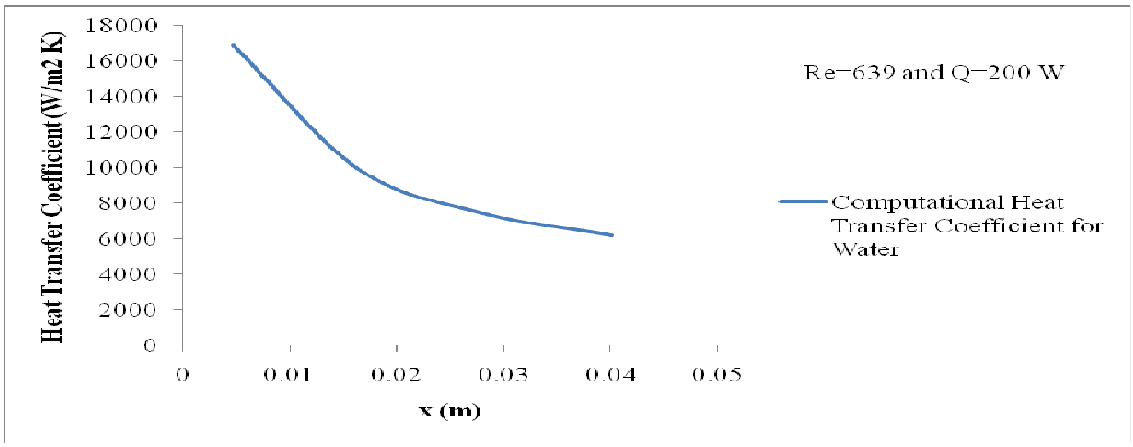

(b)

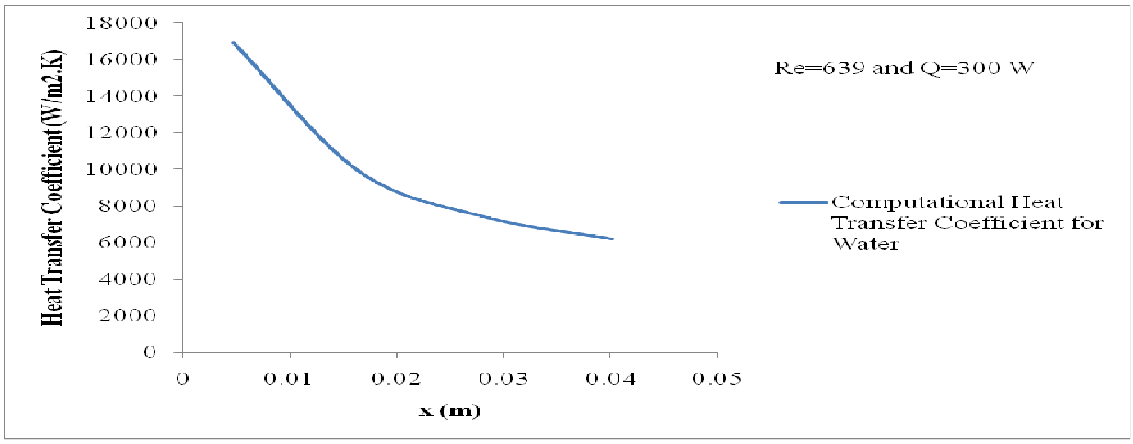

(c)

Figure 5.9: Variation of Heat Transfer Coefficient for water along micro channel at different Power inputs (a) 100 W (b) 200 W (c) 300 W

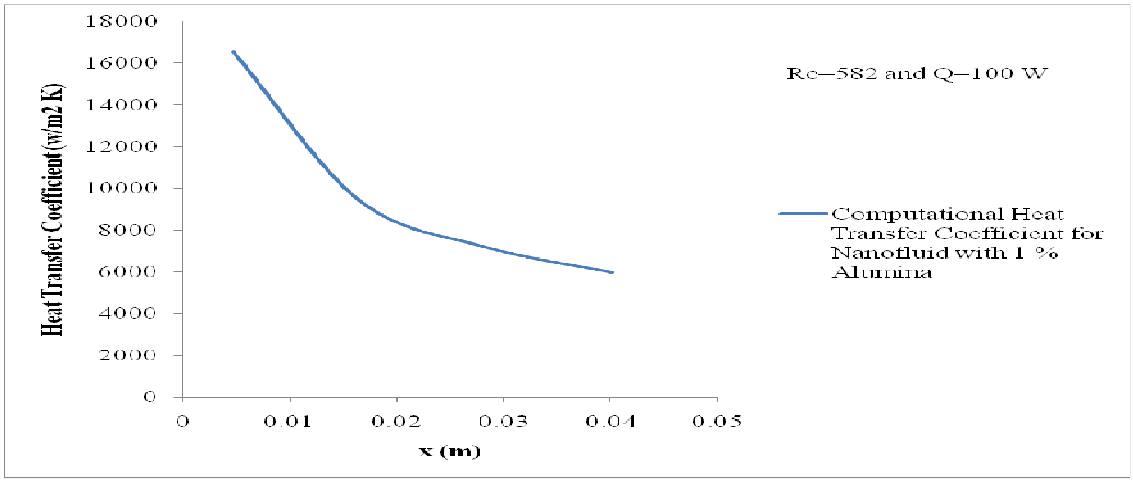

(a)

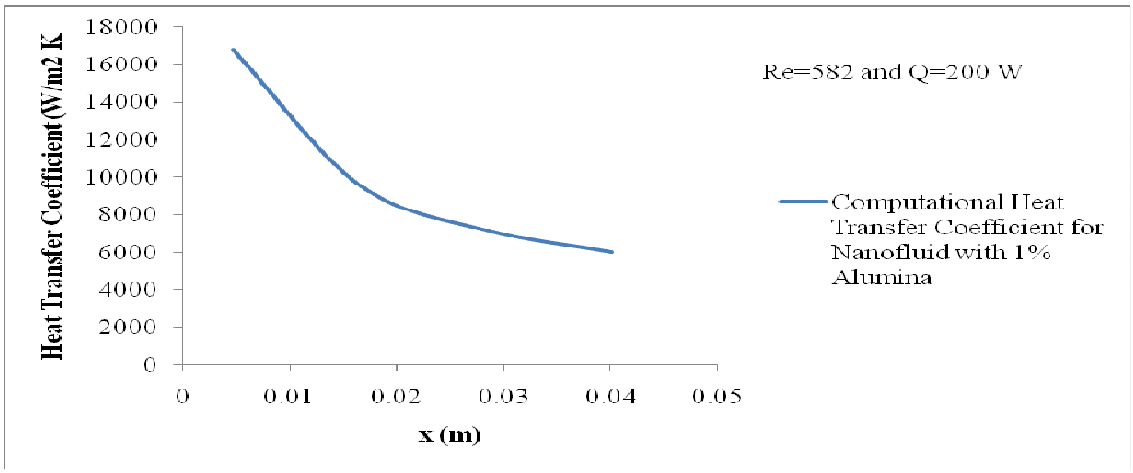

(b)

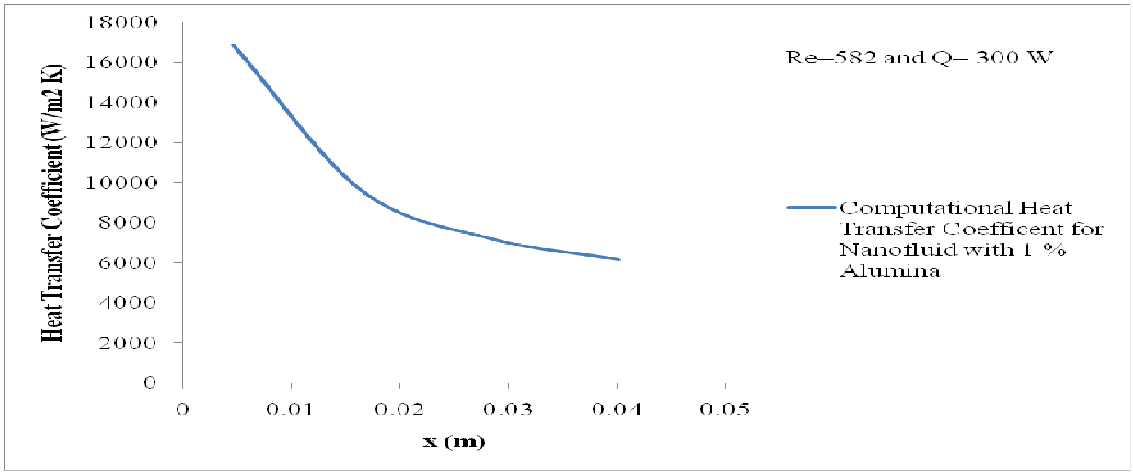

(c)

Figure 5.10: Variation of Heat Transfer Coefficient forNanofluid with 1% Alumina along micro channel at different Power inputs (a) 100 W (b) 200 W (c) 300 W.

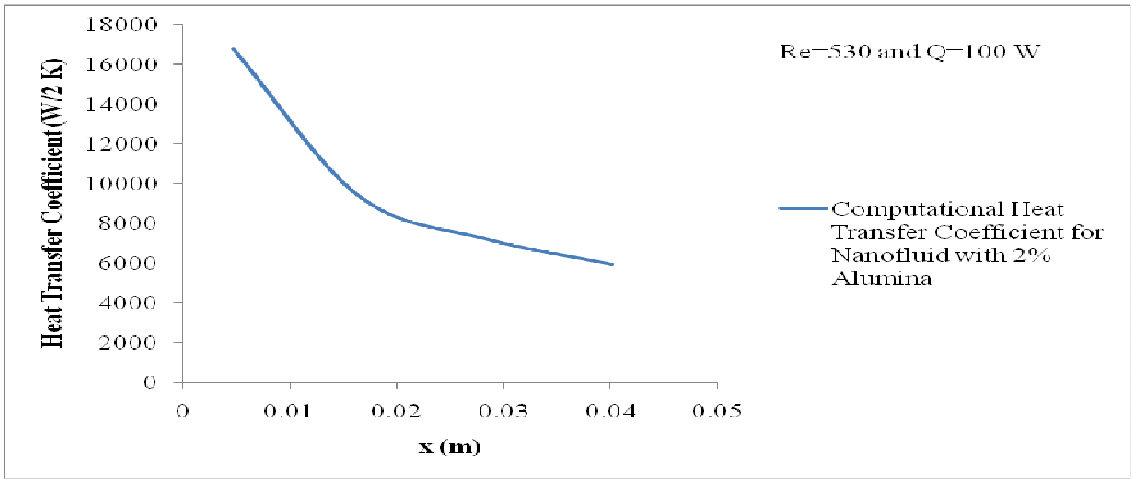

(a)

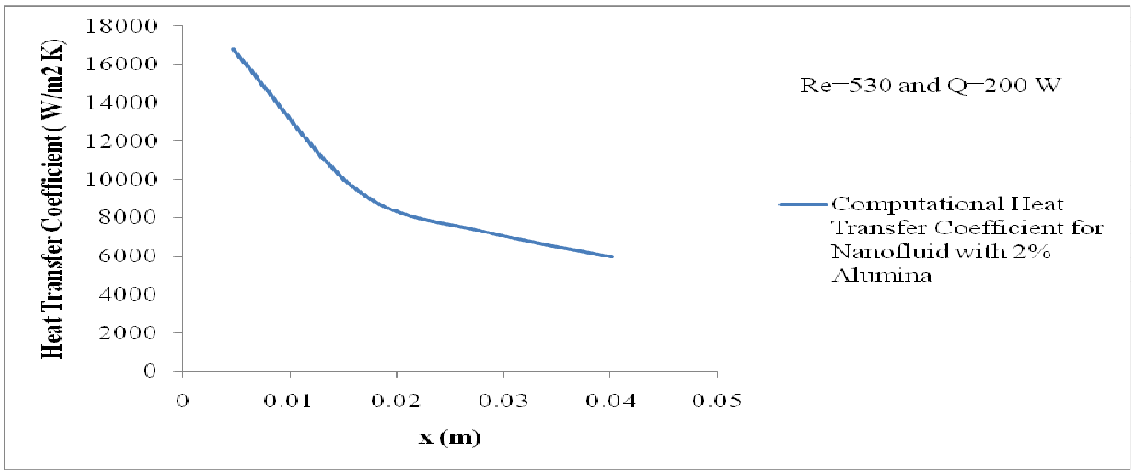

(b)

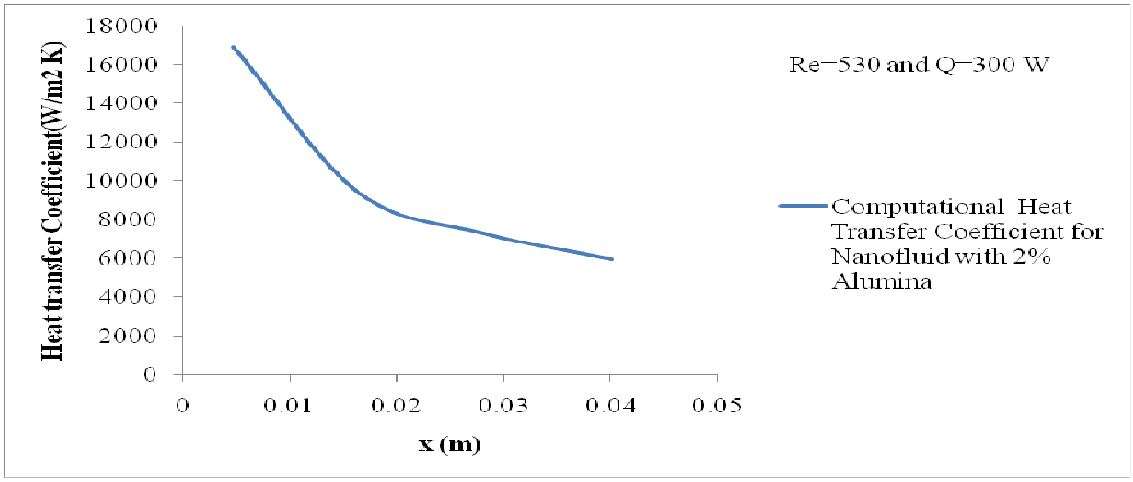

(c)

Figure 5.11: Variation of Heat Transfer Coefficient forNanofluid with 2 % Alumina along micro channel at different Power inputs (a) 100 W (b) 200 W (c) 300 W

The variation of wall temperature at different power inputs along micro channel are shown in Figs. 5.12 to 5.14 using water and its nanofluids as the coolant. The temperature is appeared to increase on the wall in the flow direction in all the cases. The rise in temperature from inlet to the outlet of the channel is found directly proportionate to heat input to the channel.

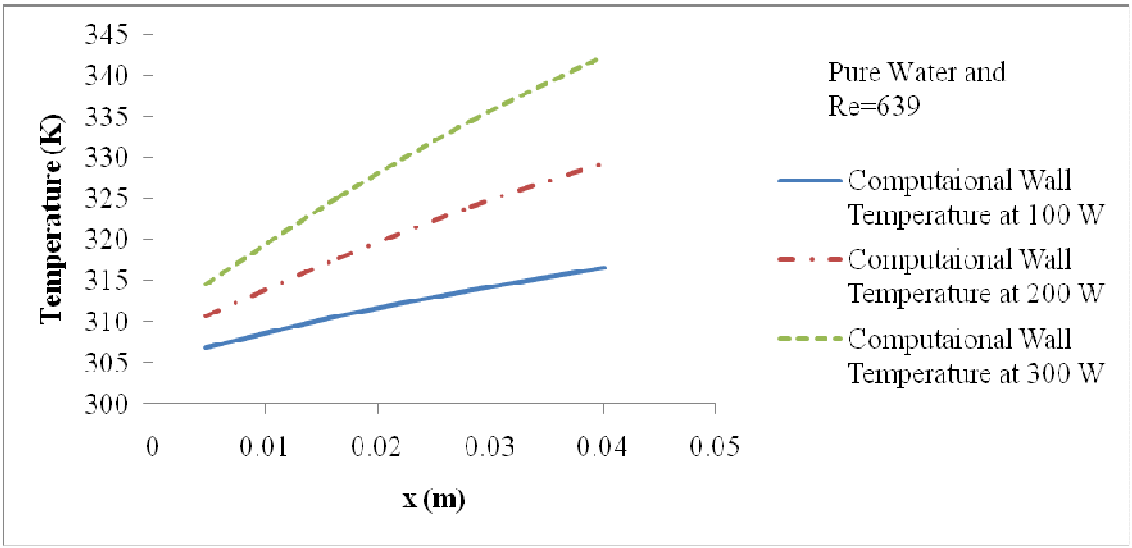

Figure 5.12: Variation of wall temperature at different power inputs along micro channel for Water

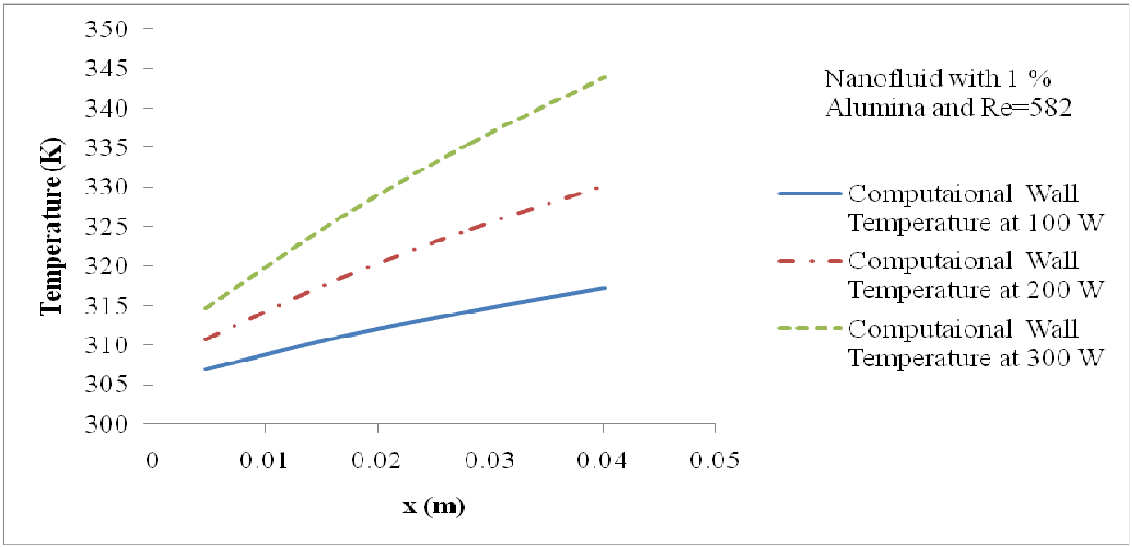

Figure 5.13: Variation of wall temperature at different power inputs along micro channel for Nanofluid with 1 % Alumina

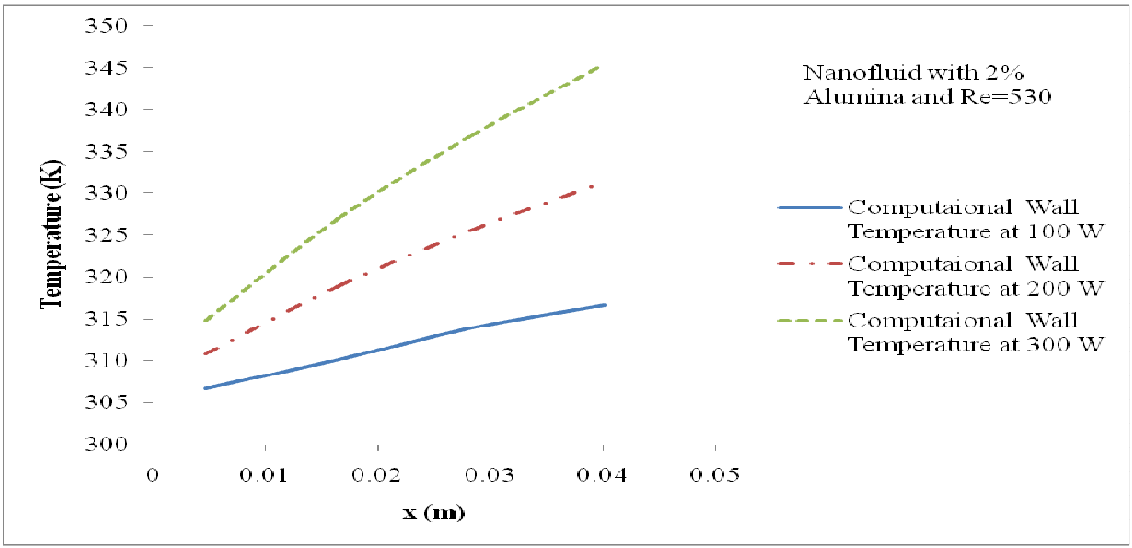

Figure 5.14: Variation of wall temperature at different power inputs along micro channel for Nanofluid with 2 % Alumina

The computed values of wall temperature in the flow direction using water and its nanofluids are compared with the experimental data (Lee and Mudawar, 2007). These are displayed in Figs. 5.15 to 5.17. The comparison shows that CFD results can predict well the experimental data.

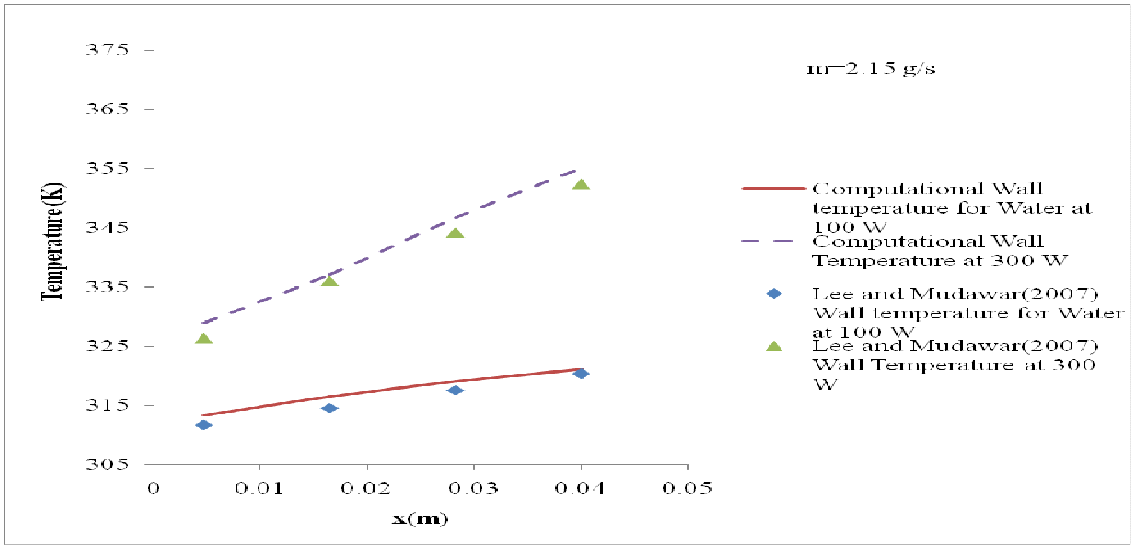

(a)

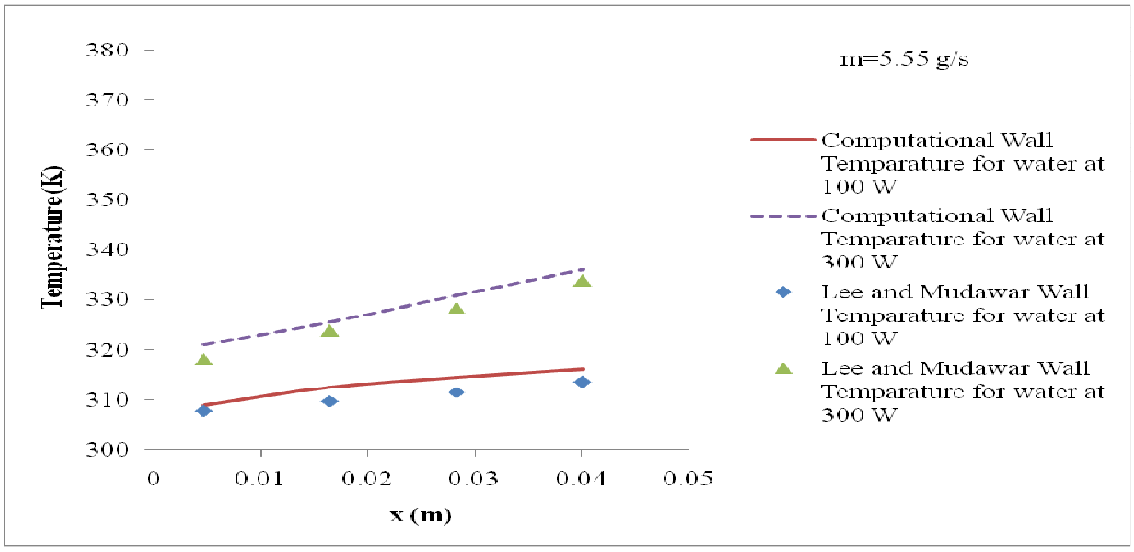

(b)

Figure 5.15: Varition of wall temperature for pure water at mass flow rate of (a) 2.15 g/s (b)5.55 g/s

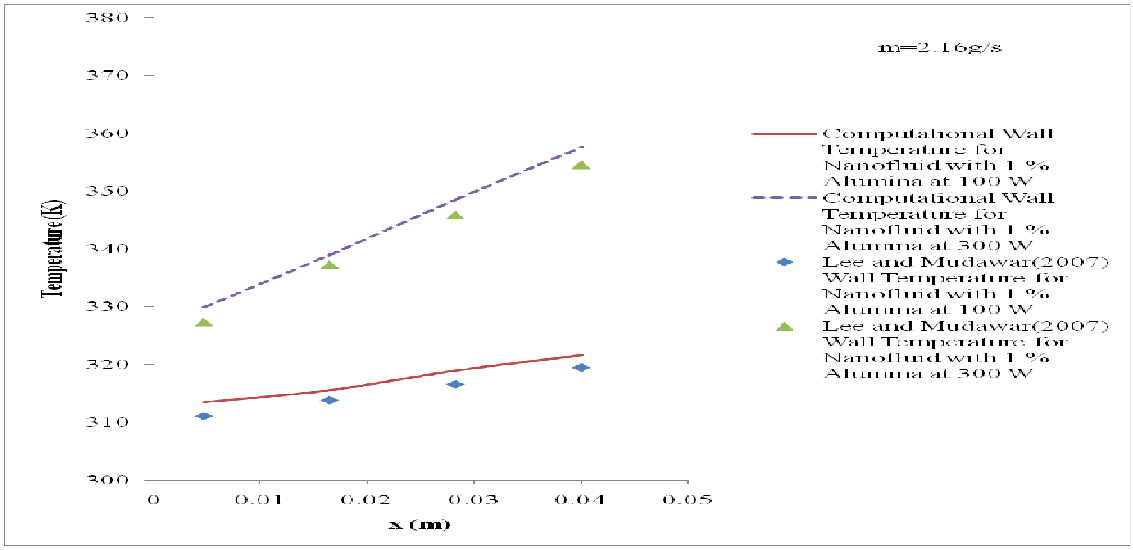

(a)

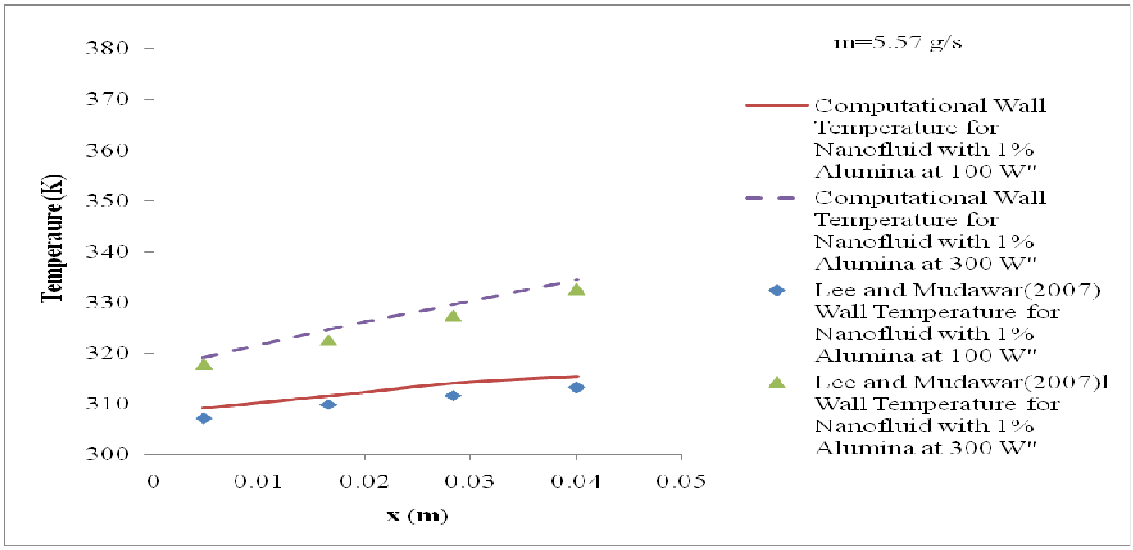

(b)

Figure 5.16: Varition of wall temperature for Nanofluid with 1 % Alumina at mass flow rate of (a) 2.16 g/s (b)5.57g/s

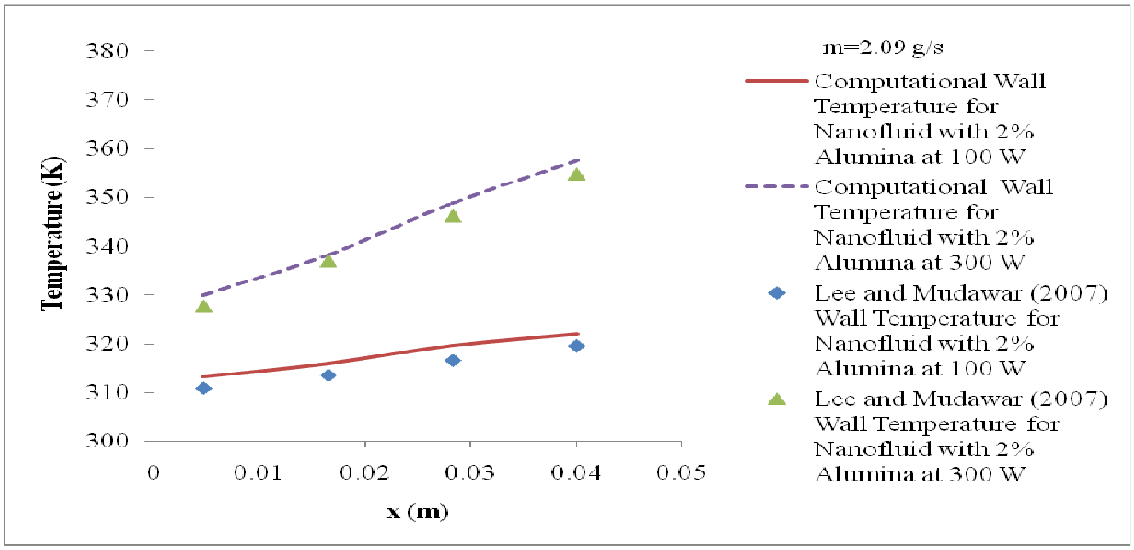

(a)

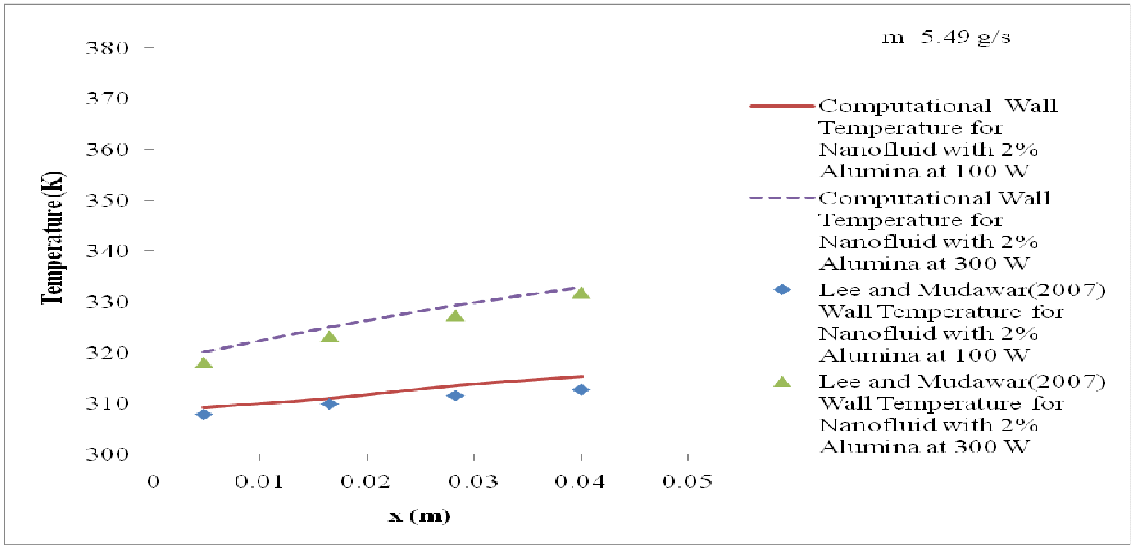

Figure 5.16a: Varition of wall temperature for Nanofluid with 2 % Alumina at mass flow rate of (a) 2.09 g/s (b)5.49g/s

The hydrodynamic and thermal behaviour are also studied in terms of contours of velocity, pressure and temperature on a surface passes through the centerline in the flow direction of the channel. The velocity contourse at different Re using water as the coolant are shown in Figs. 5.17 to 5.19. The figur shows that the entrance length increases with increases in Re.

(a) Nearer to inlet

(b) Nearer to outlet

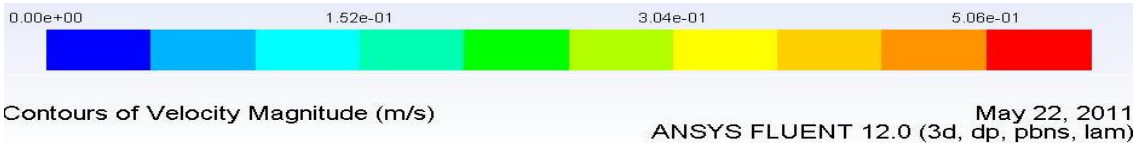

Figure 5.17 Velocity contour Plot of water At Re = 140 (a) Nearer to inlet (b) Nearer to outlet

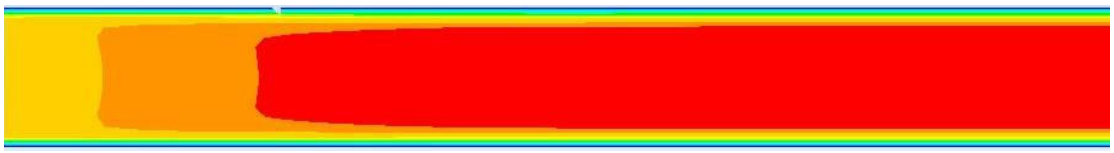

(a) Nearer to inlet

(b) Nearer to outlet

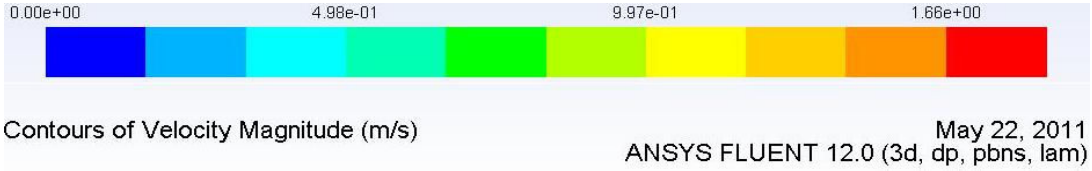

Figure 5.18 Velocity contour Plot of water At Re = 500 (a) Nearer to inlet (b) Nearer to outlet

(a) Nearer to inlet

(b) Nearer to outlet

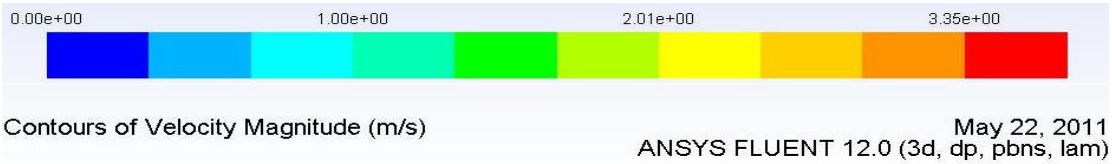

Figure 5.19 Velocity contour Plot of water At Re = 940 (a) Nearer to inlet (b) Nearer to outlet

The pressure contours at different Re are depicted in Figs. 5.20 to 5.22. It show that pressure decreases linearly in the flow direction at all Re.

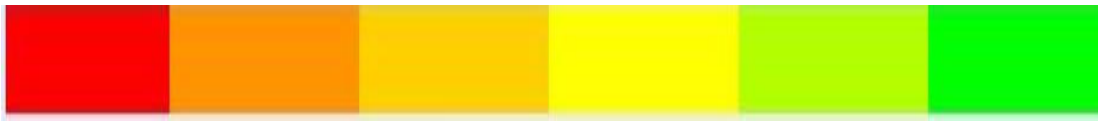

(a) Nearer to inlet

(b) Nearer to outlet

Figure 5.20 Pressure contour Plot of water At Re = 140 (a) Nearer to inlet (b) Nearer to outlet

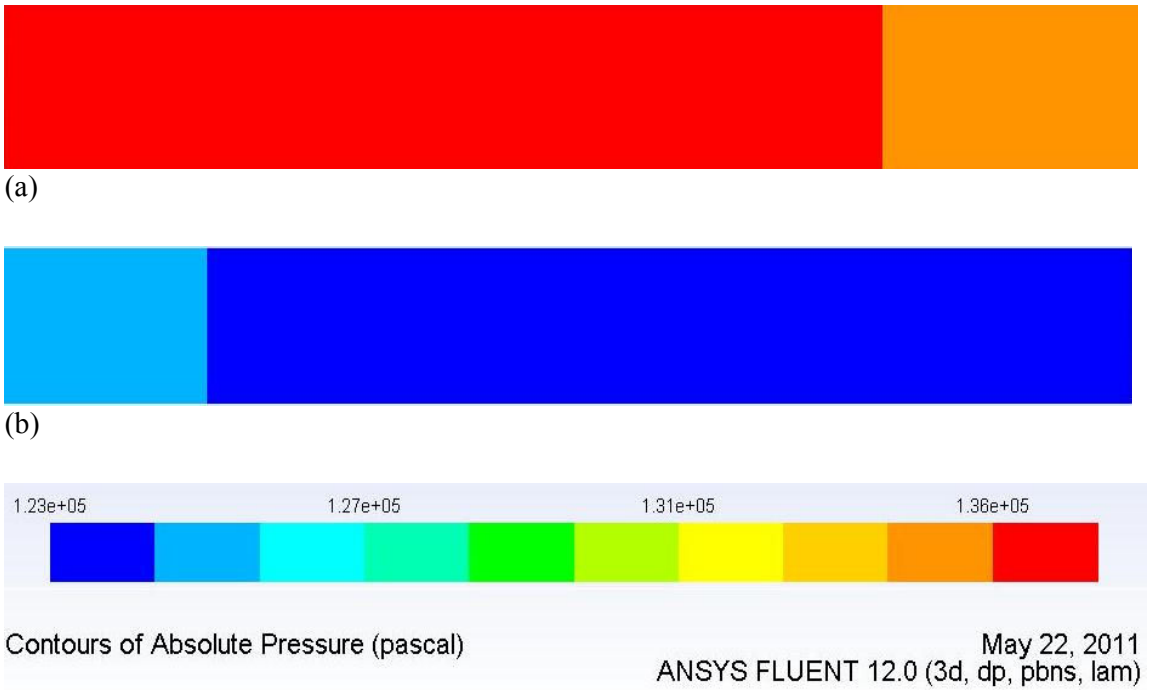

Figure 5.21 Pressure contour Plot of water At Re = 500 (a) Nearer to inlet (b) Nearer to outlet

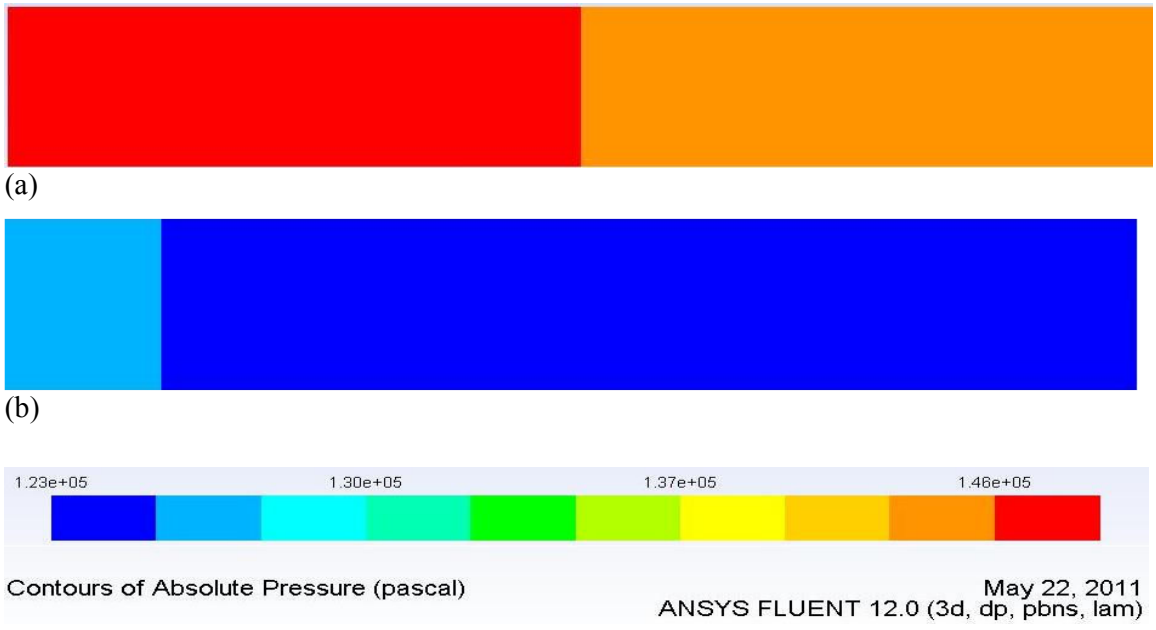

Figure 5.22 Pressure contour Plot of water At Re = 40 (a) Nearer to inlet (b) Nearer to outlet

The Temperature contour plots along microchannel are shown Figs. 5.23 to 5.25 at different Re. The plot shows that at lower re, there is distribution of temperature in the

transverse direction. But at high Re because of high Pecklet number, the inlet temperature almost reaches to outlet around the centreline and only very nears to the wall some temperature distributions are observed in transverse direction.

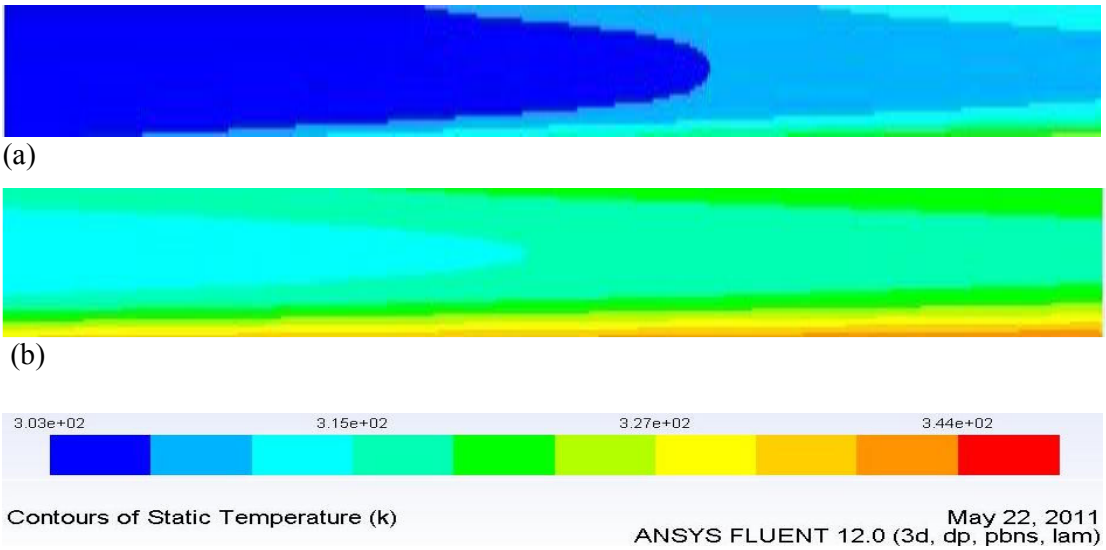

Figure 5.23: Temperature contour plot for water at Re = 140 (a) Nearer to inlet (b) Nearer to outlet

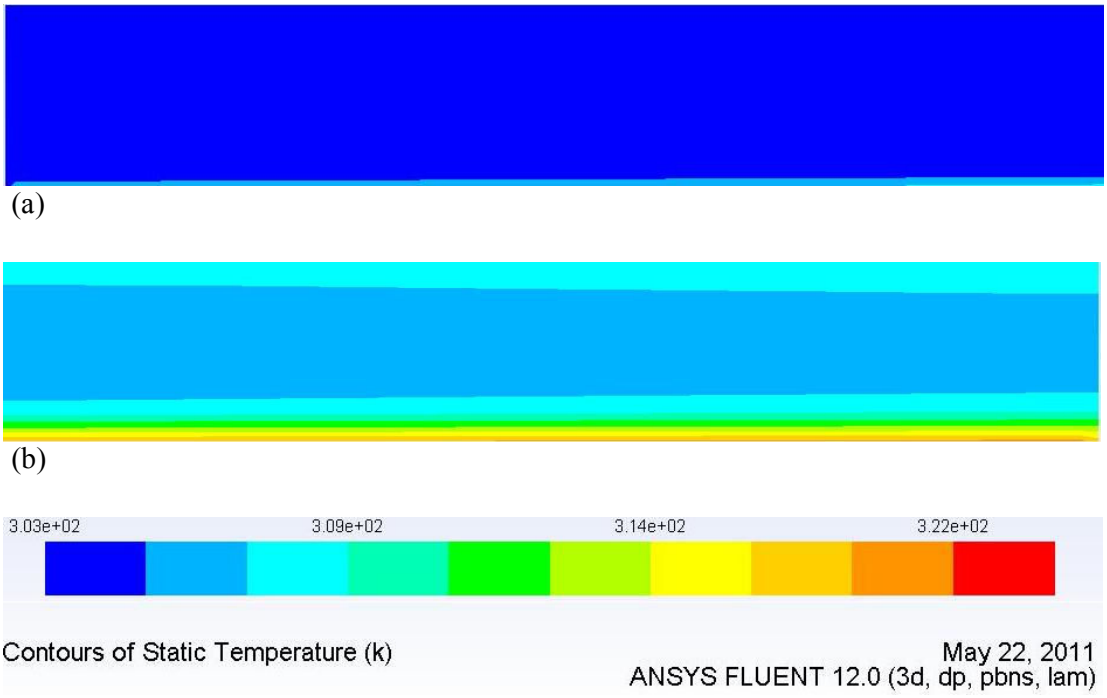

Figure 5.24: Temperature contour plot for water at Re = 500 (a) Nearer to inlet (b) Nearer to outlet

(a)

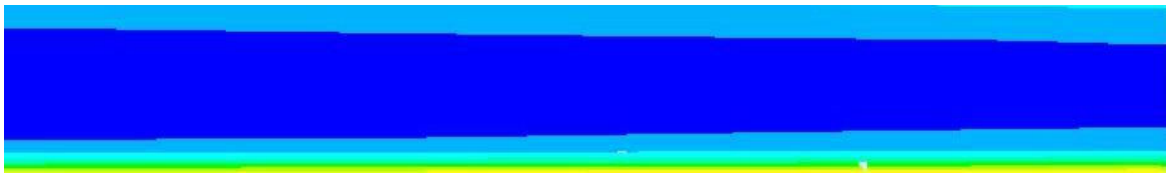

(b)

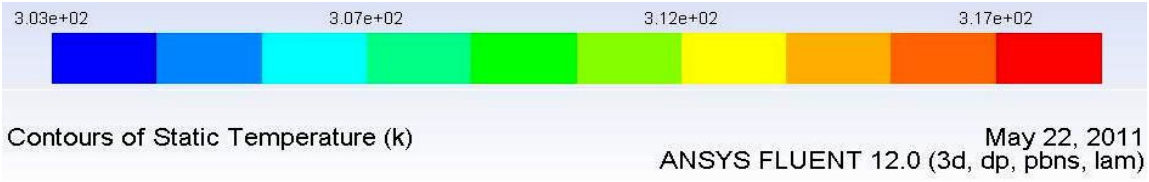

Figure 5.25: Temperature contour plot for water at Re=940(a) Nearer to inlet (b) Nearer to outlet

5.10 CONCLUSION

The theoretical work leads to the following conclusions:

- The computational result successfully validated the test data in terms of wall temperature distributions, pressure drop of the channel and friction factor.
- Pressure drop increases as Reynolds no. increases. Increasing nanoparticle concentration increases single- phase pressure drop compared to pure fluids at the same Reynolds number
- Greater heat transfer coefficient is obtained at micro channel entrance
- Wall temperature increases from entry region of micro channel to exit region.

Chapter 6

CONCLUSIONS AND FUTURE SCOPE

In this chapter the salient accomplishments and major conclusions of this work are summarized and recommendations for the future are made.

6.1 CONCLUSIONS

In this work the hydrodynamics and thermal behaviour of circular microchannel and a rectangular microchannel present in a test rig were studied. Pure water and its nanofluids (Al_2O_3) were used as the coolant in the channel. A steady state computational fluid dynamics (CFD) models was simulated by ANSYS Fluent 12.0 here. The effect of Reynolds number and Peclet number on the flow behaviour of the microchannels was found in both cases

Based on the analysis of the circular microchannel behaviour the following conclusions can be drawn

- Computed temperatures and heat transfer coefficients were found in close agreement with the analytical values.
- The use of nanofluids as the heat transport medium in the channel were found useful both in laminar and in turbulent flow conditions.
- The change of temperature from inlet to outlet was found increasing with decreasing Reynolds number.
- Temperature distribution was found independent of radial position even at very low value of Peclet number.
- Pressure drop increases with increase in Reynolds number.
- The entrance length for fully developed flow depends on Nanoparticle concentrations.
- Wall temperature has negligible variation for higher Reynolds due to greater value of Peclet no in circular micro channel.

Based on the analysis rectangular microchannel study, the following conclusions can be made

- The computational temperature variations, pressure drop and friction factor values can predict the experimental data.
- As the concentration of nanoparticle increases heat transfer coefficient also increases Greater heat transfer coefficient is obtained at rectangular micro channel entrance. Heat transfer coefficient deceases from entry to exit region in rectangular micro channel whereas it is constant in circular micro channel due to fully developed conditions
- Wall temperature increases from entry to exit region of rectangular micro channel.
- Pressure and temperature contours represent successfully the hydrodynamic and thermal behaviour of the system

6.2 FUTURE SCOPE OF THE WORK

- Modeling and Simulation of two phase flow in micro channel.
- Analysis of the boiling characteristics of nanofluids using CFD models.

References

Allen, P. W. 2007. Experimental and Numerical Investigation of Fluid Flow and Heat Transfer in Microchannels. Msc Thesis, Mechanical Engineering Department, Louisiana State University.

Al-Nimr, M.A., Maqableh, M., Khadrawi, A.F. and. Ammourah, S.A. 2009. Fully developed thermal behaviors for parallel flow microchannel heat exchanger, International Communications in Heat and Mass Transfer. 36, 385-390.

ANSYS Fluent 12.0 Theory Guide, April, (2009).

Bachok, N., Ishak, A. and Pop, I. 2011. Flow and heat transfer over a rotating porous disk in a nanofluid. Physica B. 406, 1767 – 1772.

Bayraktar, T. and Pidugu, S.B. 2006. Characterization of Liquid Flows in Microfluidic Systems. International Journal of Heat and Mass Transfer. 49, 815-824.

Bahrami, M and Jovanovich, M. M. 2006. Pressure Drop of Fully Developed Laminar Flow in Microchannels of Arbitrary Cross-Section. Journal of Fluids Engineering. 128, 1036-1044.

Bahrami, M., Jovanovich, M. M. and Culham, J.R. 2006. Pressure Drop of Fully Developed, Laminar Flow in Rough Microtubes, Journal of Fluids Engineering, 128, 632-637.

Bianco, V., Chiacchio, F., Manca, O. and Nardini, S. 2009. Numerical investigation of nanofluids forced convection in circular tubes. Applied Thermal Engineering, 29 (17-18), 3632–3642.

Chein, R. and Chuang, J. 2007. Experimental microchannel heat sink performance studies using nanofluids. International Journal of Thermal Sciences. 46, 57-66.

Choi, S.U.S., 1995. Enhancing thermal conductivity of fluids with nanoparticles. In: Proceedings of the 1995 ASME International Mechanical Engineering Congress and Exposition, San Francisco, CA, USA. 66, 99-105.

Das, S.K., Putra, N., Roetzel, W., 2003a. Pool boiling characteristics of nano-fluids. International Journal of Heat and Mass Transfer 46, 851–862.

Das, S.K., Putra, N., Roetzel, W., 2003b. Pool boiling of nano-fluids on horizontal narrow tubes. International Journal of Multiphase Flow 29, 1237–1247.

Daungthongsuk, W. and Wongwises, S. 2007. A critical review of convective heat transfer of nanofluids. Renewable and Sustainable Energy Reviews. , 11, 797–817.

Ding, Y., Chen, H., He, Y., Lapkin, Y., Yeganeh, M., Šiller, L. Butenko, Y. V. 2007. Forced convective heat transfer of nanofluids. Advanced Powder Technol., 18(6), 813–824.

Eastman, J.A., Choi, S.U.S., Li, S., Thompson, L.J., Lee, S., 1996. Enhanced thermal conductivity through the development of nanofluids. In: 1996 Fall meeting of the Materials Research Society (MRS), Boston, USA.

Eastman, J.A., Choi, S.U.S., Li, S., Yu, W., Thompson, L.J., 2001. Anomalously increased effective thermal conductivities of ethylene glycol-based nanofluids containing copper nanoparticles. Applied Physics Letters 78, 718–720.

Ergu, O. B., Sara, O.N., Yapıcı, S. and Arzutug, S. 2009. Pressure drop and point mass transfer in a rectangular microchannel. International Communications in Heat and Mass Transfer. 36. 618 – 623.

Evgeny, V., Rebrov, N., Jaap, Schouten, C. and Croon, M. 2011, Single-phase fluid flow distribution and heat transfer in micro structured reactors. Chemical Engineering Science. 66 1374–1393

Fedorov, A. G. and Raymond, V. 2000. Three-dimensional conjugate heat transfer in the micro channel heat sink for electronic packaging. International Journal of Heat and Mass Transfer. 43 399-415

Foli, K., Okabe, T., Olhofer, M., Jin, Y. and Sendhoff, B. 2006. Optimization of micro heat exchanger-CFD, analytical approach and multi-objective evolutionary algorithms, International Journal of Heat and Mass Transfer, 49, 1090-1099.

Gabriel, G., Favre-Marinet, M. and Asendrych, D. 2005. Conduction and entrance effects on laminar liquid flow and heat transfer in rectangular micro channels. International Journal of Heat and Mass Transfer. 48, 2943–2954.

Gherasim, I., Roy, G., Nguyen, C. T. and Vo-Ngoc, D. 2009. Experimental investigation of nanofluids in confined laminar radial flows. International Journal of Thermal Sciences. 48, 1486 – 1493.

Hasan, M. I., Rageb, A. A., Yaghoubi, M. and Homayoni, H. 2009. Influence of channel geometry on the performance of a counter flow microchannel heat exchanger, International Journal of Thermal Sciences, 48, 1607-1618.

Hetsroni , G., Mosyak, A., Pogrebnyak, E. and Yarin, L.P. 2005. Fluid flow in micro-channels. International Journal of Heat and Mass Transfer. 48, 1982–1998.

Hetsroni, G., Mosyak, A., Pogrebnyak, E. and Yarin, L.P. 2005. Heat transfer in micro-channels: Comparison of experiments with theory and numerical results. International Journal of Heat and Mass Transfer. 48, 5580–5601

Hong, T.K., Yang, H.S., Choi, C.J., 2005. Study of the enhanced thermal conductivity of Fe nanofluids. Journal of Applied Physics 97, 06411-1-4.

Jiang, P., Fan, M., Si, G. and Ren, Z. 2001. Thermal–hydraulic performance of small scale micro-channel and porous-media heat-exchangers. International Journal of Heat and Mass Transfer, 44, 1039-1051.

Jou, R. and Tzeng, S. 2006. Numerical research of nature convective heat transfer enhancement filled with nanofluids in rectangular enclosures. International Communications in Heat and Mass Transfer. 33, 727-736.

Jung, J., Oh, H. and Kwak, H. 2009. Forced convective heat transfer of nanofluids in microchannels. International Journal of Heat and Mass Transfer. 52, 466 – 472.

Kandlikar, S. G., Garimella, S., Li, D., Colin, S. and King, M. R. 2006. Heat Transfer and Fluid Flow In Minichannels and Microchannels, Elsevier.

Kang, S. and Tseng, S. 2007. Analysis of effectiveness and pressure drop in micro cross-flow heat exchanger, Applied Thermal Engineering. 27, 877-885.

Kawano, K., Minakami, K., Iwasaki, H. and Ishizuka, M. 1998. Micro channel heat exchangerfor cooling electrical equipment. Appl. Heat Transfer Equip., Syst. Educ. ASME HTD-361-3/PID-3, 173-180.

Khanafer, K., Vafai, K. and Lightstone, M. 2003. Buoyancy-driven heat transfer enhancement in a two-dimensional enclosure utilizing nanofluids. International Journal of Heat and Mass Transfer. 46, 3639–3653.

Khandlikar, S. G. and Grande, W.J. 2003. Evolution of Microchannel Flow Passages Thermo hydraulic Performance and Fabrication Technology. Heat Transfer Engineering. 24, 3-17.

Khandekar, S., Joshi, Y. M. and Mehta, B. 2008. Thermal performance of closed two-phase thermosyphon using nanofluids. International Journal of Thermal Sciences. 47, 659–667.

Kheram, M.A. 2011. Numerical study on convective heat transfer for water-based alumina nanofluids. International Journal of Nano Dimension Spring .1(4),297-307.

Lee, S., Choi, S.U.S., Li, S., Eastman, J.A. 1999. Measuring thermal conductivity of fluids containing oxide nanoparticles. ASME J. Heat Transfer. 121, 280–289.

Lee, J. and Mudawar, I. 2007. Assessment of the effectiveness of nanofluids for single-phase

and two-phase heat transfer in micro-channels. International Journal of Heat and Mass Transfer. 50, 452 – 463.

Lee, S., Choi, S.U.S., Li, S., Eastman, J.A., 1999. Measuring thermal conductivity of fluids containing oxide nanoparticles. Journal of Heat Transfer, Transactions ASME 121, 280–289.

Li, C. H. and Peterson, G. P. 2007. Mixing effect on the enhancement of the effective thermal conductivity of nanoparticle suspensions (nanofluids). International Journal of Heat and Mass Transfer. 50, 4668 – 4677.

Li, C.H., Wang, B.X., Peng, X.F., 2003. Experimental investigations on boiling of nano-particle suspensions. In: 2003 Boiling Heat Transfer Conference, Jamica, USA.

Li, J., Peterson, G.P. and Cheng, P. 2004. Three-dimensional analysis of heat transfer in a micro-heat sink with single phase flow. International Journal of Heat and Mass Transfer. 47, 4215–4231.

Liu, D. and Garimella, S.V. 2004, Investigation of liquid flow in micro channels, AIAA J. Thermo phys. Heat Transfer 18, 65–72.

Masuda, H., Ebata, A., Teramae, K., Hishinuma, N., 1993. Alteration of thermal conductivity and viscosity of liquid by dispersing ultra-fine particles (Dispersion of G-Al2O3, SiO2 and TiO2 ultra-fine particles). Netsu Bussei (Japan) 4, 227–233.

Mathew, B. and Hegab, H. 2009. Application of effectiveness-NTU relationship to parallel flow microchannel heat exchangers subjected to external heat transfer. International Journal of Thermal Sciences. 30, 1-10.

Mehendale, S. S., Jacobi, A.M. and Shah, R. K. 2000. Fluid Flow and Heat Transfer at Micro- and Meso-scales with Application to Heat Exchanger Design. Applied Mechanics Reviews, 53, 175-193.

Mishan, Y., Mosyak, A., Pogrebnyak, E. and Hetsroni, G. 2007. Effect of developing flow and thermal regime on momentum and heat transfer in micro-scale heat sink International Journal of Heat and Mass Transfer. 50, 3100 – 3114.

Mokrani, O., Bourouga, B., Castelain, C. and Peerhossaini, H. 2009. Fluid flow and convective heat transfer in flat micro channels. International Journal of Heat and Mass Transfer. 52, 1337–1352

Muthtamilselvan, M., Kandaswamy, P. and Lee, J. 2009. Heat transfer enhancement of copper-water nanofluids in a lid-driven enclosure. Commun Nonlinear Sci Numer Simulat. 5(7), 28 – 44.

Namburu, P. K., Das, D. K., Tanguturi, K. M. and Vajjha, R. S. 2009. Numerical study of turbulent flow and heat transfer characteristics of nanofluids considering variable properties. International Journal of Thermal Sciences. 48, 290–302.

Obot, N.T. 2003. Toward a Better Understanding of Friction and Heat/Mass Transfer in Microchannels – A Literature Review. Microscale Thermophysical Engineering. 6, 155-173. 2003.

Oztop, H. F. and Abu-Nada, E. 2008. Numerical study of natural convection in partially heated rectangular enclosures filled with nanofluids. International Journal of Heat and Fluid Flow. 29, 1326–1336.

Pak, B.C., Cho, Y.I., 1999. Hydrodynamic and heat transfer study of dispersed fluids with submicron metallic oxide particles. Experimental Heat Transfer 11, 151–170.

Peng, X. F., Wang, B. X., Peterson, G. P., and Ma, H. B. 1995. Experimental investigation of heat transfer in flat plates with rectangular micro channels. International Journal of Heat and Mass Transfer. 38,127-137.

Peng, X.F. and Peterson, G.P., 1996. Convective heat transfer and flow friction for water flow in micro channel structures. Int. J. Heat Mass Transfer. 39 12, 2599–2608

Qu, W. and Mudawar, I. 2002. Experimental and numerical study of pressure drop and heat transfer in a single-phase micro-channel heat sink. International Journal of Heat and Mass Transfer. 45, 2549 – 2565.

Qu, W. and Mudawar I. 2003, Flow boiling heat transfer in two-phase micro channel heat sinks – I. Experimental investigation and assessment of correlation methods. Int. J. Heat Mass Transfer. 46, 2755–2771.

Qu, W. and Mudawar, I. 2004. Assesment of effectiveness of nanofluids for single-phase and two-phase heat transfer in micro-channels, International Journal of Heat and Mass Transfer. 50, 452-463.

Qu, W. and Mudawar, I. 2004. Measurement and correlation of critical heat flux in two-phase micro-channel heat sinks. International Journal Heat Mass Transfer. 47, 2045–2059.

Qu, W. and Mudawar I. 2005. A systematic method for optimal design of two phase micro-channel heat sinks. ASME Journal Electron. Packaging. 127, 381–390.

Roy, G., Nguyen, C. T. and Lajoie, P. 2004. Numerical investigation of laminar flow and heat transfer in a radial flow cooling system with the use of nanofluids. Superlattices and Microstructures. 35, 497 – 511.

Sabbah, R., Farid, M. M. and Al-Hallaj, S. 2008. Micro-channel heat sink with slurry of water with micro-encapsulated phase change material: 3D-numerical study. Int. J. Applied Thermal Engineering. 29, 445–454.

Taylor, R. and Phelan, P. E. 2009. Pool boiling of nanofluids: Comprehensive review of existing data and limited new data. International Journal of Heat and Mass Transfer. , 52, 5339-5347

Trisaksria, V. and Wongwises, S. 2007. Critical review of heat transfer characteristics of nanofluids. Renewable and Sustainable Energy Reviews. 11, 512 – 523.

Tsuzuki, N., Utamura, M. and Ngo, T. 2009. Nusselt number correlations for a microchannel heat exchanger hot water supplier with S-shaped fins, Applied Thermal Engineering, 29, 3299-3308.

Tuckerman, D.B. and Pease, R.F. 1981. High-performance heat sinking for VLSI. IEEE Electronic Devices Letters. EDL-2, 5, 126-129.

Tu, J.P., Dinh, N., Theofanous, T., 2004. An experimental study of nanofluid boiling heat transfer. In: Proceedings of 6th International Symposium on Heat Transfer, Beijing, China.

Vassallo, P., Kumar, R., Damico, S., 2004. Pool boiling heat transfer experiments in silica-water nano-fluids. International Journal of Heat and Mass Transfer, 47, 407–411.

Versteeg, H. and Malalasekra, W. 2007. An Introduction to Fluids dynamics: The Finite Volume Method. 2nd Edition, Pearson.

Wang, B.X., Zhou, L.P., Peng, X.F., 2003. A fractal model for predicting the effective thermal conductivity of liquid with suspension of nanoparticles. International Journal of Heat and Mass Transfer 46, 2665–2672.

Wang, Xiang-Qi, Arun, S. and Mujumdar, 2007. Heat transfer characteristics of nanofluids: a review. International Journal of Thermal Sciences. 46, 119.

Wang, X., Xu, X. and Choi, S.U.S. 1999. Thermal conductivity of nanoparticle–fluid mixture. Journal of Thermophysics and Heat Transfer. 13 (4), 474–480.

Wen, D.S., Ding, Y.L., 2004a. Effective thermal conductivity of aqueous suspensions of carbon nanotubes (Nanofluids). Journal of Thermophysics and Heat Transfer 18 (4), 481–485.

Wen, D.S., Ding, Y.L., 2004b. Experimental investigation into convective heat transfer of nanofluids at entrance area under laminar flow region. International Journal of Heat and Mass Transfer 47 (24), 5181–5188

Wen, D.S., Ding, Y.L., 2005. Experimental investigation into the pool boiling heat transfer of aqueous based alumina nanofluids. Journal of Nanoparticle Research 7, 265–274.

Witharana, S., 2003. Boiling of refrigerants on enhanced surfaces and boiling of nanofluids. Ph.D. Thesis, The Royal Institute of Technology, Stockholm, Sweden.

Xie, H., Wang, J., Xi, T.G., Liu, Y., Ai, F., 2002. Thermal conductivity enhancement of suspensions containing nanosized alumina particles. Journal of Applied Physics 91, 4568–4572.

Xu, J.L. and Song, Y.X. 2008. Numerical simulations of interrupted and conventional micro channel heat sinks. International Journal in Heat and Mass Transfer. 51, 5906–5917.

Xuan, Y.M., Li, Q., 2000. Heat transfer enhancement of nanofluids. International Journal of Heat and Fluid Flow 21, 58–64.

Xuan, Y.M., Li, Q., 2003. Investigation on convective heat transfer and flow features of nanofluids. ASME Journal of Heat Transfer 125, 151–155.

Yang, Y., Zhang, Z., Grulke, E., Anderson, W., Wu, G., 2005. Heat transfer properties of nanoparticle-in-fluid dispersions (nanofluids) in laminar flow. International Journal of Heat and Mass transfer 48, P1107–P1116.

You, S.M., Kim, J.H., Kim, K.H., 2003. Effect of nanoparticles on critical heat flux of water in pool boiling heat transfer. Applied Physics Letters 83, 3374–3376.